Initial Excited-state Structural Dynamics of Deuterated and Methylated Uracil Derivatives by Resonance Raman Spectroscopy

by

Faranak Teimoory

A thesis submitted in partial fulfillment of the requirements for the degree of

Doctor of Philosophy

Department of Chemistry
University of Alberta

Abstract

Nucleic acids are biological macromolecules constructed of purine (guanine and adenine) and pyrimidine (cytosine, thymine and uracil) nucleobases. The interaction of ultraviolet (UV) light with pyrimidine nucleobases leads to various photoproducts, such as cyclobutane pyrimidine dimers (CPDs), pyrimidine (6-4) pyrimidinone photoproducts, the dewar photoproduct and photohydrates.

The excited-state structural dynamics are the first step of the photochemistry of the pyrimidine nucleobases after UV absorption. The similar structures of uracil and thymine only differ in the C5 substituent (the H atom on C5 in uracil is replaced by a CH_3 group in thymine). However, thymine and uracil exhibit different major photoproducts; thymine primarily forms the CPDs, while uracil mainly forms the photohydrates. We have shown that the C5 and C6 substituents determine the excited-state structural dynamics and may play a role in the different photochemistry observed. Here, deuterated and methylated C5 and C6 uracil derivatives are examined and compared for tuning the initial excited-state structural dynamics by absorption and resonance Raman spectroscopy.

In this thesis, the initial excited-state structural dynamics of 5-deuterouracil, 6-deuterouracil, 5,6-dideuterouracil and 6-methyluracil are studied. The resonance Raman spectrum is obtained quantitatively at four different UV wavelengths for each of these uracil analogs. The intensity of each resonance Raman peak is directly proportional to the slope of the excited-state potential energy surface along that normal mode at the ground-state geometry (i.e. the Franck-Condon region). Simulation of the absorption spectrum and these resonance Raman excitation profiles

with a self-consistent, time-dependent formalism yields this slope for each normal mode. The slope and mode assignments of each normal mode determined from DFT calculations at the B3LYP level, are used to calculate the excited-state reorganization energy of each internal coordinate, as a reporter of the initial excited-state structural dynamics.

The results suggest that both substituents at the C5 and C6 positions of the pyrimidine ring determine the initial excited-state structural dynamics. Substitution of deuterium for hydrogen and substitution of CH_3 for hydrogen on C5 or C6 doubles or quadruples the excited-state reorganization energy along the C5C6 stretch coordinate, respectively. However, when one site is occupied by a heavier substituent than H, the presence of a heavier mass at the second carbon does not increase this reorganization energy any further. The reorganization energies along the C5X and C6X in-plane bending coordinates are reduced by the substitution of hydrogen by deuterium or methyl on C5 and C6, except when the CH_3 group is substituted on C5. In this case, an unexpectedly high reorganization energy is observed along these in-plane bending coordinates.

Therefore, the high reorganization energy along all these internal coordinates (C5C6 stretch and C5X + C6X in-plane bends) when a CH_3 group is on C5 confirms the highest initial excited-state structural dynamics in thymine, as observed previously. Interestingly, among all the deuterated uracil derivatives, 5-*d*-U has the highest reorganization energies along these internal coordinates, which highlights the significance of the C5 position further in determining the initial excited-state structural dynamics of these uracil analogs.

Preface

Chapter 2 of this thesis has been published by Ng, S. S.; Teimoory, F.; Loppnow, G. R. as "Mass-Tuned Initial Excited-State Structural Dynamics of DNA Nucleobases from UV Spectroscopy: 5-Deuterouracil". *J. Phys. Chem. Lett.* **2011,** *2*, 2362-2365. I was responsible for performing DFT calculations to assign the vibrational modes in the Gaussian09 package. I also did a single point calculation on the optimized structure of uracil with the additional replacement of the natural abundance mass with the isotopic mass of 2 for deuterium at the substituent at C5. I used GAR2PED to construct the set of non-redundant symmetry coordinates of 5-*d*-U and to determine the normal modes and potential energy distributions (PEDs) in terms of these symmetry coordinates. Ng, S. S contributed in the experimental part including the measurement of the resonance Raman and absorption spectra, as well as simulating the absorption and resonance Raman excitation profiles in order to obtain the slopes of excited-state potential energy surface for each normal mode. G. R. Loppnow oversaw the whole project and wrote the manuscript.

Chapter 3 has been published by Teimoory, F.; Loppnow, G. R. as "Initial Excited-state Structural Dynamics of 6-substituted Uracil Derivatives: Femtosecond Angle and Bond Lengthening Dynamics in Pyrimidine Nucleobase Photochemistry" in *J. Phys. Chem. B* **2014,** *118*, 12161–12167. I did the experiment and calculations of this project: measured the absorption and resonance Raman spectra and simulated the absorption and resonance Raman excitation profiles in order to obtain the slope of excited-state potential energy surface each normal mode. In addition, I obtained the vibrational modes of 6-methyluracil by performing DFT calculations in the Gaussian09 package. I also obtained the vibrational modes of 6-deuterouracil by a single point calculation, similar to that of 5-deuterouracil, on the optimized structure of uracil with the replacement of an H to a deuterium at the C6 substituent. I wrote the manuscript and G. R. Loppnow supervised the whole project and proofread the manuscript. A version of Chapter 4 of this thesis is also ready to submit for publication.

Dedicated to

My husband, Hamid Mokhtari,
My lovely daughter, Shaghayegh Mokhtari
for their encouragement, support and understanding
during my PhD

Acknowledgement

Foremost, I am pleased to express my sincerest gratitude to my supervisor Prof. Glen R. Loppnow for his continuous support and great guidance during my PhD. Immense knowledge in chemistry is not the only thing that I learned from him. I benefited from his enthusiasm, patience, motivation, and immense knowledge during the entire research process and writing this thesis. I could say that I was lucky to have such a supportive advisor and mentor in my scientific journey in PhD study for the past five years. It would not be so exciting and rewarding without his help.

Besides my supervisor, I would like to thank my supervisory committee; Dr. Alexander Brown and Dr. Michael J. Serpe for monitoring my research progress, support and encouragement with brilliant comments. I'd also like to thank Dr. Mariusz Klobukowski, Dr. Chris Le, Dr. Rylan Lundgren and Dr. Judy Kim for attending my candidacy and PhD defense sessions. I benefited from their encouragement, insightful comments, and hard questions.

My sincerest thanks also goes out to my colleagues and friends Dr. Swaroop Sasidharanpillai, Dr. Amira El-Yazbi, Sindhu G. Nair, Nazanin Assempour and Farnaz Shakib for their friendship, support and for the stimulating discussions. Of course, paving the road of PhD without them would not have been so easy and joyful. I will never forget the long days we spent studying and working together, and the fun we have had in these past couple of years. I acknowledge all the supports from Analytical and Instrumentation Laboratory, electronic shop and machine shop, especially Dr. Wayne Moffat, Jing Zheng, Allan Chilton and Paul Crothers and a special thanks to Dr. Masao Fujinaga in Information Services & Technology for helping me in running all my calculation in WestGrid. I am also grateful of Shelley Garrett and Tyler Peterson in Information Technology of Chemistry Department for solving our computer issues.

I'd like to thank the Department of Chemistry staff, especially Anita Weiler, the kind and supporting secretary of department, who is always available and ready to help. I appreciate the GSA and FGSR, and the University of Alberta for offering me the teaching assistantship, financial support, Provost, and travel awards that not only helped me financially, but also provided me with

ample teaching in undergraduate labs under supervision of Dr. Norman Gee and Dr. Anna D. Jordan.

Last but not the least, I would like to thank my family; my parents and my lovely sisters, who supported me spiritually throughout my life. Also, I appreciate my husband, Hamid Mokhtari and my lovely daughter, Shaghayegh for their unequivocal support, patience, understanding and encouragement.

Table of Content

List of Tables

Table of Figures

List of Abbreviations

5-*d*-U	5-deuterouracil
6-*d*-U	6-deuterouracil
5-MeU	5-methyluracil (Thymine)
6-MeU	6-methyluracil
5,6-d_2-U	5,6-dideuterouracil
5,6-Me_2U	5,6-dimethyluracil
A	Adenine
a. u.	arbitrary unit
BBO	Barium Borate
C	Cytosine
CPD	Cyclobutyl pyrimidine dimer
DFT	Density function theory
DNA	Deoxydibonucleic acid
G	Guanine
IC	Internal Conversion
IR	Infrared
IS	Internal standard
ISC	Intersystem crossing
LBO	Lithium triborate
PED	Potential energy distribution
PES	Excited-state potential surface
RNA	Ribonucleic acid
S	Singlet state
SA	Self-absorption
T	Thymine
U	Uracil
UV	Ultraviolet
UVA	Ultraviolet A
UVB	Ultraviolet B
UVC	Ultraviolet C
Vis	Visible
VR	Vibrational relaxation

List of Symbols

α	Polarizability
α_0	Equilibrium polarizability
α_1	Change in polarizability with vibration
β	Hyperpolarizability
$\beta/\hbar$	Excited-state potential surface slope (PES)
Δ	Difference between the equilibrium geometry of ground and excited-state
ε	Molar extinction coefficient
ε_i	Energy of the initial vibrational state
ε_v	Energy of the virtual vibrational state
$(\frac{d\sigma}{d\Omega})$	Differential resonance Raman cross Section
Γ	Homogeneous linewidth
μ	Dipole moment
ν	Frequency of vibration
ν_0	Frequency of incident light
ρ	Depolarization ratio
σ_A	Absolute absorption cross section
σ_R	Absolute resonance Raman cross section
θ	Inhomogeneous linewidth
Θ	Standard deviation in inhomogeneous linewidth
$\|i\rangle$	Initial vibrational state
$\|f\rangle$	Final vibrational state
$\|v\rangle$	Virtual vibrational state
$\bar{E}_0$	Average energy
C	Concentration
d	Raman sample pathlength
E	Electric field or the efficiency of the spectrometer

E_0	Zero-zero energy of the electronic transition
E_L	Energy of the incident light
E_S	Energy of the scattered light
$\bar{E}_0$	Normalized inhomogeneous distribution of zero-zero energies around an average energy
E	Spectrometer efficiency
h	Planck's constant
Ω	Solid angle
ρ	polarization index
I	Resonance Raman intensity
L	Internal field correction
n	Refractive index
S	Electronic state
V	Vibrational state

Chapter 1

1. Introduction

Nucleic acids include deoxyribonucleic acid (DNA) and ribonucleic acid (RNA). Nucleic acids and proteins are the most important polymeric biological molecules that are responsible for encoding, transmitting and expressing genetic information. DNA and RNA tend to be double-stranded and single-stranded, respectively. Nucleic acids are constructed of the units known as nucleotides, which consist of a pentose sugar, a phosphate group, and a purine or pyrimidine nucleobase. Changes in the structure of DNA and RNA leads to nucleic acid damage. Nucleic acid damage can lead to the breaking of DNA strands, as well as missing bases in the DNA backbone.[1, 2] The structural change can lead to the formation of photoproducts, such as cyclobutyl pyrimidine dimers (CPD), pyrimidine photohydrates and 8-oxoguanosine.[3, 4] DNA damage is known as one of the main causes of variety of diseases such as cancer. Various reasons are introduced and proposed for DNA damage, which among them, ultraviolet (UV) light is a well-known cause of cancer. Numerous scientists, all around the world, have been focusing on the study of the different types of DNA and RNA damage by UV light.[1, 5-7]

1.1 Nucleotides and Nucleic acids

Purine nucleobases are adenine (A) and guanine (G) (Figure 1.1) and pyrimidines are uracil (U), thymine (T) and cytosine (C) (Figure 1.2). RNA has the same nucleobases as DNA, except thymine (T), which is replaced with uracil (U) (Figure 1.2). The sugar in DNA and RNA backbones are deoxyribose and ribose, respectively. The backbone of a single-stranded DNA is formed by phosphodiester bonds between the sugars and phosphate groups that are connected to each other alternatively. The nucleobases are bound to the sugars. Phosphate groups attach to the 3'-end and the 5'-end of the sugar. The nucleobases are joined to the 1' carbon of sugars via an N-glycosidic linkage from the N1 (nucleobase ring nitrogen) of pyrimidines or N9 of purines.

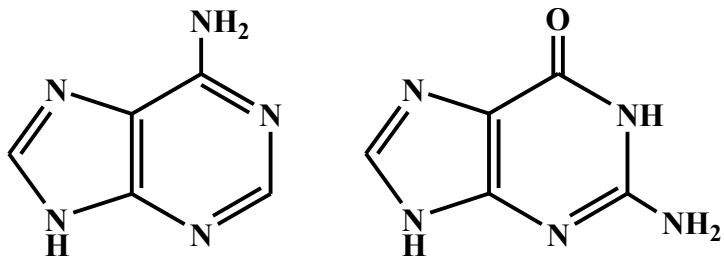

Adenine **Guanine**

Figure 1.1 The structures of purine nucleobases

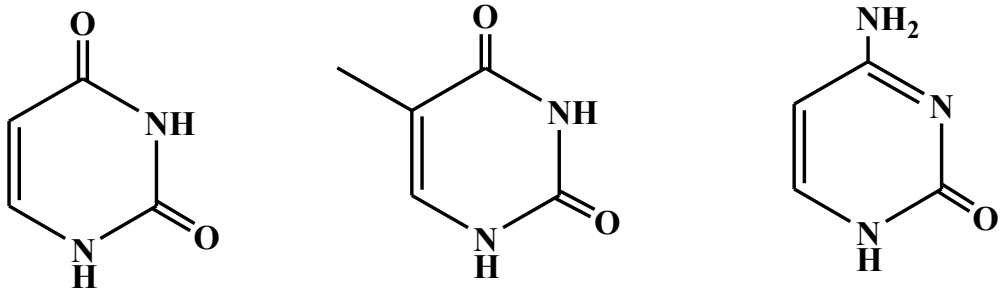

uracil **thymine** **cytosine**

Figure 1.2 The structures of pyrimidine nucleobases

Figure 1.3 illustrates the structures of a uracil nucleobase, a nucleoside, and a nucleotide. A nucleoside is formed by a nucleobase attached to a sugar. A nucleotide includes a nucleobase attached to a sugar and a phosphate. Double-stranded nucleic acids are formed by two sets of complementary sequences based on Watson-Crick base pairing. Indeed, adenine (A) is complementary to thymine (T) and bound to T via two hydrogen bonds and cytosine (C) is complementary to guanine (G) and bound to G via three hydrogen bonds (shown in Figure 1.4).

The genetic information found within proteins in living cells is encoded by sequences of nucleic acids. The code is transcribed by copying the DNA into RNA. The long DNA strands in cells are organized in chromosomes and are duplicated during cell division. This process is called DNA replication.[8] The structures and functionality of certain nucleobases in the nucleic acids are changed upon UV irradiation, resulting in the formation of different photoproducts. This evolution can break the DNA or RNA strand or make the uni- or bimolecular change in the nucleobases structures. The most common is the pyrimidine photodimer formation by the effect of radiation. UV light is an energetic radiation, which is one of the main causes of nucleic acid damage. The amount of UV light that reaches the surface of earth from the sun is significantly less than the visible and infrared. The UV light spectrum (190-380 nm) is classified into three regions: UVC (190-290 nm), UVB (290-320 nm), and UVA (320-380 nm). UVC of sunlight does not reach earth, because these low wavelengths are absorbed by the ozone layer in the stratosphere.[1] UVB radiation reaches the surface of earth and involves the upper end of the DNA absorption spectra. It is mainly responsible for making direct photochemical damage to DNA and is a potent carcinogen.[5, 6] UVA is weakly absorbed by DNA but it is photo-carcinogenic and is involved in photoaging, because DNA damage is indirectly induced by UVA through highly reactive chemical intermediates.[7] Nucleic acids and proteins absorb UV light and form photoproducts. The structural changes and the resulting photoproducts, if not repaired, can ultimately result in mutation in the gene and cause different diseases such as cancer.

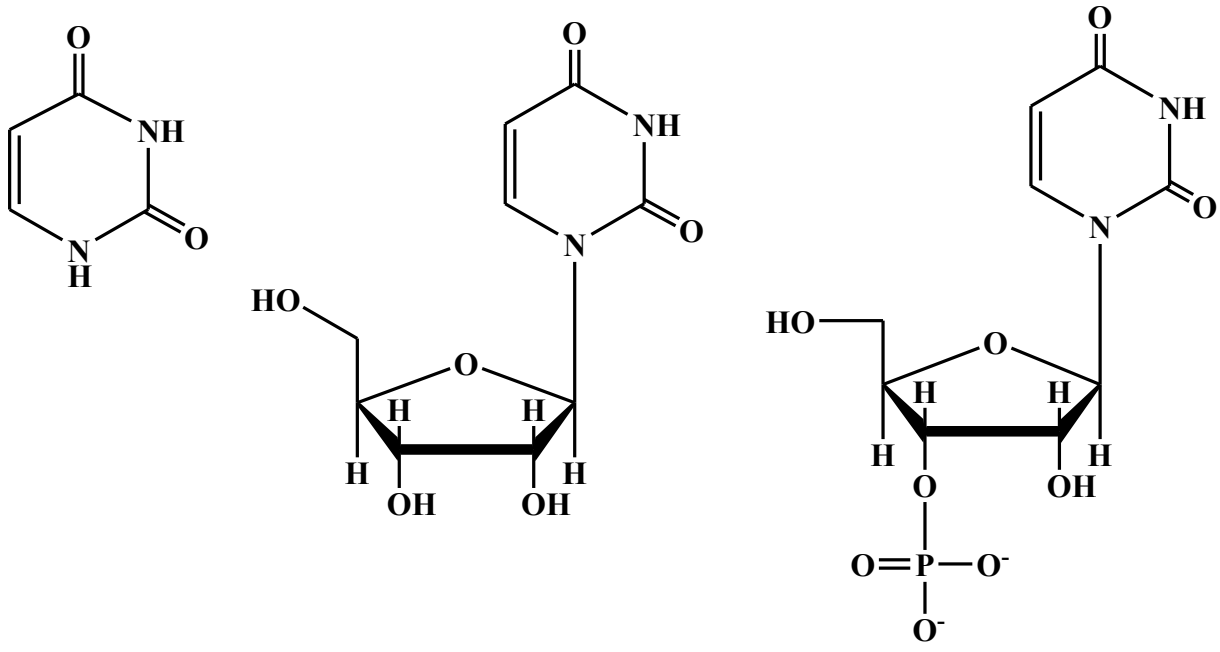

Figure 1.3 The structure of uracil (nucleobase), uridine (nucleoside) and uridine 3'-monophosphate

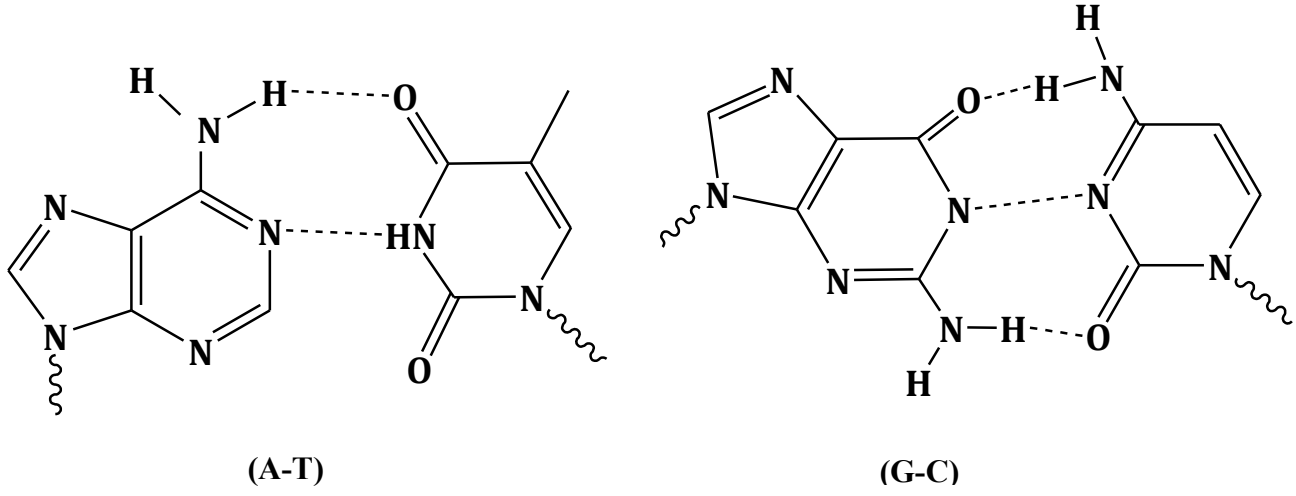

Figure 1.4 The structure of A-T and C-G base pair and the correspondent hydrogen bonds

1.2 The Pyrimidine Nucleobases Photoproducts

The pyrimidine photoproducts are formed by either the addition of the pyrimidine nucleobases to each other or by addition of a water molecule to a pyrimidine nucleobase. However, a different quantum yield is observed on the photoproducts. The most common pyrimidine photoproducts are cyclobutyl pyrimidine dimer (CPD), pyrimidine [6-4]-pyrimidone photoproducts ([6-4]-PPs) and the photohydrate, which will be introduced in more detail in the following paragraphs.[8]

1.2.1 Cyclobutyl Photodimer

Cyclobutyl pyrimidine dimer (CPD) is one of the most common photoproducts observed in the DNA damage. CPD structure is shown in Figure 1.5. CPD is formed by a [2+2] cycloaddition of C5C6 double bonds of two adjacent pyrimidines. It is mostly observed by two thymines (T<>T) or cytosines (C<>C) or a thymine and a cytosine (T<>C). The formation of CPD has a very fast kinetic (less than 1ps).[9] Basically, CPD has cis, trans, syn, and anti isomers, based on the position of both nucleobases. However, formation of trans and anti isomers are restricted by the parallel orientation of the bases in a DNA strand. Cis and syn most strongly dominate CPD isomers in a double-stranded DNA.[10-13] The CPDs lack the aromaticity of the parent nucleobases, thus, there is a loss of maximum absorption band around 260-270 nm. Indeed, the photoreversion of CPD into the parent bases is confirmed by the residual absorption band at 254 nm.[14, 15] Consequently, the CPD formation reaches reaches a plateau.[12, 13]

1.2.2 Pyrimidine [6-4] Pyrimidinone Photoproducts

Pyrimidine [6-4]-pyrimidinone photoproducts ([6-4]-PPs) are the other main photoproducts observed in adjacent pyrimidines. The structure of [6-4]-pp is shown in Figure 1.5, which is the result of decomposition of the heterocyclic intermediate of oxetane in thymine and the intermediate of azetidine at the 3' end of cytosine.[16, 17] The intermediates are formed in a Paterno-Büchi reaction[18]. The secondary photoreaction is also observed in [6-4]-PPs with a high quantum yield. Indeed, an intramolecular cycloaddition following the isomerization into a dewar valence

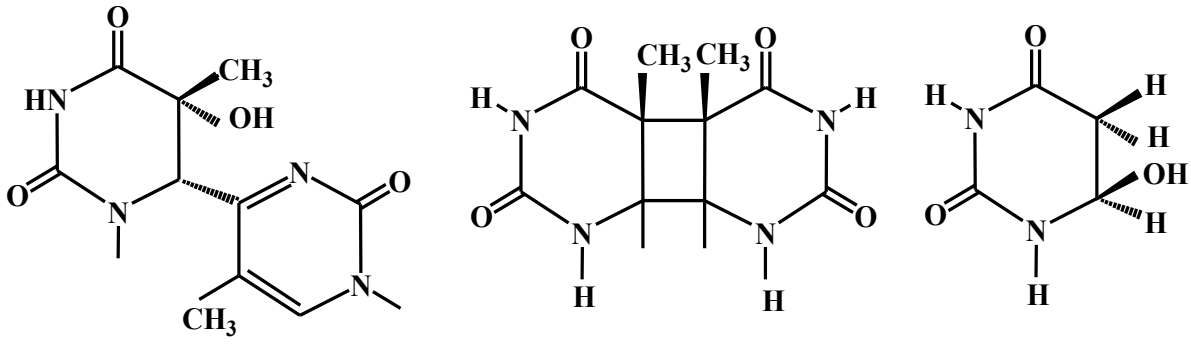

Figure 1.5 The structures of high quantum yield pyrimidine photoproducts

isomer occurs at the pyrimidinone ring upon excitation in the 310-350 nm region.[19-22] Upon high doses of UVB irradiation, dewar isomers are formed on DNA and cells.[23-25]

1.2.3 Photohydrates

Photohydrates are the next photoproduct that include a single pyrimidine base in DNA or RNA (the structure is shown in Figure 1.5). Extensive studies on this photoproduct indicate that photohydrates are formed by nucleophilic addition of water onto the C6 of the intermediate compound derived from the singlet excited-state. The reaction proceeds with a nonstereospecific water addition across the C5C6 double bond, which can occur either on C5 or C6 and result in both stereoisomers. The relative efficiency of this photoproduct among pyrimidine bases at neutral pH is sorted as Cyd ≈ Urd >> Thd.[23-25]

1.3 The Pyrimidine Differences in Photoproduct Quantum Yields

Table 1.1 shows the photoproduct quantum yields (Φ) of the three pyrimidine bases (U, T, and C). The low quantum yield of CPD is observed in U-U and U-T with a reduced efficiency by a factor of 0.5 to 0.75. Research in this area have shown that the photoproducts and their quantum yields differ for uracil and thymine.[9-11]The quantum yield of the thymine photohydrate (10^{-5}) is significantly less than that of cytosine and uracil (10^{-2}). The structures of uracil and thymine are similar with the only difference on the C5 substituent, which is H in uracil and CH_3 group in thymine (as shown in Figure 1.2). Therefore, the presence of the electron donating group of CH_3 on the C5 position is assumed to be the main reason for different CPD and photohydrate quantum yields in thymine and uracil. Ultraviolet irradiation of uracil dinucleotides results in the production of the photohydrate with a 66% quantum yield (Φ = 0.018) and the cyclobutyl photodimer (CPD) with a 33% quantum yield (Φ = 0.007). The photoproducts of thymine dinucleotides are quite different, with the CPD and the [6,4]-PP quantum yields of 81% (Φ = 0.013) and 19% (Φ = 0.003), respectively; thymine does not show any significant amount of the photohydrate

Table 1.1 The quantum yields of a number of pyrimidine photoproducts[8]

Pyrimidine Photoproduct	Φ CPD	Φ [6-4]-PP	Φ Photohydrate
dTpdT	0.016	0.0005	_
dTpdU	0.0082	0.00045	0.00065
dUpdU	0.007	_	0.018
CpC	0.04	_	0.006
T<>T	0.015	_	_

formation. A recent ultrafast time-resolved infrared measurement of dT_{18} indicates that the CPD forms within 1 ps, which leads to the low CPD formation in the oligonucleotides.[9, 23-25] Moreover, the measurement of the photochemical rates of thymine (dTpdT) and uracil (dUpdU) dideoxyribonucleoside monophosphates found that the higher energy UV light is ascribed to the photoreversibility of the CPD reaction.[12] In this thesis, I have focused on the initial excited-state structural dynamics of four uracil derivatives to be able to make a clear comparison between U, T, and the mass tuned C5 and C6 methylated and deuterated uracil derivatives.

1.4 Jablonski Diagram

Spectroscopy introduces numerous powerful techniques for studying nucleic acid damage. Spectroscopy is defined by the interaction between matter and light which can change different characters of either of the two. Therefore, irradiation of light to nucleobases (known as the bricks of life) can change the light properties, which appears by changing the spectrum. It can report any change in the molecular properties of the nucleobases. Light is an electromagnetic wave, with perpendicular oscillating electric and magnetic fields. The magnetic fields of light can be absorbed by molecules. Molecules are excited to higher-energy levels by absorbing the energy of photons. According to the energy and intensity of the incident light, molecules can be excited to different electronic and vibrational states (these processes are discussed later in this chapter). Subsequently, emission occurs in the reverse direction from the higher to lower states. Relaxation process from these higher-energy levels may occur through either radiative or non-radiative transitions. All of these processes, as well as other possible processes, are well described in Jablonski diagram.[26, 27]

Jablonski diagram was developed by Aleksander Jablonski, a Polish scientist, who extensively studied the molecular absorbance and emission of light. A Jablonski diagram is a written representation that (as shown in Figure 1.6) illustrates the transition of molecules between different electronic and vibrational energy states within a molecule. This simple model can easily describe a series of quantum mechanical phenomena such as absorbance, fluorescence, phosphorescence, internal conversion, and intersystem crossing. [26, 27]

1.4.1 Absorption

Absorption is the first transition in the Jablonski diagram, in which the molecules in the ground state (S_0) absorb energy from light and get excited to the higher electronic states (S_1, S_2, etc.). The energy of a photon is then transferred to a molecule and it transitions to a different state. The absorption of the light occurs only if the light's energy is the same as the difference between the two energy states. Absorption is a very fast process on the order of 10^{-15} seconds, which usually occurs from the lowest (ground) electronic state of molecules. The population in the ground state is determined by the Boltzmann distribution within the lower vibrational states and the available energy of the molecules at that temperature. [26-28]

1.4.2 Vibrational Relaxation and Internal Conversion

The relaxation from the excited vibrational level to the lowest vibrational level within that electronic state is called *vibrational relaxation*, which is a non-radiative process. The energy is transferred to the other molecules as heat. This fast process (10^{-14} and 10^{-11} seconds) is extremely probable to occur immediately after absorbance. Transitions between overlapping vibrational energy levels of different electronic states of the same spin multiplicity is called *internal conversion* (IC). As the distance between electronic energy states decreases, the probability of a transition between the vibrational levels increases. As internal conversion is mechanistically identical to vibrational relaxation, it occurs in the same time-scale. [26, 27]

1.4.3 Fluorescence

Fluorescence is another relaxation pathway for molecules in excited-state and occurs by radiation emission. Upon fluorescence, the energy of the excited molecules is released radiatively between molecular vibrational states of the same spin multiplicity. Fluorescence, as a slow process (on the order of 10^{-9} to 10^{-7} seconds), is not a common relaxation pathway, especially from the second and higher electronic energy states. The higher probability of internal conversion and vibrational relaxation in the higher excited electronic states, as the faster processes, reduces the probability

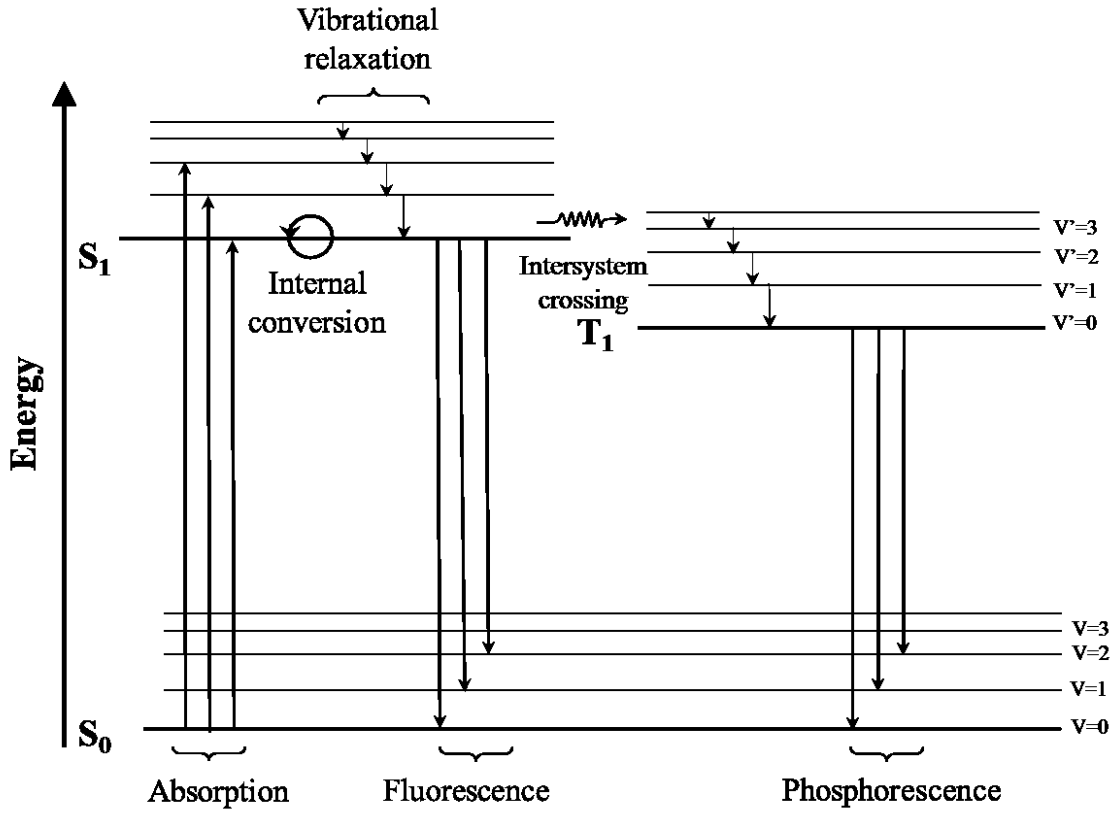

Figure 1.6 Jablonski diagram. In this diagram, S_0 and S_1 represent the ground and the first excited-singlet electronic states, respectively (shown as thick horizontal lines). v represents the vibrational energy states (shown as thinner horizontal lines). Molecules in S_0 absorb energy from light and get excited to the higher electronic states (S_1, S_2, etc.). Absorption is represented by a straight arrow pointing up. The excited molecules relax back in different pathways, including vibrational relaxation, fluorescence, internal conversion, intersystem crossing and phosphorescence. Fluorescence is represented as a straight line pointing down on the energy axis between molecular vibrational states of the same spin multiplicity. Vertical columns show each spin multiplicity. The two excited states show singlet (left S_1) and triplet (right T_1) spin multiplicity of an electron in excited state. Within each column, horizontal lines represent the vibrational (thin) and electronic (thick) eigenstates for those particular molecules. The arrows between vibrational levels also indicate the vibrational relaxation and curved arrow between columns show intersystem crossing. On the other hand, T_1 represents the first excited-triplet state from where phosphorescence occurs to S_0. All the vertical arrows show the radiative transitions, except those which are involved in vibrational relaxation in which energy is released as heat.

of fluorescence. The exciting photons always have more energy than the fluorescent photons. It comes from the fact that some portion of the energy is dissipated by vibrational relaxation. Fluorescence (as well as absorbance) occurs usually within a wide range of wavelengths, because a large number of vibrational levels can be coupled with the transitions between different electronic states. [26, 27]

1.4.4 Intersystem Crossing (ISC) and Phosphorescence

The other non-radiative relaxation is called *intersystem crossing* (ISC), in which the spin multiplicity of an excited state changes from a singlet to a triplet state. It is represented as a horizontal arrow in Figure 1.6. Given that ISC is a forbidden transition, it is a much slower process than fluorescence. The radiative transition from an excited triplet state to a singlet ground state is called phosphorescence, which is also a forbidden transition. Phosphorescence occurs at even lower energies than fluorescence, since triplet excited states have lower energies than singlet excited states, the probability of a transition between the vibrational levels increases. As internal conversion is mechanistically identical to vibrational relaxation, it occurs in the same time-scale. [26, 27]

1.4.5 Photochemical Reactions

Photochemical reactions involve the reaction of the excited molecules with each other, or it can be through a unimolecular mechanism, such as isomerization. Upon excitation, the structure of a molecule is evolved, which is the first step of photoproduct formation. To study the mechanism of photoproduct formation, it is essential to know the main characteristics of the molecule in the excited state.[29] Studying the initial excited-state structural dynamics of molecules is one of the main determining factors in understanding the mechanism of photoreaction. In other words, it is important to know the initial excited-state structural dynamics of the molecule immediately after excitation.[30] In this thesis, the evolution of the molecule on the excited-state potential energy surface is used to probe the photochemical mechanism of a few uracil derivatives. The importance of these molecules are discussed in a later section.

1.5 Spectroscopy

According to the quantum theory, the particular energy of a photon, which is absorbed by a molecule, E, is calculated by $E = h\nu$, where h is Planck's constant, 6.6256×10^{-34} J sec and ν is the frequency. According to the classical model, the nuclei of the atoms in a molecule are considered as mathemathical points with mass. The position of each mass point is defined by three coordinates x, y, and z in a cartesian coordinate system. Therefore, each mass point has three independent degrees of freedom for motion. A molecule with N atoms has 3N degrees of freedom in space. Translation of molecule, which is the movement of the center of mass of the molecule, requires three degrees of freedom in the three directions of the space. The remaining degrees of freedom correspond to the vibration and rotation of the molecule. Spectroscopy involves studying the interaction of the molecules with light. The energy can affect the molecules with electronic, vibrational or rotational transitions. According to that energy, spectroscopy is categorized in electronic, vibrational and rotational spectroscopy. The latter is not described in this thesis, because it is out of the scope of this research.

1.5.1 Electronic Spectroscopy

Electronic spectroscopy relies on absorption of energy. An electron is excited from the initial ground state to a higher excited state. The vibrational (v = 1, 2, 3,...) and rotational energy levels (j= 1, 2, 3, ...) are embedded into the electronic states. Electronic spectroscopy relies on absorption of energy. An electron is excited from the initial ground state to a higher excited state. The vibrational (v=1,2,3,...) and rotational energy levels (j=1,2,3,...) are embedded into the electronic states. Thus, a vibrational and rotational transition also occurs at the onset of an electronic transition.

In other words, when n (electronic states number) = 0, v and j might not be necessarily 0. In addition, as the Franck-Condon Factor is dependent on the overlap between vibrational states of two electronic states, the vibrational bands are involved in the absorption bands. The absorption and fluorescence peaks are assigned by knowing whether the transition is symmetrically allowed,

based on the Laporte Rules, electron spin, or vibrational coupling. The more allowed a transition is, the greater the intensity and the extinction coefficient of this transition will be. Every compound usually has a unique energy spacing between electronic states. For example, aromatic compounds have (π π^*) and (n π^*) transitions. In absorption spectroscopy, the light from a source passes through a monochrometer of a spectrophotometer and hits the sample. Some wavelengths are absorbed. Absorbance is the ratio of the initial intensity of the incident light to the final intensity of the light.[26, 31]

1.5.2 Vibrational Spectroscopy

Generally, the periodic motion of atoms in a molecular structure is called molecular vibration. If the molecule is nonlinear, the number of normal or fundamental vibrations will be 3N-6 and if it is linear, it will be 3N-5, where N is the total number of atoms of the molecule. When a molecule absorbs the required energy for a transition between two adjacent energy levels, it is known as the excitation of a fundamental vibration. The vibrational frequency ν_k and the normal coordinate Q_k characterize the kth normal mode, which describes the vibration and can be expressed as intramolecular coordinates. A molecular vibration involves a periodic distortion away from the equilibrium structure. This distortion can be described as one internal coordinate.

Valence coordinates are a kind of internal coordinates, by which the changes in the bonds length and angles or dihedral angles are measured. For example, the length of a bond changes symmetrically or asymmetrically in a stretch coordinate (ν), the angle between a group of atoms changes; the atoms in the group vibrate in the same plane in a bend (be) coordinate. The angle between the plane of a group of atoms changes out of the plane of the molecule in a wagging **(γ)** (out-of-plane) coordinate.[31]Valence coordinates are usually used for expressing the potential energy of the molecule. Group coordinate is another useful internal coordinate, which consists of a linear combination of valence coordinates to describe the vibration.

Cartesian displacement coordinate is the other type of internal coordinate, in which the displacement of a fixed atom at its equilibrium position is measured in terms of Cartesian axes. The application of valence and group coordinates are more customary, however, expressing the

kinetic energy of the molecule is simpler by using the Cartesian displacement coordinate. As the atom displacements are involved in this type of coordinate, it is also more appropriate for depicting the form of the vibration. Internal coordinate representation is known as Z-matrix. The description of the atoms in a molecule, such as their atomic numbers, bond lengths and angles are all provided by the Z-matrix. [32, 33]

Absorption of two quanta of energy is called the first overtone. In addition, the energy level differences between the ground state (v = 0) and the first excited-state (v = 1) is not the same as (v = 1) and (v = 2), which is the consequence of anharmonicity of the transitions. In fact, the transition from (v = 1) to (v = 2) with a less energy is called the hot band. The vibrational transitions are probed by Infrared (IR) and Raman spectroscopy.[34]

1.5.3 Infrared Spectroscopy (IR)

In this technique, absorption of energy in the infrared region of the electromagnetic spectrum is measured. The IR spectrum is obtained by IR spectrophotometer. IR spectrum is used to identify the molecular structure, since some special functional groups absorb at certain energy bands. The vibrational frequencies (ν) are determined by the specificity of atoms, the potential energy surfaces of the molecules and the vibrational coupling.

According to the proximity to the visible region, IR region is divided into three regions. The first region is called near-IR, 14000-4000 cm^{-1} (0.8-2.5 μm), in which the fundamental and overtone vibrations can be excited. The second region is called mid-IR, 4000-400 cm^{-1} (2.5-25 μm), which involves the fundamental vibrations and rotational-vibrational movements and the final region is known as far- IR, 400-10 cm^{-1} (25-1000 μm), which is close to the microwave region and is usually used for rotational spectroscopy. The absorbed energy of the molecules from one vibrational state to another is measured by IR spectroscopy.[35]

1.6 Raman Effect

Molecules interact with electromagnetic radiation in various ways. Light can be transmitted,

absorbed or scattered. Light scattering occurs by particles (such as smoke) or molecules, which are known as the Tyndall effect and Rayleigh scattering, respectively. The wavelength of the photons do not change during these processes. Raman effect is another type of scattering in which the molecules are irradiated by a monochromatic and intense light source (usually a laser in the visible region) and are scattered. When this light interacts with a molecule, the molecule is raised to a higher and unstable state. Rayleigh scattering is the elastic collision of the incident photon and the molecule, in which the incident and scattered lights have the same frequency. Rayleigh scattering is the most intense component in a Raman spectrum. The scattered light from the molecules is collected and detected in a spectrometer and detector.

The energy of the scattered light can differ from the energy of the incident light. These different frequencies come from the inelastic collision of the incident light and the molecules. This phenomenon is called the Raman effect (Figure 1.7). However, a smaller number of the raised molecules in the virtual state relax back to the higher vibrational state in the ground state (S_0). Therefore, these lower energy scattered photons shift to a Stokes line. Another possibility occurs when the molecules are in a higher vibrational state in the ground state (v = 1). When these molecules are irradiated and sent to the virtual state, the scattered photons can relax to a lower vibrational energy state in the ground state (v = 0). This leads to anti-Stokes shifts, with lower frequencies than Rayleigh line. Generally, since most of the population is in the lower vibrational levels of the ground state at ambient temperature, the Stokes lines are more intense than anti-Stokes lines.[32]

1.6.1 Polarizability

The electrons and protons of the atoms within a molecule are affected oppositely by irradiation of the electric vector of electromagnetic light. In fact, the electrons of a molecule are displaced and the molecules become polarized by the external electric field. The polarized molecules have an induced dipole moment, μ, which is obtained by Eq. 1.1 [29, 36]

$$\mu = \alpha E \qquad (1.1)$$

where α is the polarizability, which is the deformability of the electron cloud of the molecule by the electric field and E is the strength of the electric field. The electric field of the incident radiation interacting with the molecule varies by time, according to Eq. 1.2

$$E = E_0 \cos 2\pi\nu t \tag{1.2}$$

where E_0 is the maximum value of the electric field, ν is the radiation frequency and t is time.

Eq. 1.3 is derived by combining Eqs. 1.1 and 1.2, which indicates the relationship between the induced dipole moment and the initial electric field of the incident irradiation

$$\mu = \alpha E_0 \cos 2\pi\nu t \tag{1.3}$$

It must be noted that the polarization, α, is not a constant value, because the electron clouds of the atoms do not change identically, when the molecular shape changes during a vibration. The polarizability is expanded for a small displacement by the Taylor series as shown in Eq. 1.4

$$\alpha_k = \alpha_0 + \left(\frac{\partial\alpha}{Q_k}\right)_0 Q_{k_0} \cos 2\pi\nu_k t \tag{1.4}$$

where Q_k and Q_{k0} are the k^{th} normal mode of vibration and the amplitude of the normal mode, respectively. It is observed that, the amplitude of the induced dipole moment oscillation is modulated when polarizability changes vibrationally and causes a rise in the Raman frequency amplitude.[37]

1.6.2 Raman Spectroscopy

Since laser is an intense, collimated, monochromatic, and polarized light, one or more lasers are usually used as the source of light in Raman spectroscopy. These properties of a laser makes it the best source of light to interact with molecular vibrations. The laser light with an energy in near-IR, visible or UV region is usually required to excite molecules, therefore, it is the structure of the samples that dictate the wavelength of the laser light. With the advent of the tunable laser at the early 1970s, the signal to noise ratio (S/N) of Raman spectra improved significantly. In addition, the inexpensive and smaller, hollow cathode UV laser, generates 244 and 248 nm excitation

wavelengths. Some other commonly used lasers are, UV diode lasers, double Ar^+ lasers and excimer lasers.

Light is scattered in all directions after hitting the sample, which can be in gas, liquid or solid states. By placing the optical probes at any angle, the signals can be collected. The angle is usually set at 90˚, 135˚ or 180˚ with respect to the exciting laser. Fiber-optic cables are sometimes used to transmit the incident laser light to the sample and the scattered light back to the detector. These cables can transmit light 100 m or more and enable the sample analysis under the experimental conditions.

The scattered radiation from the illuminated spot is collected with a lens and is sent to a monochromator. Since Raman signals are typically very weak, it is usually difficult to separate the weak Raman scattered light (inelastic) from the intense Rayleigh scattered laser light. Rayleigh scattered radiation at the wavelength corresponding to the laser light is usually filtered out by a holographic filter and a grating disperses the rest of the collected light onto a detector. In the past, holographic gratings and multiple dispersion stages were used in Raman spectrometers to obtain a high degree of laser rejection. The oriented detectors at angles greater than 90° are generally called back-scattering, because the detectors are oriented in the same direction as the incident laser, thus the radiation must scatter back. Charge-coupled device (CCD) detectors, photodiodes and photomultipliers are used as the common detectors for Raman setups. However, the latter takes a longer acquisition time. However, modern Raman setups are usually equipped by notch or edge filters for laser rejection. The energy shift is observed in the scattered light and is detected by a detector. In general, NIR detectors are less sensitive than UV detectors.

In the past, one of the typical problems of Raman spectroscopy was the low intensity of Raman signals; i.e. the number of Raman scattered photons was quite small. However, this problem has been solved and the sensitivity of a Raman measurement has been enhanced by the advent of multichannel and the other advanced processes. Some of the developed advanced types of Raman spectroscopy include surface-enhanced Raman, resonance Raman, tip-enhanced Raman, polarized Raman, stimulated Raman (analogous to stimulated emission), transmission Raman, spatially offset Raman, and hyper Raman.[27, 38, 39]

1.7 Comparison of IR and Raman Spectroscopy

Although Infrared and Raman both provide vibrational spectra of diatomic and polyatomic molecules, the two techniques differ and are complementary to each other, such that some IR active vibrational transitions are not Raman active, and vice versa. In fact, in the Raman process the energy of incident photon distorts the electron distribution around a bond, which results in a change in the polarizability of molecules. However, in IR spectroscopy, the induced dipole moment of the molecules changes in an IR active vibration. This is one of the main differences between IR and Raman spectroscopy.

In addition, although the vibrational states are involved in both IR and Raman spectroscopy, they measure two different phenomena. In IR spectroscopy, the absorption of IR energy between different vibrational states is recorded, whereas in Raman spectroscopy the energy of the scattered photons is recorded. As a result of gross selection rules, in a molecule with a center of symmetry, the polarization is preserved but the dipole moment changes. Therefore, in these types of molecules, symmetrical stretching and bending is IR inactive and Raman active. However, in a molecule with no center of symmetry, the vibrational modes may be both IR and Raman active, or not active at all. The symmetrical stretches and bends are mostly Raman active. In the IR setup the sample holder and any other optical components (lenses, mirrors, etc.) must not be glass, quartz or plastic, because they absorb IR light. However, glass or quartz can be used as any of those parts in Raman spectroscopy setup, because the energy of the incident laser is usually in the visible region. This is one of the advantages of Raman over IR spectroscopy. The strong OH band of water in IR spectrum usually masks the other signals. Therefore, water cannot be used as a solvent in IR spectroscopy. However, aqueous samples can be measured in Raman spectroscopy, because water shows a weak signal in Raman. This advantage of Raman spectroscopy makes it a powerful technique for biological systems.[27, 35, 38]

1.7.1 IR and Raman Selection Rules

The IR and Raman selection rules are derived by solving the Schrödinger wavefunctions. The first rule states that a transition is only allowed for a harmonic oscillator, when $\Delta v = \pm 1$, where v is a vibrational quantum number. This excludes overtones, because they are anharmonic vibrations.[34] The other IR selection rule states that a vibrational mode in a molecule is called "IR active" only if, the permanent dipole of the molecule changes upon vibration and only the asymmetric molecules are “IR active”. However, a vibration is Raman active, only if the polarizability of the molecules changes upon the vibration.[32, 35]

1.8 Resonance Raman Spectroscopy

The resonance Raman spectroscopy occurs when the frequency of the incident laser beam corresponds to an electronic transition of the molecule, as illustrated in Figure 1.7.[30, 39] Resonance Raman spectroscopy, as well as Raman and IR spectroscopy, are often used to identify the structure and to provide information about the vibrations of the molecules. Because the energy spacing of different electronic states is dependent on molecular structure, one tunable laser is required for different chemicals in resonance Raman spectroscopy. The tunable lasers are tuned to the energy difference of two electronic states and enhance the Raman band intensities.[39] This enhancement is observed only in the bonds corresponding to those transitions, for example, the stretching modes of π bonds in a $\pi\pi^*$ transition are affected and enhanced in a resonance Raman spectrum and the other bonds are affected much less.

In fact, in resonance Raman, an extreme enhancement (10^5-10^8 fold) of Raman bands is obtained around the electronic transition. Therefore, very low concentrations (about 10^{-8} M) of samples can be measured by resonance Raman spectroscopy. The higher sensitivity of resonance Raman spectroscopy makes it a powerful technique to study a few vibrational modes of a molecule at a particular excitation wavelength. Molecules can be the large bioinorganic or biomolecules with the chromophores, such as nucleobases in nucleic acids. Resonance Raman spectroscopy is also suited to study some individual chromophores in a complex molecule, such as a protein, only

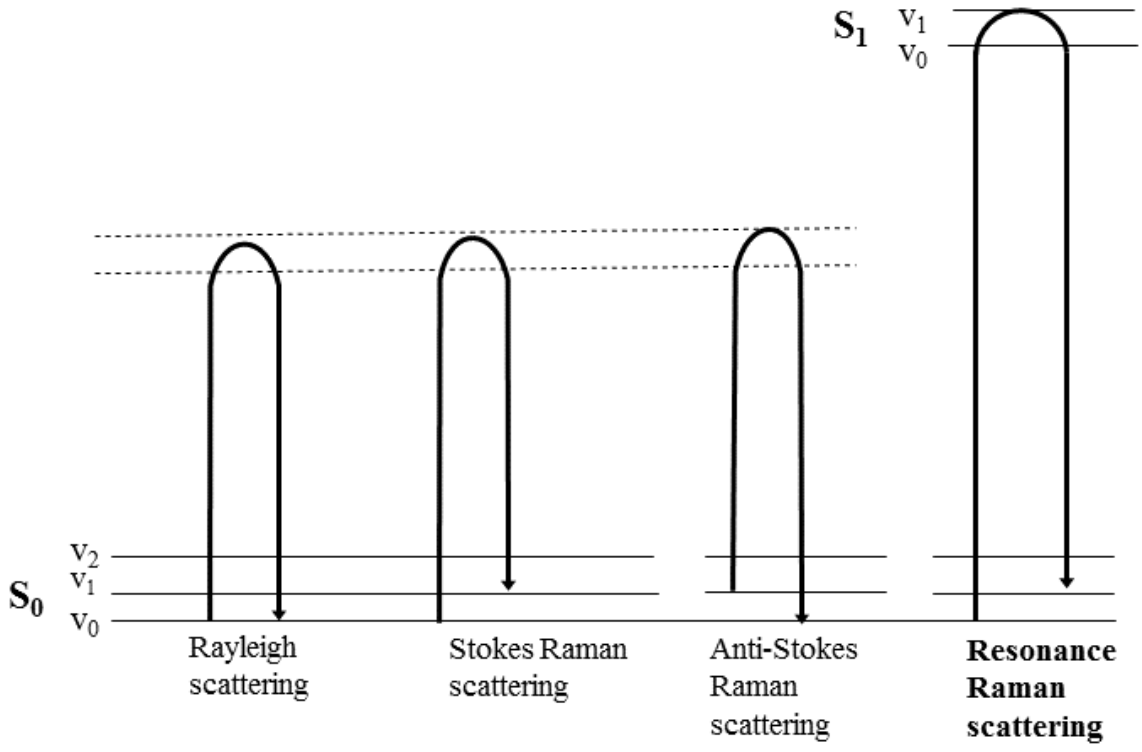

Figure 1.7 Schematic form of Raman and resonance Raman scattering, v represents the vibrational levels in the ground and the first excited states (S_0 and S_1).

if the chromophores have different charge transfer bands.[40-42]

Fluorescence is a typical interference in Raman spectroscopy, which is minimized by the excitation wavelengths in UV resonance Raman spectroscopy. However, the highly intense UV laser increases the risk of heating and photodegradation of the molecules of the sample. This problem is also solved by flowing the sample (if in solution) in a flow cell or spinning it in a NMR tube.[40, 43]

1.8.1 Resonance Raman Setup

A schematic diagram of a resonance Raman instrumental setup is shown in Figure 1.8. The sample is excited by a laser light with a particular excitation wavelength. The sample can be stored in a glass or quartz tube. Heating or photodegradation of the sample by the laser beam is not so probable, since the laser is only focused on a small point. This problem becomes worse when the sample is excited in UV region, however, heating or photodegradation of sample is minimized by flowing or spinning the sample, as mentioned above. The collected scattered light from the sample is sent to a monochromator, which usually consists of a diffraction grating that disperses the light. The grating is rotated and collects the scattered wavelengths reaching to the detector. The detectors are usually CCD or diode array.[28, 29, 39]

1.9 Theory of Resonance Raman and Absorption Cross Sections Calculations

The vibrational frequencies obtained by the resonance Raman spectra provide information about the geometry and electronic structure of the molecules. In addition, the intensities of the Raman and resonance Raman peaks provide information about the symmetry, equilibrium geometry and the excited electronic state structural dynamics. Indeed, the intensities of the resonance Raman modes project the geometry from the ground-state to excited-state. Tang and Albrecht showed the relationship between resonance Raman intensities and the excited-state structure for the first time. Sum-over-state model, time-dependent theory of Raman and transform methods are three

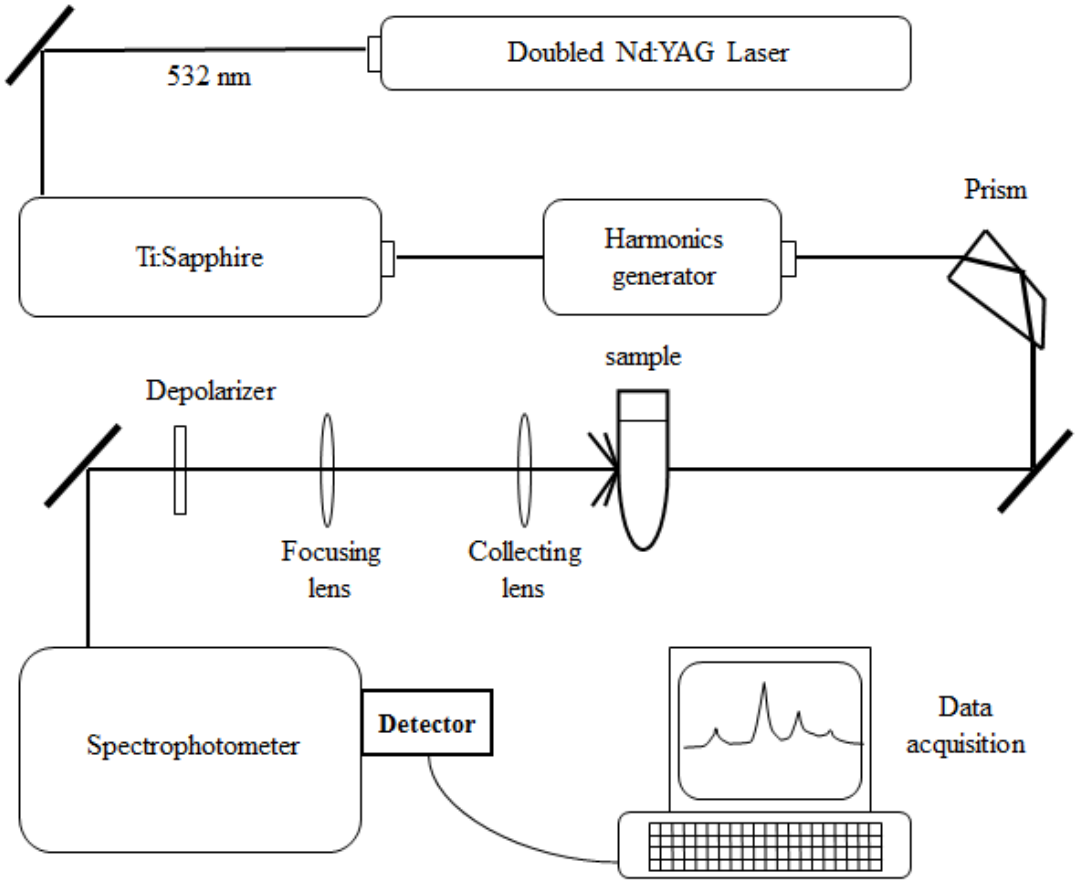

Figure 1.8 Resonance Raman spectrophotometer. Laser excitation is obtained with a doubled Nd:YAG pumped, picosecond mode-locked Ti:Sapphire laser and harmonic generator. Wavelengths of interest were obtained by doubling the Ti:Sapphire fundamental in a lithium triborate (LBO) crystal followed by third-harmonic generation in a β-barium borate (β-BBO) crystal. The entire fundamental beam and its second and third harmonics pass through a prism and are refracted. Only the third harmonic laser beam (in UV region) is sent toward the sample. The resonance Raman scattering was excited by spherically focusing the laser onto an open stream of flowing solution in a 135° backscattering geometry. The scattered beam is collected by a collecting lens and is focused into a depolarizer and a double-grating spectrophotometer with a diode array detector. Then, the resonance Raman spectrum is recorded on a computer.

theoretical methods that are used to evaluate the resonance state structure. [30, 35, 44, 45]

1.9.1 Sum-over-state Method

This model, which is the summation over all the vibrational levels of the excited electronic state, involves the dispersion expressions, derived by Kramers, Heisenberg and Dirac, from the second-order time-dependent perturbation theory.[46, 47] This theory arises from the fact that the power of the scattered light is obtained by a Raman transition from the initial state (I) to the final state (F) over all directions and polarizations of the scattered light. According to Eq. 1.5, the radiated power, $P_{(I\rightarrow F)}$ (photons sec^{-1}) depends on the incident photon flux, I (photons cm^{-2} sec^{-1}) and the cross section of a peak, $\sigma_{(I\rightarrow F)}$ (cm^2).

$$P_{(I\rightarrow F)} = I\,\sigma_{(I\rightarrow F)}\,(E_L) \tag{1.5}$$

On the other hand, resonance Raman cross section is also derived by Eq. 1.6

$$\sigma_{(I\rightarrow F)}(E_L) = \frac{8\pi e^4 E_S^3 E_L}{9\hbar^4 c^4} \sum_{\rho,\lambda} \left|(\alpha_{\rho,\lambda})_{(I\rightarrow F)}\right|^2 \tag{1.6}$$

where E_L and E_S are the energies of the incident, and scattered lights, respectively. I and F are the initial and final vibrational states, respectively. $\alpha_{\rho,\lambda}$ is the resonance Raman polarizability, and the subscripts ρ and λ are the vertical and horizontal polarization indices.

The resonance Raman polarizability is also derived by considering Raman scattering as a two-photon process, involving absorption from the initial state (I) to the excited vibrational state (ν) and a virtual emission to the final state (F). Since there is not any measurement of the system during the intermediate time, we must use the sum of the contributions of all the intermediate states, followed by using several approximations, such as Born-Oppenheimer and Condon approximation. The sum derives the resonance Raman polarizability expression as shown in Eq. 1.7

$$(\alpha_{\rho\lambda})_{I\rightarrow F} = M^2 \sum_V \frac{\langle f|\nu\rangle\langle\nu|i\rangle}{\varepsilon_\nu - \varepsilon_i + E_0 - E_L - i\Gamma} \tag{1.7}$$

where E_0 is the zero-zero energy, which stands for the energy difference between the lowest vibrational level of the ground and excited electronic states. $|i\rangle$ and $|f\rangle$ are the initial and final vibrational wave functions in the Raman process, respectively, ε_ν and ε_i are the energies of the vibrational states of $|\nu\rangle$ and $|i\rangle$, Γ is the homogeneous linewidth, and M is transition electronic length. Therefore, the resonance Raman cross section is obtained by Eq. 1.8

$$\sigma_{(I\to F)}(E_L) = 5.87\times 10^{-19} M^4 E_S^3 E_L \left| \sum_\nu \frac{\langle f|\nu\rangle\langle\nu|i\rangle}{\varepsilon_\nu - \varepsilon_i + E_0 - E_L - i\Gamma} \right|^2 \qquad (1.8)$$

in which, all the energies (E_L, E_S, E_0, ε_ν , ε_i) and Γ are in cm^{-1}, M is in Å, and σ is in Å/molecule. The absorption cross section is also calculated in the same level of approximations and depends on the same excited-state parameters as the Raman cross section does, shown in Eq. 1.9

$$\sigma_{(i\to f)}(E_L) = \frac{4\pi^2 e^2 M^2 E_L}{3\hbar cn} \sum_\nu \frac{\Gamma}{\pi} \frac{|\langle\nu|i\rangle|^2}{(\varepsilon_\nu - \varepsilon_i + E_0 - E_L - i\Gamma)^2 + \Gamma^2} \qquad (1.9)$$

where n is refractive index of the solution.[30]

1.9.2 Time-Dependent Method

The second approach to express the resonance Raman cross section is the time-dependent method, developed by Lee and Heller in 1979, which is a computationally simpler approach than the sum-over-state method.[44] This method can calculate the resonance Raman cross section by using time-dependent perturbation theory directly. However, time dependent method can be started by the sum-over-states formula. In this method the denominator of the Raman polarizability is written as a half Fourier transform (Eq. 1.10).

$$\alpha_{(i\to f)} = \sum_\nu \frac{\langle f|\nu\rangle\langle\nu|i\rangle}{\varepsilon_\nu - \varepsilon_i + E_0 - E_L - i\Gamma} = \frac{i}{\hbar}\int_0^\infty \sum_\nu \langle f|\nu\rangle\langle\nu|i\rangle \exp\left[\frac{-i(\varepsilon_\nu - \varepsilon_i + E_0 - E_L - i\Gamma)t}{\hbar}\right] dt \qquad (1.10)$$

Therefore,

$$\langle\nu|e^{-i(\varepsilon_\nu + E_0)t/\hbar} = \langle\nu|e^{-iHt/\hbar} \qquad (1.11)$$

where *H* is the excited-state Hamiltonian.

$$\alpha_{(i\to f)} = \frac{i}{\hbar}\int_0^\infty \sum_\nu \langle f|\nu\rangle\langle\nu|e^{-iHt/\hbar}|i\rangle \exp\left[\frac{i(\varepsilon_i + E_L + i\Gamma)t}{\hbar}\right]dt \tag{1.12}$$

The operator $e^{-iHt/\hbar}$operates on the right side

$$e^{-iHt/\hbar}|i\rangle = |i(t)\rangle \tag{1.13}$$

and the sum over v is removed by closure and Eq. 1.14 becomes

$$\alpha_{(i\to f)} = \frac{i}{\hbar}\int_0^\infty \langle f|i(t)\rangle \exp\left[\frac{i(\varepsilon_i + E_L)t}{\hbar}\right]e^{-\Gamma t/\hbar}dt \tag{1.14}$$

The absorption and resonance Raman and cross sections are obtained by Eqs. 1.15 and 1.16

$$\sigma_A(E_L) = \frac{4\pi e^2 E_L M^2}{6\hbar^2 cn}\int_{-\infty}^\infty \langle i|i(t)\rangle \exp\left[\frac{i(\varepsilon_i + E_L)t}{\hbar}\right]G(t)dt \tag{1.15}$$

$$\sigma_{(i\to f)}(E_L) = \frac{8\pi e^4 E_S^3 E_L M^4}{9\hbar^4 c^4}\left|\int_0^\infty \langle f|i(t)\rangle \exp\left[\frac{i(\varepsilon_i + E_L)t}{\hbar}\right]e^{-\Gamma t/\hbar}dt\right|^2 \tag{1.16}$$

which are evolved by entering the effect of inhomogeneous and homogeneous broadenings and shown in Eqs. 1.17 and 1.18

$$\sigma_A = \frac{4\pi\ E_L e^2 M^2}{6\hbar^2 cn}\int_0^\infty dE_0 H(E_0)\int_{-\infty}^\infty dt < i\,|\,i(t) > exp\left\{\ i\left(E_L + \varepsilon_i\right)\ t/\hbar\right\}\ G(t) \tag{1.17}$$

$$\sigma_R = \frac{8\pi\ E_s^3 E_L e^4 M^4}{9\hbar^6 c^4}\int_0^\infty dE_0 H(E_0)\left|\int_0^\infty dt < f\,|\,i(t) > exp\left\{\ i\left(E_L + \varepsilon_i\right)\ t/\hbar\right\}\ G(t)\right|^2 \tag{1.18}$$

The inhomogeneous broadening is expressed as $H(E_0)$, which is a normalized inhomogeneous distribution of zero-zero energies around an average energy ($\bar{E}_0$) and is derived by Eq. 1.19

$$H(E_0) = (2\pi)^{-1/2}\theta^{-1}\int_0^{\infty} dE_0 exp\left\{\frac{-(E_0 - \bar{E}_0)^2}{2\theta^2}\right\} \quad (1.19)$$

where θ is the standard deviation of the distribution, |i(t)⟩ is the initial ground-state vibrational wave function propagated on the excited-state potential energy surface. The ⟨i|i(t)⟩ and ⟨f|i(t)⟩ represent the overlaps between |i⟩ and |i(t)⟩ and between |i(t)⟩ and |f⟩, respectively. G(t) is the homogeneous linewidth function, which represents the dynamics of the chromophore-solvent coupling for molecules interacting with a bath. Mukamel and co-workers developed the Brownian oscillator model, in which the solute-solvent interactions contribute to the solvent-induced homogeneous broadening.[30, 45]

1.9.3 Transform Methods

The multimode information in the absorption spectrum is used in the transform method, developed by Blazej and Peticolas, and a relationship between the Raman intensity of a mode and its excited-state displacement is derived. It started by the sum-over-states by Tonks and Page involving more mathematics and the finite-temperature effects.[46-48] This method also started by the time-dependent theory by Hizhnyakov and Tehver.[49] The relationship between the resonance Raman and absorption cross sections is utilized in both formalisms. The imaginary part of the Rayleigh scattering is proportional to the absorption cross section. Kramers-Kronig relations relate the real and imaginary parts of the scattering amplitude. There is no direct relationship between the scattering amplitude and the absorption cross section in Raman scattering. More details for this method are not discussed further, because it is far from the scope of this thesis.

1.10 Experimental Differential Resonance Raman Cross Section

The relation between the differential and absolute Raman cross sections is shown in Eq. 1.20

$$\sigma_S = \frac{8\pi(1+2\rho)}{3(1+\rho)}\frac{d\sigma_R}{d\Omega} \quad (1.20)$$

where σ_R is the absolute Raman cross section, and $\frac{d\sigma_R}{d\Omega}$ is the differential Raman cross section, Ω is the solid angle and ρ is the depolarization ratio. The absolute Raman cross section is calculated by Eq. 1.21

$$\sigma_S = \sigma_{std} \frac{I_S[std]E_{std}L_S n_S (\frac{1+2\rho}{1+\rho})_S}{I_{std}[S]E_S L_{std} n_{std} (\frac{1+2\rho}{1+\rho})_{std}} 10^{dc(\varepsilon_S - \varepsilon_{std})} \quad (1.21)$$

where σ_S and σ_{Std} are the absolute resonance Raman cross sections of the sample and the internal standard, respectively, I is the resonance Raman intensity, E is the spectrometer efficiency. L is the internal field correction, which is equal to $[(n^2+3)/3]^4$, where n is the refractive index. d is the pathlength of the sample, C is the concentration of the absorbents and ε is the molar extinction coefficient. Because internal standard is used, $L_S = L_{Std}$ and $n_S = n_{Std}$. The common internal standard used in Raman spectroscopy are cyclohexane, acetonitrile, benzene, sulfate and nitrate salts. The Raman cross sections of these compounds are known at different excitation wavelengths. The term $10^{dC(\varepsilon_S - \varepsilon_{Std})}$ represents the differential self-absorption, where d is the pathlength of the incident laser light in the half power of this laser and ε is the extinction coefficient at the excitation wavelength.

Now Eq. 1.22 is derived by combining Eqs. 1.20 and 1.21, to give us the equation for calculating the differential cross section of the sample and internal standard

$$\frac{d\sigma_S}{d\sigma} = (\frac{d\sigma_{std}}{d\Omega}) \frac{I_S[std]E_{std}}{I_{std}[S]E_S} 10^{dc(\varepsilon_S - \varepsilon_{std})} \quad (1.22)$$

After measuring the resonance Raman spectrum, the peak area is measured and used as the intensity of each peak. The self-absorption correction factor is found by using the extinction coefficient of the sample and internal standard at the particular excitation wavelength. Hence, the differential cross section of the sample is calculated by using the known differential cross section of the internal standard and the relative area under the peaks.[54]

1.11 Initial Excited-state Structural Dynamics

The resonance Raman intensities directly reflect the initial excited-state structural dynamics. This theory is explained through the separable harmonic oscillator approximation. The $\langle i \mid i(t) \rangle$ and $\langle f \mid i(t) \rangle$ overlaps are significantly sensitive to the difference of the equilibrium geometry of a normal mode from ground- to excited-state (Δ) (shown in Figure 1.9). In other words, these overlaps are related to the initial force on the molecule along the vibrational coordinate in the electronic excited-state, which is called excited-state potential energy surface (PES) slope.

The excited-state PES slope is presented as $\beta/\hbar$ and is derived by $\beta/\hbar=\Delta\bar{\nu}$ (shown in Figure 1.8), where $\bar{\nu}$ is the wavenumber of each normal mode. Because the average relative resonance Raman intensities are proportional to Δ^2, a simulation is scaled so that Δ value in each mode reproduces the experimentally observed absorption and resonance Raman excitation profiles. Therefore, the Δ values in each normal mode are obtained and used as an initial excited-state structural dynamics projection.

The resonance Raman excitation profiles can be simulated by using the time-dependent wave packet formalism based on Eqs. 1.18 and 1.19. All the experimental fundamental modes are included in the time-dependent calculations. Overtone vibrations are also used to constrain the simulation. An iterative optimization of the parameters is obtained by the best possible agreement between the calculated and experimental absorption spectra and resonance Raman excitation profiles. The equilibrium change of the potential energy surface between the ground and excited states is denoted as Δ. The excited-state PES slope in the Franck-Condon region is denoted as $\beta/\hbar$ and the electronic and vibrational states are denoted as S and v, respectively.[29, 30, 55]

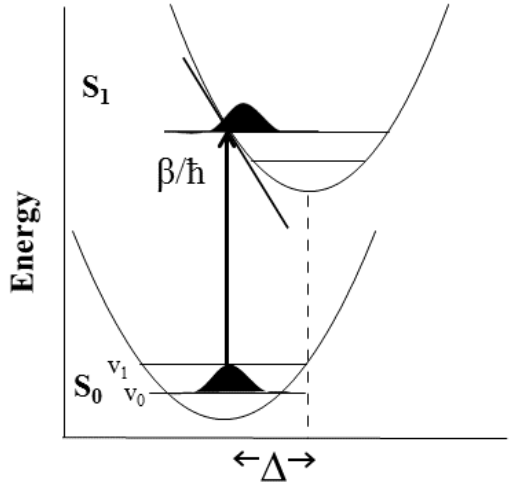

Figure 1.9 Ground and excited-state potential energy diagram

1.12 The Mechanism of the CPD and Photohydrate Formation

UV irradiation of uracil and thymine results in the photoproducts with different quantum yields. CPD and photohydrate are the most frequent types of photoproducts by UV irradiation of thymine and uracil, respectively.[8] Uracil and thymine absorb the UV irradiation and the first effect of the UV light absorption on the structure of these molecules appear as a change in the excited-state structural dynamics. Much computational and experimental research have been confirmed the sub-picosecond excited-state lifetimes of pyrimidine nucleobases through transient UV absorption, fluorescence spectroscopy and ab initio calculation.[56-64] For example, Laubereau and coworkers' studies by transient absorption spectroscopy showed that the first excited electronic states S_1 lifetimes in uracil and thymine are 0.9 ps and 1.2 ps, respectively.[58] Therefore, the initial excited-state dynamics is a crucial step in the mechanism of CPD and photohydrate formation.

These very short excited-state lifetimes showed the significance of the initial excited-state dynamics in determining the mechanism of the photoproduct formation, since the excited molecules cannot experience any further structural dynamics evolution on the extremely short time scale at excited state. The importance of the C5 and C6 substituents of the pyrimidine nucleobases in the photoproduct formation comes from the initial difference of the C5 substituents in uracil and thymine, the structures of uracil and thymine photoproducts (Figure 1.5), and as well, the different quantum yields of these photoproducts. Therefore, in this thesis, I have mainly focused on studying the first effect of the UV light absorption on the structure of the C5 and C6 substituted uracil derivatives, which appears as the change in the initial excited-state structural dynamics by varying mass along the C5 and C6 substituents. The excited-state potential energy surface (PES) slopes along each mode are calculated and compared in the C5 and C6 deuterated and methylated uracil derivatives. The excited-state PES slopes along each mode reflect the initial excited-state structural dynamics. The following results presented in this thesis can explain the mass effect in changing the initial excited-state structural dynamics along the C5C6 stretch and the C5X and C6X bends, where X is a hydrogen, deuterium or a CH_3 group.

Generally, much experimental and computational research involve the excited-state *electronic*

dynamics by femtosecond up-conversion spectroscopy, transient absorption spectroscopy and ab initio calculation.[64-75] There are also various techniques to study the excited-state *structural* dynamics, including experimental techniques; time-resolved fluorescence, IR, and Raman spectroscopy and resonance Raman spectroscopy and also, computational techniques such as, time dependent DFT (B3LYP) potential energy profiles.[69, 70, 76-82] Kohler et al. collected the excited-state *electronic* dynamics of the nucleobases and nucleotides found by different studies in a published review.[83] This review includes numerous studies reporting the photoproduct formation of uracil and thymine within a few hundred femtoseconds and essentially along a barrierless process.[83] The short lifetimes of these pyrimidine nucleobases in excited state clearly show the significance of the initial excited-state structural dynamics in determining the mechanism of the photoproduct formation. This is because the molecules do not have enough time for further evolution in the structural dynamics at excited state. Therefore, a technique is required to probe the initial excited-state structural dynamics.

Among all the experimental techniques for studying the excited-state *structural* dynamics of nucleobases, only resonance Raman spectroscopy is a unique technique for studying the initial excited-state structural dynamics of these molecules in such a short time after excitation, (10-30 fs). Our model in Chapers 2-4 proposes the mass effect on the initial excited-state *structural* dynamics of the C5 and C6 substituted uracil derivatives, therefore, we need a technique that can provide the excited-state *structural* dynamics along the individual internal coordinates. In this thesis, we observe how the intensity of a peak in the resonance Raman spectrum provides the PES slope of that normal mode and how it reflects the initial excited-state structural dynamics of the internal coordinates. In this way, resonance Raman spectroscopy provides the initial excited-state *structural* dynamics of the photochemical active internal coordinates, which is worthy detailed information for understanding the molecular structural change after excitation.

Many computational and experimental techniques have studied the excited-state electronic dynamics of the nucleobases and their derivatives and reported sub-picosecond excited-state lifetimes for these nucleobases.[71, 72] Although, these excited-state *electronic* dynamics information are valuable in understanding the mechanism of the photoproducts formation, more

detailed excited-state *structural* dynamics studies are required. Time-resolved fluorescence, IR and Raman spectroscopy, as well as, computational technique, TD-DFT, are powerful techniques to study the excited-state *structural* dynamics of nucleobabses and other systems.[69, 70, 78, 84] The computational results, also, need to be confirmed by experimental results.[78] As the short lifetimes of the nucleobases at excited state (a few hundred femtoseconds) dictate, the first few femtoseconds after excitation play a major role in determining the photoproduct formation mechanism. However, using time-resolved experimental techniques, it is very difficult to obtain the initial excited-state structural dynamics in the very short time-scale (10-30 fs). Therefore, a technique is required to measure the initial excited-state *structural* dynamics in such a short time.

In resonance Raman spectroscopy the exciting laser is tuned into the absorption band and results in the resonant enhancement of the vibrational modes coupled to the electronic excitation. The intensity of the resonance Raman peak is directly proportional to the excited-state PES slope along that vibrational mode. Therefore, the greater change in the molecular structure along a normal mode is attributed to the more intense resonance Raman vibrational band. Resonance Raman spectroscopy is the best experimental technique to probe excited-state molecular structure and initial in a simpler way, because not only it provides the initial excited-state dynamics in the extremely short time after excitation, but also it provides the valuable excited-state *structural* dynamics along the individual photochemical internal coordinates.[82, 85-88]

Gustavsson et al., have studied the excited-state electronic dynamics of a few uracil derivatives by means of femtosecond fluorescence up-conversion and quantum chemical calculations. The longer excited-state lifetime of the C5-substituted uracil compared to other derivatives indicates the major impact of the C5 substitution on the electronic dynamics. The same study showed the less importance of the C6 substitution on the electronic dynamics.[69] However, a more specific excited-state *structural* dynamics research was required to confirm these results. Zheng et al. studied the excited-state structural dynamics of 1,3-dimethyluracil (DMU), 5-bromo-1,3-dimethyluracil (5BrDMU), uracil, and thymine in water and acetonitrile by resonance Raman spectroscopy. However, no research has ever been performed on the initial excited-state *structural* dynamics of the C6 substituted uracil derivatives. Hence, it was necessary to examine the C6

substituent impact on the initial excited-state structural dynamics along the photochemical active internal coordinates. This is the main difference of the projects in Chapters 3 and 4 and all the other competitors' in this field. Therefore, using resonance Raman spectroscopy, as a powerful technique to provide a detailed initial excited-state *structural* dynamics, we can compare the excited-state *structural* dynamics of uracil, thymine, and their derivatives with slightly different mass, such as deuterated derivatives. The resulting excited-state *structural* dynamics along the photochemical active internal coordinates are valuable information for understanding the photoreactions of these nucleobases.

1.13 References

(1) Knowland, J.; McHugh, P. J.; Dunford, R., Eds.; In *Sunscreen Photobiology;* Gasparo, F. P. Ed.; Molecular, Cellular and Physiological Aspects; Springer: New York, 1997; Vol. 1, pp 47.

(2) Peak, J. G.; Peak, M. J. Comparison of Initial Yields of DNA-to-Protein Cross-Links and Single-Strand Breaks Induced in Cultured Human-Cells by Far- and Near-Ultraviolet Light, Blue-Light and X-Rays. *Mutat. Res.* **1991**, *246*, 187-191.

(3) Kundu, L. M.; Loppnow, G. R. Direct Detection of 8-Oxo-Deoxyguanosine using UV Resonance Raman Spectroscopy. *Photochem. Photobiol.* **2007**, *83*, 600-602.

(4) Faichuk, M.; Mah, A.; Loppnow, G. R. Photochemistry of 5-Fluorouracil Dideoxyribonucleoside Monophosphate. *Photochem. Photobiol.* **2007**, *83*, 1491-1496.

(5) Urbach, F. Potential Effects of Altered Solar Ultraviolet-Radiation on Human-Skin Cancer. *Photochem. Photobiol.* **1989**, *50*, 507-513.

(6) Cadet, J.; Vigny, P. Eds.; In *Bioorganic Photochemistry, Vol. 1: Photochemistry and the Nucleic Acids;* Morrison, H., Ed.; Photochemistry and the Nucleic Acids; John Wiley & Sons: New York, 1990; pp 1.

(7) Martincigh, B. S.; Allen, J. M.; Allen, S. K., Eds.; In *Sunscreen Photobiology;* Gasparo, F. P., Ed.; Molecular, Cellular and Physiological Aspects ; Springer: New York, 1997; pp 11.

(8) Lemaire, D. G. E.; Ruzsicska, B. P., Eds.; In *Organic Photochemistry and Photobiology;* Horspool, W. M., Song, P.-S., Eds.; DNA Damage and Repair; CRC Press: 1995; pp 1295-1329.

(9) Schreier, W. J.; Schrader, T. E.; Koller, F. O.; Gilch, P.; Crespo-Hernandez, C. E.; Swaminathan, V. N.; Carell, T.; Zinth, W.; Kohler, B. Thymine Dimerization in DNA is an Ultrafast Photoreaction. *Science* 2007, *315*, 625-629.

(10) Patrick, M. H.; Gray, D. M. Independence of Photoproduct Formation on DNA Conformation. *Photochem. Photobiol.* 1976, *24*, 507-513.

(11) Patrick, M. H. Studies on Thymine-Derived UV Photoproducts in DNA-I. Formation and Biological Role of Pyrimidine Adducts in DNA. *Photochem. Photobiol.* 1977, *25*, 357-372.

(12) Douki, T.; Cadet, J. Individual Determination of the Yield of the Main UV-Induced Dimeric Pyrimidine Photoproducts in DNA Suggests a High Mutagenicity of CC Photolesions. *Biochemistry* 2001, *40*, 2495-2501.

(13) Douki, T.; Court, M.; Sauvaigo, S.; Odin, F.; Cadet, J. Formation of the Main UV-Induced Thymine Dimeric Lesions within Isolated and Cellular DNA as Measured by High Performance Liquid Chromatography-Tandem Mass Spectrometry. *J. Biol. Chem.* 2000, *275*, 11678-11685.

(14) Lemaire, D. G. E.; Ruzsicska, B. P. Quantum Yields and Secondary Photoreactions of the Photoproducts of dTpdT, dTpdC and dTpdU. *Photochem. Photobiol.* 1993, *57*, 755-769.

(15) Johns, H. E.; Delbruck, M.; Rapaport, S. A. Photochemistry of Thymine Dimers. *J. Mol. Biol.* 1962, *4*, 104-114.

(16) Varghese, A. J.; Wang, S. Y. Ultraviolet Irradiation of DNA in Vitro and in Vivo Produces a 3rd Thymine-Derived Product. *Science* 1967, *156*, 955-957.

(17) Wang, S. Y.; Varghese, A. J. Cytosine-Thymine Addition Product from DNA Irradiated with Ultraviolet Light. *Biochem. Biophys. Res. Commun.* 1967, *29*, 543-549.

(18) Palmer, I. J.; Ragazos, I. N.; Bernardi, F.; Olivucci, M.; Robb, M. A. An Mc-Scf Study of the (Photochemical) Paterno-Buchi Reaction. *J. Am. Chem. Soc.* 1994, *116*, 2121-2132.

(19) Douki, T.; Voituriez, L.; Cadet, J. Characterization of the (6-4) Photoproduct of 2'-Deoxycytidylyl-(3'-Greater-than-5')-Thymidine and of its Dewar Valence Isomer. *Photochem. Photobiol.* 1991, *53*, 293-297.

(20) Taylor, J. S.; Cohrs, M. P. DNA, Light, and Dewar Pyrimidinones - the Structure and Biological Significance of TpT3. *J. Am. Chem. Soc.* 1987, *109*, 2834-2835.

(21) Taylor, J. S.; Lu, H. F.; Kotyk, J. J. Quantitative Conversion of the (6-4) Photoproduct of TpdC to its Dewar Valence Isomer upon Exposure to Simulated Sunlight. *Photochem. Photobiol.* 1990, *51*, 161-167.

(22) Perdiz, D.; Grof, P.; Mezzina, M.; Nikaido, O.; Moustacchi, E.; Sage, E. Distribution and Repair of Bipyrimidine Photoproducts in Solar UV-Irradiated Mammalian Cells - Possible Role of Dewar Photoproducts in Solar Mutagenesis. *J. Biol. Chem.* 2000, *275*, 26732-26742.

(23) Fisher, G. J.; Johns, H.E. Ed.; In *Photochemistry and Photobiology of Nucleic Acids;* Wang, S. Y., Ed.; Pyrimidine Photohydrates; Academic Press: 1976; Vol. 1, pp 169.

(24) Liu, F. T.; Yang, N. C. Photochemistry of Cytosine Derivatives. 2. Photohydration of Cytosine Derivatives - Proton Magnetic-Resonance Study on Chemical-Structure and Property of Photohydrates. *Biochem.* 1978, *17*, 4877-4885.

(25) Wechter, W. J.; Smith, K. C. Nucleic Acids. XI. Structure and Chemistry of Uridine Photohydrate. *Biochem.* 1968, *7*, 4064-4068.

(26) Lakowicz, J. R. In *Principles of Fluorescence Spectroscopy;* 2006; Vol. 3, pp 954.

(27) Skoog, D. A.; Holler, F. J.; Crouch, S. R., Eds.; In *Principles of Instrumental Analysis;* Thomson Brooks/Cole: CA, 2007; pp 1039.

(28) Griffiths, P. R., Ed.; In *Handbook of Vibrational Spectroscopy;* Chalmers, J. M., Griffiths, P. R., Eds.; John-Wiley & Sons Ltd.: Chichester, UK, 2002; Vol. 1, pp 33-43.

(29) Loppnow, G. R.; Billinghurst, B. E.; Oladepo, S. A., Eds.; In *Radiation Induced Molecular Phenomena in Nucleic Acids - A Comprehensive Theoretical and Experimental Analysis Series: Challenges and Advances in Computational Chemistry and Physics;* Leszczynski, J., Ed.; Springer: Netherland, 2008; Vol. 5, pp 237-263.

(30) Myers, A. B.; Mathies, R. A., Eds.; In *Biological applications of Raman spectroscopy;* Spiro, T. G., Ed.; Resonance Raman Spectra of Polyenes and Aromatics; Wiley-Interscience: New York, 1987; Vol. 2, pp 1-58.

(31) Harris, D.; Bertolucci, M. In *Symmetry and Spectroscopy.* An Introduction to Vibrational and Electronic Spectroscopy. Dover Publications: New York, 1989.

(32) Smith, E.; Dent, G. In *Modern Raman Spectroscopy - A Practical Approach;* Modern Raman Spectroscopy - A Practical Approach; John Wiley & Sons, Ltd: Chichester, England, 2005; pp 1-210.

(33) Fava, R. A., Ed.; In *Polymers, Part A: Molecular Structure and Dynamics.* Academic Press: Pennsylvania, 1980; Vol. 16, pp 89-91.

(34) Gordon, M. S.; Pople, J. A. Approximate Self-Consistent Molecular-Orbital Theory .6. Indo Calculated Equilibrium Geometries. *J. Chem. Phys.* **1968**, *49*, 4643-4650.

(35) Colthup, N. B.; Daly, L. H.; Wiberly, S. E. In *Introduction to Infrared and Raman Spectroscopy;* Academic Press, INC.: San Diego, 1990, pp 60-64.

(36) Keresztury, G., Ed.; In *Handbook of Vibrational Chemistry;* Chalmers, J. M., Griffiths, P. R., Eds.; John-Wiley & Sons Ltd.: Chichester, UK, 2002; Vol. 1, pp 71-87.

(37) Long, D. A. In *The Raman Effect: A Unified Treatment of the Theory of Raman Scattering by Molecules;* John-Wiley & Sons Ltd.: Chichester, UK, 2002; pp 1-597.

(38) Clark, R. J. H.; Dines, T. J. Resonance Raman-Spectroscopy, and its Application to Inorganic-Chemistry. *Angew. Chem. Int. Ed.* **1986**, *25*, 131-158.

(39) McHale, J. L., Ed.; In *Handbook of Vibrational Spectroscopy;* Chalmers, J. M., Griffiths, P. R., Eds.; Chichester, UK, 2002; Vol. 1, pp 534-556.

(40) Asher, S. A. Ed.; In *Handbook of Vibrational Spectroscopy;* Chalmers, J. M., Griffiths, P. R., Eds.; John-Wiley & Sons Ltd.: Chichester, UK, 2002; pp 557-571.

(41) Asher, S. A. UV Resonance Raman-Spectroscopy for Analytical, Physical, and Biophysical Chemistry .1. *Anal. Chem.* **1993**, *65*, A59-A66.

(42) Pezolet, M.; Yu, T. J.; Peticolas, W. L. Resonance and Preresonance Raman-Spectra of Nucleotides using Ultraviolet Lasers. *J. Raman Spectrosc.* **1975**, *3*, 55-64.

(43) Asher, S. A.; Johnson, C. R. Raman-Spectroscopy of a Coal Liquid shows that Fluorescence Interference is Minimized with Ultraviolet Excitation. *Science* **1984**, *225*, 311-313.

(44) Lee, S. Y.; Heller, E. J. Time-Dependent Theory of Raman-Scattering. *J. Chem. Phys.* **1979**, *71*, 4777-4788.

(45) Mukamel, S. In *Principles of nonlinear optical spectroscopy;* Oxford University Press: New York, 1995.

(46) Blazej, D. C.; Peticolas, W. L. Ultraviolet Resonance Raman Excitation Profiles of Pyrimidine Nucleotides. *J. Chem. Phys.* **1980**, *72*, 3134-3142.

(47) Tonks, D. L.; Page, J. B. 1st-Order Resonance Raman Profile Line Shapes from Optical-Absorption Lineshapes - Consistency Test of Standard Theoretical Assumptions. *Chem. Phys. Lett.* **1979**, *66*, 449-453.

(48) Page, J. B.; Tonks, D. L. On the Separation of Resonance Raman-Scattering into Orders in the Time Correlator Theory. *J. Chem. Phys.* **1981**, *75*, 5694-5708.

(49) Hizhnyak.V; Tehver, I. Theory of Resonant Secondary Radiation due to Impurity Centres in Crystals. *Physica. Status. Solidi.* **1967**, *21*, 755-768.

(50) Pecourt, J. M. L.; Peon, J.; Kohler, B. Ultrafast Internal Conversion of Electronically Excited RNA and DNA Nucleosides in Water. *J. Am. Chem. Soc.* **2000**, *122*, 9348-9349.

(51) Pecourt, J. M. L.; Peon, J.; Kohler, B. DNA Excited-State Dynamics: Ultrafast Internal Conversion and Vibrational Cooling in a Series of Nucleosides. *J. Am. Chem. Soc.* **2001**, *123*, 10370-10378.

(52) Hovorun, D. M.; Kondratyuk, I. V. The Quantum Mechanical Calculations Evidence Molecular-Zwitterionic Features of Prototropic Tautomerism of Canonical Nucleotide Bases. 1. Pyrimidines. *Biopolimery i Kletka* **1996**, *12*, 42-48.

(53) Crespo-Hernandez, C. E.; Cohen, B.; Hare, P. M.; Kohler, B. Ultrafast Excited-State Dynamics in Nucleic Acids. *Chem. Rev.* **2004**, *104*, 1977-2019.

(54) Yoshikawa, A.; Matsika, S. Excited Electronic States and Photophysics of Uracil-Water Complexes. *Chem. Phys.* **2008**, *347*, 393-404.

(55) Yarasi, S.; Brost, P.; Loppnow, G. R. Initial Excited-State Structural Dynamics of Thymine are Coincident with the Expected Photochemical Dynamics. *J. Phys. Chem. A* **2007**, *111*. 5130-5135.

(56) Oraevsky, A. A.; Sharkov, A. V.; Nikogosyan, D. N. Picosecond Study of Electronically

Excited Singlet-States of Nucleic-Acid Components. *Chem. Phys. Lett.* **1981**, *83*, 276-280.

(57) Ballini, J. P.; Daniels, M.; Vigny, P. Wavelength-Resolved Lifetime Measurements of Emissions from DNA Components and Poly-RA at Room-Temperature Excited with Synchrotron Radiation. *J. Lumin.* **1982**, *27*, 389-400.

(58) Reuther, A.; Nikogosyan, D. N.; Laubereau, A. Primary Photochemical Processes in Thymine in Concentrated Aqueous Solution Studied by Femtosecond UV Spectroscopy. *J. Phys. Chem.* **1996**, *100*, 5570-5577.

(59) Reuther, A.; Iglev, H.; Laenen, R.; Laubereau, A. Femtosecond Photo-Ionization of Nucleic Acid Bases: Electronic Lifetimes and Electron Yields. *Chem. Phys. Lett.* **2000**, *325*, 360-368.

(60) Haupl, T.; Windolph, C.; Jochum, T.; Brede, O.; Hermann, R. Picosecond Fluorescence of Nucleic Acid Bases. *Chem. Phys. Lett.* **1997**, *280*, 520-524.

(61) Nikogosyan, D. N.; Oraevsky, A. A.; Letokhov, V. S.; Arbieva, Z. K.; Dobrov, E. N. 2-Step Picosecond UV Excitation of Polynucleotides and Energy-Transfer. *Chem. Phys.* **1985**, *97*, 31-42.

(62) Nikogosyan, D. N.; Angelov, D. A.; Oraevsky, A. A. Determination of Parameters of Excited-States of DNA and RNA Bases by Laser UV Photolysis. *Photochem. Photobiol.* **1982**, *35*, 627-635.

(63) Morsy, M. A.; Al-Somali, A. M.; Suwaiyan, A. Fluorescence of Thymine Tautomers at Room Temperature in Aqueous Solutions. *J. Phys. Chem. B* **1999**, *103*, 11205-11210.

(64) Nir, E.; Kleinermanns, K.; Grace, L.; de Vries, M. S. On the Photochemistry of Purine Nucleobases. *J. Phys.Chem. A* **2001**, *105*, 5106-5110.

(65) Middleton, C. T.; de La Harpe, K.; Su, C.; Law, Y. K.; Crespo-Hernandez, C. E.; Kohler, B. DNA Excited-State Dynamics: From Single Bases to the Double Helix. *Annu. Rev. Phys. Chem.*

2009, *60*, 217-239.

(66) Barbatti, M.; Aquino, A. J. A.; Szymczak, J. J.; Nachtigallova, D.; Hobza, P.; Lischka, H. Relaxation Mechanisms of UV-Photoexcited DNA and RNA Nucleobases. *Proc. Natl. Acad. Sci. U. S. A.* **2010**, *107*, 21453-21458.

(67) Pancur, T.; Schwalb, N. K.; Renth, F.; Temps, F. Femtosecond Fluorescence Up-Conversion Spectroscopy of Adenine and Adenosine: Experimental Evidence for the πσ* State? *Chem. Phys.* **2005**, *313*, 199-212.

(68) Gustavsson, T.; Sarkar, N.; Lazzarotto, E.; Markovitsi, D.; Improta, R. Singlet Excited State Dynamics of Uracil and Thymine Derivatives: A Femtosecond Fluorescence Up-conversion Study in Acetonitrile. *Chem. Phys. Lett.* **2006**, *429*, 551-557.

(69) Gustavsson, T.; Banyasz, A.; Lazzarotto, E.; Markovitsi, D.; Scalmani, G.; Frisch, M. J.; Barone, V.; Improta, R. Singlet Excited-State Behavior of Uracil and Thymine in Aqueous Solution: A Combined Experimental and Computational Study of 11 Uracil Derivatives. *J. Am. Chem. Soc.* **2006**, *128*, 607-619.

(70) Kwok, W.; Ma, C.; Phillips, D. L. Femtosecond Time- and Wavelength-Resolved Fluorescence and Absorption Spectroscopic Study of the Excited States of Adenosine and an Adenine Oligomer. *J. Am. Chem. Soc.* **2006**, *128*, 11894-11905.

(71) Merchan, M.; Gonzalez-Luque, R.; Climent, T.; Serrano-Andres, L.; Rodriuguez, E.; Reguero, M.; Pelaez, D. Unified Model for the Ultrafast Decay of Pyrimidine Nucleobases. *J. Phys. Chem. B* **2006**, *110*, 26471-26476.

(72) Hare, P. M.; Crespo-Hernandez, C. E.; Kohler, B. Internal Conversion to the Electronic Ground State Occurs Via Two Distinct Pathways for Pyrimidine Bases in Aqueous Solution. *Proc. Natl. Acad. Sci. U. S. A.* **2007**, *104*, 435-440.

(73) Crespo-Hernandez, C. E.; Kohler, B. Influence of Secondary Structure on Electronic Energy Relaxation in Adenine Homopolymers. *J. Phys. Chem. B* **2004**, *108*, 11182-11188.

(74) Buchvarov, I.; Wang, Q.; Raytchev, M.; Trifonov, A.; Fiebig, T. Electronic Energy Delocalization and Dissipation in Single- and Double-Stranded DNA. *Proc. Natl. Acad. Sci. U. S. A.* **2007**, *104*, 4794-4797.

(75) Kwok, W.; Ma, C.; Phillips, D. L. A Doorway State Leads to Photostability or Triplet Photodamage in Thymine DNA. *J. Am. Chem. Soc.* **2008**, *130*, 5131-5139.

(76) Sobolewski, A. L.; Domcke, W.; Dedonder-Lardeux, C.; Jouvet, C. Excited-State Hydrogen Detachment and Hydrogen Transfer Driven by Repulsive $^1\pi\sigma^*$ States: A New Paradigm for Nonradiative Decay in Aromatic Biomolecules. *Phys. Chem. Chem. Phys.* **2002**, *4*, 1093-1100.

(77) Schreier, W. J.; Schrader, T. E.; Koller, F. O.; Gilch, P.; Crespo-Hernandez, C. E.; Swaminathan, V. N.; Carell, T.; Zinth, W.; Kohler, B. Thymine Dimerization in DNA is an Ultrafast Photoreaction. *Science* **2007**, *315*, 625-629.

(78) Sun, S.; Brown, A. Simulation of the Resonance Raman Spectrum for Uracil. *J. Phys. Chem. A* **2014**, *118*, 9228-9238.

(79) Billinghurst, B. E.; Loppnow, G. R. Excited-State Structural Dynamics of Cytosine from Resonance Raman Spectroscopy. *J. Phys. Chem. A* **2006**, *110*, 2235-2359.

(80) El-Yazbi, A. F.; Palech, A.; Loppnow, G. R. Initial Excited-State Structural Dynamics of 2'-Deoxyguanosine Determined Via UV Resonance Raman Spectroscopy. *J. Phys. Chem. A* **2011**, *115*.

(81) Sasidharanpillai, S.; Loppnow, G. R. Initial Excited-State Structural Dynamics of 5,6-Dimethyluracil from Resonance Raman Spectroscopy. *J. Phys. Chem. A* **2014**, *118*, 4680-4687.

(82) Oladepo, S. A.; Loppnow, G. R. Initial Excited-State Structural Dynamics of 9-

Methyladenine from UV Resonance Raman Spectroscopy. *J. Phys. Chem. B* **2011**, *115*, 6149-6156.

(83) Crespo-Hernandez, C. E.; Cohen, B.; Hare, P. M.; Kohler, B. Ultrafast Excited-State Dynamics in Nucleic Acids. *Chem. Rev.* **2004**, *104*, 1977-2019.

(84) Li, M.; Liu, M.; Zhao, Y.; Pei, K.; Wang, H.; Zheng, X.; Fang, W. H. Excited State Structures and Decay Dynamics of 1,3-Dimethyluracils in Solutions: Resonance Raman and Quantum Mechanical Calculation Study. *J. Phys. Chem. B* **2013**, *117*, 11660-11669.

(85) Myers, A. B.; Mathies, R. A., Eds.; In *Biological applications of Raman spectroscopy;* Spiro, T. G., Ed.; Resonance Raman spectra of polyenes and aromatics; Wiley-Interscience: New York, 1987; Vol. 2, pp 1-58.

(86) Loppnow, G. R.; Mathies, R. A. Excited-State Structure and Isomerization Dynamics of the Retinal Chromophore in Rhodopsin from Resonance Raman Intensities. *Biophys. J.* **1988**, *54,* 35-43.

(87) Yarasi, S.; Brost, P.; Loppnow, G. R. Initial Excited-State Structural Dynamics of Thymine are Coincident with the Expected Photochemical Dynamics. *J. Phys. Chem. A* **2007**, *111*, 5130-5135.

(88) Billinghurst, B. E.; Yeung, R.; Loppnow, G. R. Excited-State Structural Dynamics of 5-Fluorouracil. *J. Phys. Chem. A* **2006**, *110*, 6185-6191.

Chapter 2

Mass-Tuned Initial Excited-state Structural Dynamics of DNA Nucleobases from UV Resonance Raman Spectroscopy: 5-Deuterouracil

2.1 Introduction

RNA and DNA contain the common nucleobases of adenine, cytosine, guanine, with uracil and thymine (Figure 2.1) being the fourth base in RNA and DNA, respectively. This distinction is strictly observed in biology with very few examples of uracil on DNA and thymine on RNA.[1,2] Because uracil and thymine exhibit surprisingly different photochemistry, this compositional difference has important consequences for the stability of the two nucleic acids in the presence of UV light; the primary photoproduct of UV irradiation of uracil is photoinduced addition of water to the C5=C6 double bond to form the photohydrate, while thymine forms cyclobutane photodimers (CPDs) via [2+2] cycloaddition reactions with neighboring nucleobases, primarily with other thymines.[3]

Previous work has shown that the excited-state electronic structure of uracil and thymine are very similar at the Franck-Condon geometry, but that the initial excited-state structural dynamics are quite different.[4-7] This difference has been attributed to the mass of the different substituents at C5.[5,6] In this Chapter, we test this model via UV resonance Raman and computational characterization of the initial excited-state structural dynamics of 5-deuterouracil (5-*d*-U, Figure 2.1) and show that its structural dynamics are qualitatively and quantitatively intermediate to those of uracil and thymine, as predicted by this model. Thus, the excited-state structural dynamics in the pyrimidine nucleobases can be tuned by the mass nature of the substituent at the C5 position.

---

*A version of this chapter has been published: Ng, S. S.; Teimoory, F.; Loppnow, G. R. *J. Phys. Chem. Lett.* **2011,** *2*, 2362-2365.

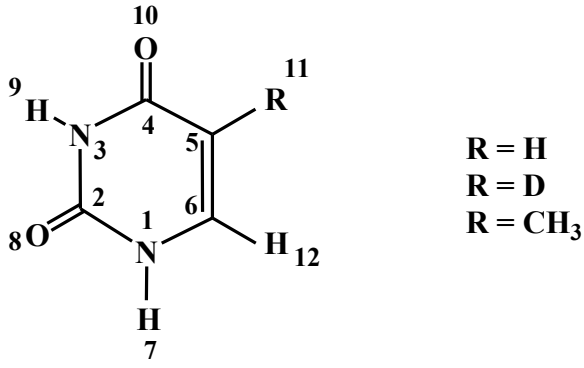

Figure 2.1 Structure of uracil and thymine nucleobases.

2.2 Experimental

UV resonance Raman spectra (Figures 2.2 and 2.3) were obtained of 2.4-3.6 mM aqueous (nanopure water, Barnsted, Boston, MA) solutions of 5-*d*-U (99%, C/D/N Isotopes, Pointe-Claire, Quebec) containing 0.3 M lithium sulfate (99%, EMD Chemicals Inc., Gibbstown, NJ) as an internal standard at excitation wavelengths throughout 5-*d*-U's 260 nm absorption band as previously described.[4-7] Typical laser powers were 5-15 mW. The addition of the internal standard had no noticeable effect on either the absorption or resonance Raman spectra. Spectral measurements and quantitative determinations of intensities were repeated on three freshly prepared samples of 5-*d*-U at each excitation wavelength. Absorption spectra (Hewlett-Packard, model 8452A, Sunnyvale, CA) acquired before and after each Raman measurement demonstrate photoalteration of less than 5% during resonance Raman spectral acquisition. Spectra were frequency calibrated, baseline-corrected, and corrected for spectrometer efficiency with a standard lamp as previously described.[4-9] Frequency calibration against standard solvents introduce errors of up to 5-10 cm^{-1}. Spectral peaks were integrated (Microcal Origin 7.0, Piscataway, NJ) to yield the peak intensities, which were converted into differential cross sections by using the following differential Raman cross sections for sulfate: 3.54 x 10^{-12}, 2.71 x 10^{-12}, 2.28 x 10^{-12}, 1.93 x 10^{-12}, and 1.49 x 10^{-12} $Å^2$ (molecule sr)$^{-1}$ at 244, 257, 266, 275, and 290 nm, respectively.[10]

Theory

The absorption spectrum and resonance Raman excitation profiles were simulated with the parameters in Table 2.1 and the time-dependent wave packet formalism of Eqs. 2.1 and 2.2

$$\sigma_A = \frac{4\pi\ E_L e^2 M^2}{6\hbar^2 cn} \int_0^\infty dE_0 H(E_0) \int_{-\infty}^{\infty} dt < i \mid i(t) > exp\left\{\ i\left(E_L + \varepsilon_i\right)\ t/\hbar\right\}\ G(t) \qquad (2.1)$$

$$\sigma_R = \frac{8\pi\ E_s^3 E_L e^4 M^4}{9\hbar^6 c^4} \int_0^\infty dE_0 H(E_0) \left| \int_0^\infty dt < f \mid i(t) > exp\left\{\ i\left(E_L + \varepsilon_i\right)\ t/\hbar\right\}\ G(t) \right|^2 \qquad (2.2)$$

where E_S and E_L are the scattered and incident photon energies, respectively.[10,11] M is the transition length, <i|i(t)> and <f|i(t)> denote the overlap of the initial and final vibrational state

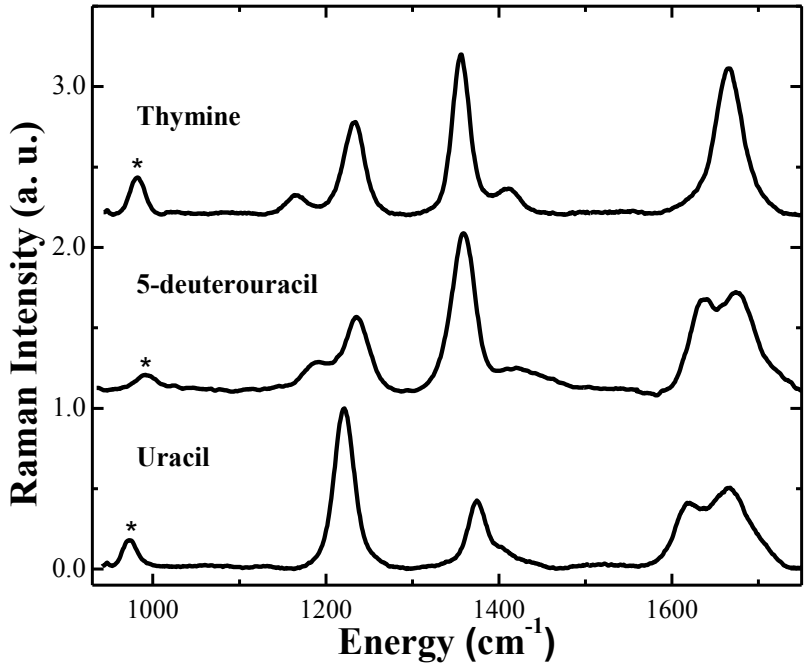

Figure 2.2 Resonance Raman spectra of 3 mM solutions of thymine, 5-*d*-U and uracil in water excited at 275 nm. Intensities have been normalized to the most intense peak in each spectrum. The bands due to the internal standard (0.3 M lithium sulfate for 5-*d*-U and 0.4 M sodium sulfate for thymine and uracil) are indicated by asterisks (*)

Table 2.1 Raman frequencies, excited-state PES slopes and assignments for 5-*d*-U.

Mode (cm^{-1})	Uracil β /ħ (cm^{-1})	Thymine β /ħ (cm^{-1})	5-*d*-U β /ħ (cm^{-1})	Mode Assignment
1666	1000	-	920	ν (C4O10) [71], ν (C4C5) [-9]
1629	490	820	730	ν (C5C6) [59], be(C6H12) [15], ν (N1C6) [-8]
1354	610	650	920	be(C6H12) [30], ν (N1C2) [-17], ν (C2N3) [16], ν (C5C6) [-15], be(C5D11) [-6], be(C2O8) [6]
1230	910	490	550	ν (C2N3) [23], be(C6H12) [-19], be(N1H7) [17], ν (N3C4) [-10], ν (N1C6) [-9], ν (C4C5) [6]
1187	100	260	330	ν (N3C4) [29], ν (N1C6) [-25], be(C4O10) [-10], ν (N1C2) [9], ν (C2N3) [-8], ν (C4C5) [-6]

Mode wavenumbers are the experimentally determined wavenumbers for 5-*d*-U. Excited-state PES slopes (β/ħ) in cm^{-1} were obtained by fitting Eqs. 2.1 and 2.2 with the following parameters: temperature $T = 298$ K, Brownian oscillator line shape $\kappa = \Lambda/D = 0.1$, Gaussian homogeneous linewidth $\Gamma_G = 1300$ cm^{-1}, inhomogeneous linewidth $\theta = 975$ cm^{-1}, zero-zero energy $E_0 = 36575$ cm^{-1} and transition length $M = 0.67$ Å. The "-" indicates the mode was not observed. Values for β/ħ for uracil and thymine are taken from references 5 and 4, respectively. Mode assignments are from Gaussian09 computations and GAR2PED decomposition into internal coordinates. Potential energy distributions (PEDs) in % are shown in square brackets and the sign indicates the phase. For these assignments, ν = stretch and be = bend. Only internal coordinates with PEDs > 5% are shown. The definition of the Ring def. coordinates is shown in Table A of Appendix.

wave functions with the intermediate wavefunction, respectively, ν_i is the energy of the initial vibrational state, E_0 is the energy difference between the lowest vibrational levels of the ground and excited electronic state, G(t) is a homogeneous linewidth function encompassing the decay of the excited state and $H(E_0)$ is the inhomogeneous linewidth function accounting for the broadening of peaks due to differences in the environment of individual molecules. Within the separable harmonic oscillator approximation, the <i|i(t)> and <f|i(t)> overlaps are sensitive to the excited-state potential energy surface slope ($\beta/\hbar$) along each normal mode. As such, the absorption and resonance Raman cross sections are directly related and provide complementary information, though through different mathematical implications. The implementation of these equations have been described previously.[4-6, 10, 11, 13-18]

2.3 Results

In assessing the spectra of 5-*d*-U, thymine and uracil (Figure 2.2), it is immediately apparent that the 5-*d*-U spectrum has similar features to those found in both nucleobases. 5-Deuterouracil has a shoulder at 1187 cm^{-1} that is similar to the small peak in thymine at 1186 cm^{-1} and the ratio of the 1230 and 1354 cm^{-1} peaks has a greater resemblance to the corresponding peaks in thymine than uracil. However, 5-*d*-U has a weaker shoulder at 1400 cm^{-1} than thymine and two peaks between 1600 and 1700 cm^{-1}, more similar to uracil than thymine.

Five vibrational bands are observed between 1100 and 1800 cm^{-1} (Table 2.1). To assign the vibrational modes, DFT calculations at the B3LYP/6-311G(d,p) level of theory using the default gradients implemented in the Gaussian09 package were performed on the initial planar, C_s structures of uracil in the diketo tautomer form. To calculate the isotope effect on the frequencies of uracil, a single point calculation was performed on the optimized structure with the addition al replacement of the natural abundance mass with the isotopic mass of 2 for deuterium at the substituent at C5.[5, 7, 8] The calculated frequencies were not scaled. GAR2PED was used to construct the set of non-redundant symmetry coordinates of 5-*d*-U as well as to determine the normal modes and potential energy distributions (PEDs) in terms of these symmetry coordinates (Table 2.1).[9] From highest wavenumber to lowest, the 5 most intense vibrations of 5-*d*-U are the

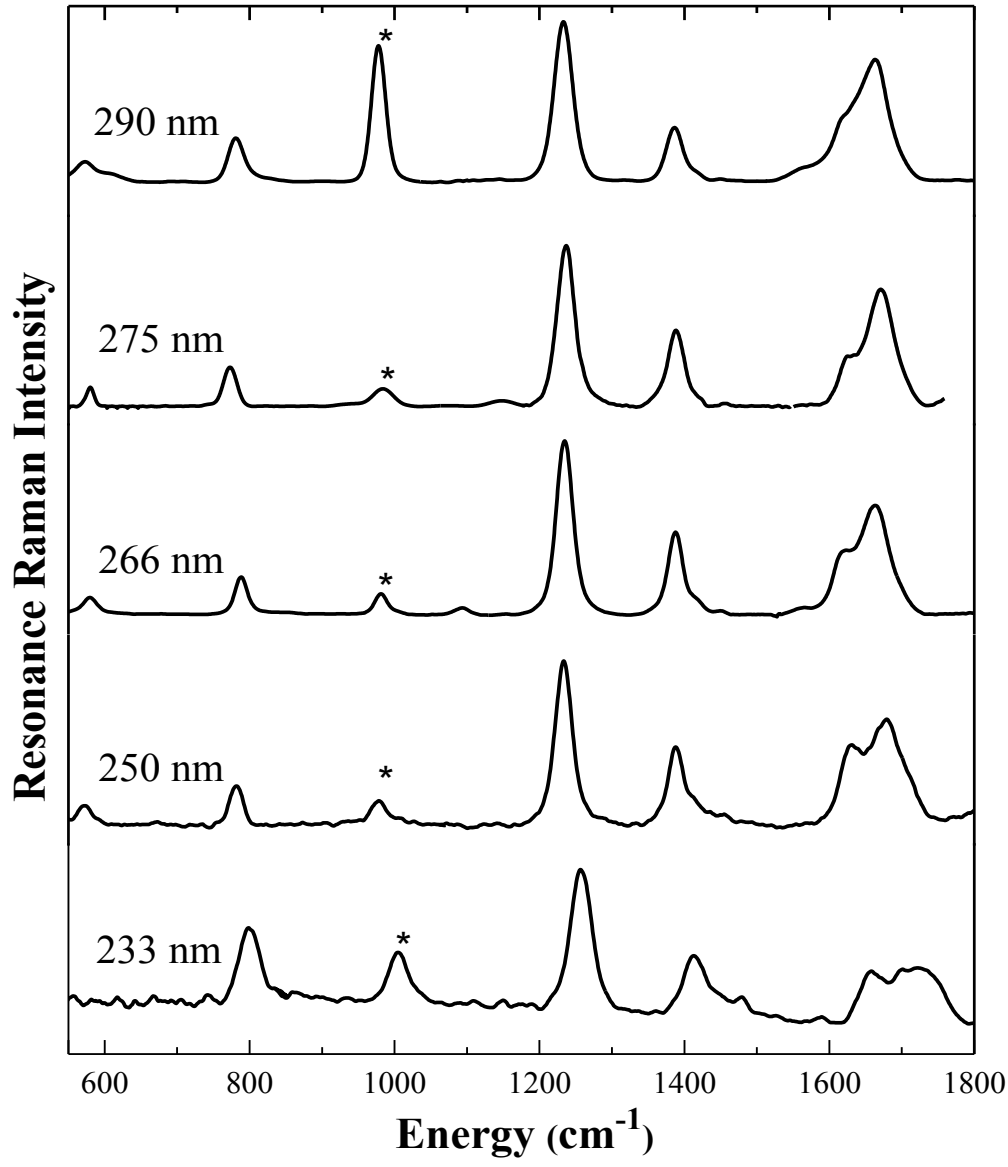

Figure 2.3 Resonance Raman spectra of 2.4-3.6 mM solutions of 5-*d*-U containing 0.3 M lithium sulfate as an internal standard at excitation wavelengths throughout its ca. 260 nm absorption band. The bands due to the internal standard are indicated by asterisks (*).

C4=O stretch, the C5=C6 stretch, a C6H deformation, a ring stretch and a ring breathing vibration.

The absorption spectrum and resonance Raman excitation profiles of 5-*d*-U are shown in Figures 2.3 and 2.4. Discrepancies between the simulated and experimental absorption spectra above 38,000 cm^{-1} are attributed to higher energy electronic transitions, which are not modeled here. The agreement between experimental and calculated absorption and resonance Raman differential cross sections is good and indicates an accurate characterization of the initial excited-state structural dynamics of 5-*d*-U.

2.4 Discussion

The resonance Raman spectrum of 5-*d*-U is found to be intermediate between that of thymine and uracil, supporting the hypothesis that the substituent on the C_5 position heavily influences the excited-state structural dynamics. Subsequent analysis of the resonance Raman spectra yields the excited-state potential energy slopes at the Franck-Condon geometry along each normal coordinate (Table 2.1). To quantitatively compare the initial excited-state structural dynamics of uracil, 5-*d*-U, and thymine, their potential energy slopes are collected in Table 2.1.

As Table 2.1 shows, the initial excited-state structural dynamics of 5-*d*-U lie quantitatively intermediate between those of uracil and thymine, indicating that the mass of the substituent at C5 dictates the excited-state dynamics near the Franck-Condon region. For example, the 1629 cm^{-1}/1666 cm^{-1} mode slope ratio, discriminating photochemically related bond lengthening of the C5=C6 double bond from a non-photochemical carbonyl bond lengthening, are 0.5, 0.8 and undefined (∞) for uracil, 5-*d*-U and thymine, respectively, indicating 5-*d*-U shows more relative motion in the excited-state along the photochemical C5=C6 bond-lengthening motion than uracil does, but not as much as thymine.

Similar intermediate behavior can be observed for the 1629 cm^{-1}/1230 cm^{-1} mode excited-state slope ratio, discriminating between C5=C6 bond lengthening related to CPD formation and C5, C6 pyramidalization related to photohydrate formation, which are 0.54, 1.3 and 1.7 for uracil, 5-*d*-U and thymine, respectively, indicating that the 5-*d*-U has more relative C5=C6 bond lengthen-

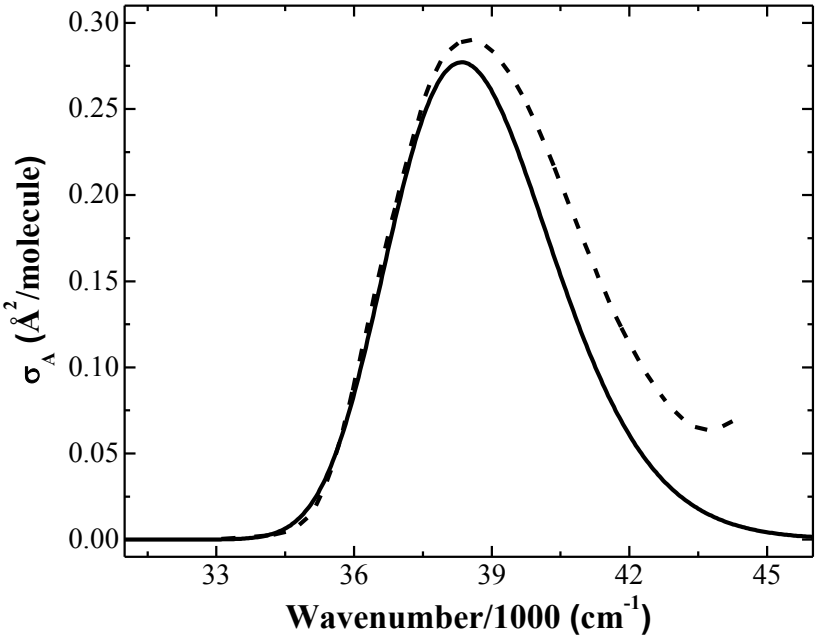

Figure 2.4 Experimental (dashed line) and simulated (solid line) absorption spectra of 5-*d*-U. The absorption spectrum was calculated using Eq. 2.2 and the parameters in Table 2.1.

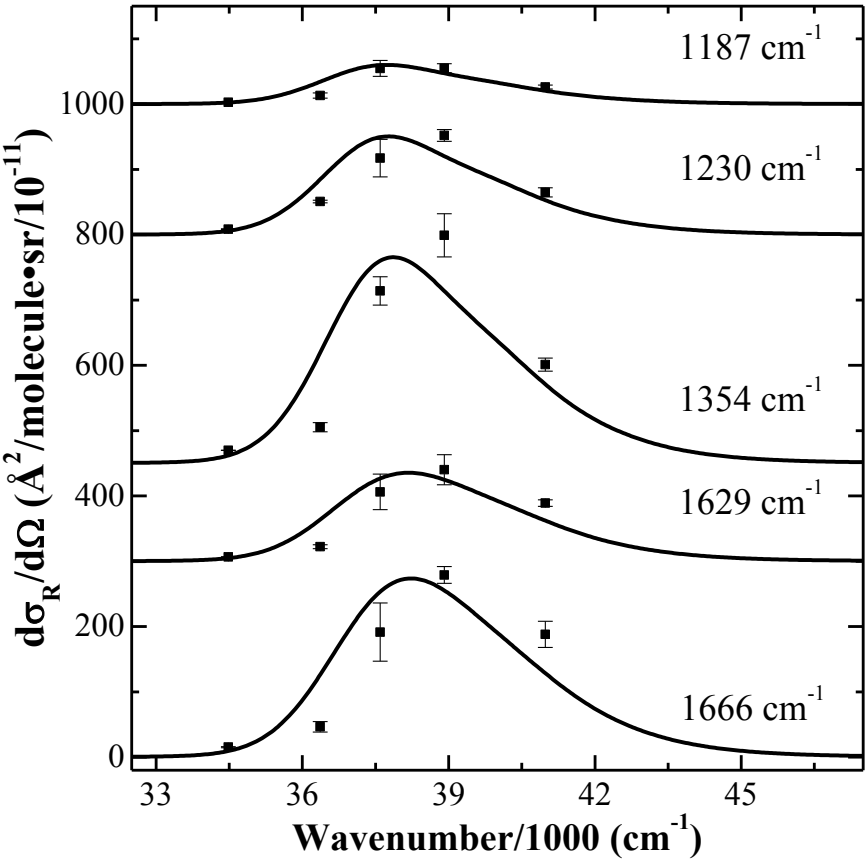

Figure 2.5 Experimental (points) and calculated (solid line) resonance Raman excitation profiles of 5-*d*-U. The excitation profiles were calculated using Eq. 2.1 and the parameters in Table 2.1. The excitation profiles have been offset along the ordinate for increased clarity of presentation. Error bars are on the order of the point size.

-ing compared to uracil. However, the intermediate behavior of 5-*d*-U is less clear when the 1629 cm^{-1}/1354 cm^{-1} ratio is calculated. For this ratio, values of 0.80, 0.79 and 1.26 are obtained for uracil, 5-*d*-U and thymine, respectively. Thus, the molecular motions may be more complex than a simple partitioning between bond lengthening and pyramidalization coordinates.

2.5 Conclusion

The results presented here demonstrate that the mass of the C5 substituent on uracil-like pyrimidine nucleobases determines their initial excited-state structural dynamics. Similar results have been observed for 5-fluorouracil and other 5-substituted halouracils, indicating that this model is relatively independent of the nature of the C5 substituent.[6] The initial excited-state structural dynamics are significant in determining the photochemistry of the nucleobases due to their rapid excited-state relaxation times.[12-15] Although the photochemistry of any molecular system is determined not only by the initial excited-state structural dynamics, but also by the "later" dynamics on both the excited- and ground-state potential energy surfaces, by the location and nature of state crossings, and by the nature of the initial excited electronic state, the results presented here provide a clear discrimination of pathways based on the mass of the C5 substituent.

2.6 References

(1) el-Hajj, H. H.; Wang, L.; Weiss, B. Multiple Mutant of Escherichia Coli Synthesizing Virtually Thymineless DNA during Limited Growth. *J. Bacteriol.* **1992**, *174*, 4450-4456.

(2) Duncan, B. K.; Warner, H. R. Metabolism of Uracil-containing DNA: Degradation of Bacteriophage PBS2 DNA in Bacillus Subtilis. *J. Virol.* **1977**, *22*, 835-838.

(3) Ruzsicska, B. P.; Lemaire, D. G. E. DNA photochemistry. In *CRC Handbook of Organic Photochemistry and Photobiology;* Horspool, W. H.; Song, P.-S., Eds.; CRC Press: New York, 1995; pp 1289-1317.

(4) Yarasi, S.; Brost, P.; Loppnow, G. R. Initial Excited-State Structural Dynamics of Thymine are Coincident with the Expected Photochemical Dynamics. *J. Phys. Chem. A* **2007**, *111*, 5130-

5135.

(5) Yarasi, S.; Ng, S.; Loppnow, G. R. Initial Excited-State Structural Dynamics of Uracil from Resonance Raman Spectroscopy are Different from Those of Thymine (5-Methyluracil). *J. Phys. Chem. B* **2009**, *113*, 14336-14342.

(6) Billinghurst, B. E.; Yeung, R.; Loppnow, G. R. Excited-State Structural Dynamics of 5-Fluorouracil. *J. Phys. Chem. A* **2006**, *110*, 6185-6191.

(7) Yarasi, S.; Loppnow, G. R. Vibrational Properties of Thymine, Uracil and Their Isotopomers. *J. Raman Spectrosc.* **2007**, *38*, 1117-1126.

(8) Frisch, M. J.; Trucks, G. W.; Schlegel, H. B.; Scuseria, G. E.; Robb, M. A.; Cheeseman, J. R.; Scalmani, G.; Barone, V.; Mennucci, B.; Petersson, G. A.; et al. In Gaussian 09; revision B.01.2009; Gaussian, Inc.:Wallingford,: CT, 2010.

(9) Martin, J. M. L.; Van Alsenoy, C. In GAR2PED; University of Antwerp: Antwerp: The Netherlands, 1995.

(10) Lee, S. Y.; Heller, E.J. Time-Dependent Theory of Raman Scattering. *J. Chem. Phys.* 1979, 71, 4777-4788.

(11) Myers, A.B. Excited Electronic State Properties from Ground-state Resonance Raman Intensities. In *Laser Techniques in Chemistry* Myers, A.B.; Rizzo, T.R.; Eds.; Wiley: New York, 1995; pp 325-384.

(12) Kang, H.; Taek Lee, K.; Jung, B; Jae Ko, Y.; Keun Kim, S. Intrinsic Lifetimes of the Excited State of DNA and RNA Bases. *J. Am. Chem. Soc.* **2002**, *124*, 12958-12959.

(13) He, Y.; Wu, C.; Kong, W. Decay Pathways of Thymine and Methyl-Substituted Uracil and Thymine in the Gas Phase. *J. Phys. Chem. A* **2003**, *107*, 5145-5148.

(14) Gustavsson, T.; Banyasz, A.; Sarkar, N.; Markovitsi, D.; Improta, R. Assessing Solvent Effects on the Singlet Excited State Lifetime of Uracil Derivatives: A Femtosecond Fluorescence Upconversion study in Alcohols and D_2O. *Chem. Phys.* **2008**, *350*, 186-192.

(15) Schreier, W.J.; Schrader, T.E.; Koller, F.O.; Gilch, P.; Crespo-Hernandez, C.E.; Swaminathan, V.N.; Carell, T.; Zinth, W.; Kohler, B. Thymine Dimerization in DNA is an Ultrafast Photoreaction. *Science* **2007**, *315*, 625-629.

(16) Billinghurst, B. E.; Loppnow, G. R. Excited-State Structural Dynamics of Cytosine from Resonance Raman Spectroscopy. *J. Phys. Chem. A* **2006**, *110*, 2353-2359.

(17) Oladepo, S. A.; Loppnow, G. R. Initial Excited-State Structural Dynamics of 9-Methyladenine from UV Resonance Raman Spectroscopy. *J. Phys. Chem. B* **2011**, *115,* 6149-6156.

(18) El-Yazbi, A. F.; Palech, A.; Loppnow, G. R. Initial Excited-state Structural Dynamics of 2'-deoxyguanosine from UV Resonance Raman Spectroscopy. *J. Phys. Chem. A* **2011,** *115*, 10445-10451.

Chapter 3

Initial Excited-state Structural Dynamics of 6-Substituted Uracil Derivatives: Femtosecond Angle and Bond Lengthening Dynamics in Pyrimidine Nucleobase Photochemistry

3.1 Introduction

DNA and RNA are polymers of nucleotides and have the functions of storing genetic information and regulating gene expression, respectively. Their chemical composition is similar, except for the sugars which make up the sugar-phosphate backbone and for one of the four nucleobases. For the latter difference, uracil is found exclusively in RNA, while thymine (5-methyluracil) is found exclusively in DNA (Figure 3.1). Despite the very similar structure between uracil and thymine- the only difference is the replacement of a hydrogen on C5 in uracil by a methyl group in thymine - the photochemistry is very different. The photohydrate is the major photoproduct of uracil induced by UV irradiation, while the cyclobutyl photodimer (CPD) is the major photoproduct of thymine.[1]

To understand the determinants of such a difference in photochemical reactivity for this difference in structure, a probe of the initial excited-state structural dynamics is needed. However, uracil and thymine have sub-picosecond excited-state lifetimes, and sufficient probes of structural dynamics on that timescale are rare.[2,3] Resonance Raman intensities can yield initial excited-state structural dynamics and have shown that uracil and thymine have different molecular structural changes within the first few tens of femtoseconds after excitation; thymine appears to undergo

[*]A version of this chapter has been published: Teimoory, F.; Loppnow, G. R. *J. Phys. Chem. B* **2014,** *118*, 12161–12167.

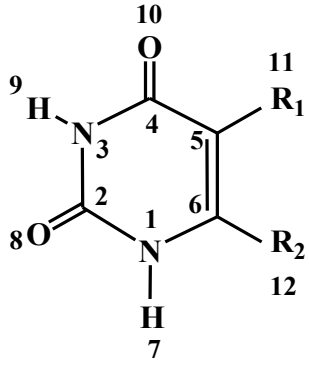

R_1	R_2	Compound
H	H	uracil
D	H	5-deuterouracil (5-*d*-U)
H	D	6-deuterouracil (6-*d*-U)
D	D	5,6-dideuterouracil (5,6-d_2-U)
CH_3	H	5-methyluracil (5-MeU or thymine)
H	CH_3	6-methyluracil (6-MeU)
CH_3	CH_3	5,6-dimethyluracil (5,6-Me_2U)

Figure 3.1 Structures of the C5 and C6 substituted uracil derivatives

more C5-C6 bond lengthening, while uracil undergoes more delocalized motions and more C5X and C6X bending.[4-7] The differences in the structural dynamics appear to be correlated with the mass of the substituent on C5, one of the carbons at the photochemical site.[6,7] The C5 mass effect on the initial excited-state structural dynamics was confirmed previously by self-consistently simulating the resonance Raman excitation profiles and the absorption spectra of 5-deuterouracil (discussed in Chapter 2) and 5-fluorouracil.[8] The latter shows similar initial excited-state structural dynamics as thymine, while 5-deuterouracil, as discussed in Chapter 2, shows intermediate initial excited-state structural dynamics between uracil and thymine, as the model predicted.[8]

In this Chapter, we measure the resonance Raman-derived initial excited-state structural dynamics for a uracil derivative in which the substituent on C6 (Figure 3.2), the other carbon at the photochemical site (C5C6), is changed to each of a methyl group (6-MeU) and a deuterium (6-*d*-U) in order to better understand the role of substituents on the uracil ring in determining nucleobase photochemistry. The reorganization energies of the photochemical active internal coordinates indicate that the initial excited-state structural dynamics of the C5C6 stretching internal coordinate remains the same upon methylation at either the C5 or C6 position.[5, 9] Lesser excited-state structural dynamics along the C5X and C6X in-plane bends are observed upon heavy-group substitution in 6-MeU, 6-*d*-U and even 5-*d*-U. In contrast, 5-MeU (T) exhibits much higher initial excited-state structural dynamics along the C5X and C6X in-plane bends. These results will be discussed to develop a clearer model of pyrimidine nucleobase photochemistry from ground-state structural differences and excited-state structural dynamics.

3.2 Experimental

Solutions of 6-deuterouracil (6-*d*-U, 99%, C/D/N isotopes, Pointe-Claire, Quebec) and 6-methyluracil (6-MeU, 97%, Sigma-Aldrich Canada Ltd., Oakville, Ontario) were dissolved in nanopure water obtained from a Barnstead (Boston, MA) water filtration system. The 3 mM solutions of 6-*d*-U and 6-MeU contained 0.3 M lithium sulfate (99%, EMD Chemicals Inc., Gibbstown, NJ) as an internal standard. The lithium sulfate did not noticeably affect either the

absorption or resonance Raman spectra of 6-*d*-U and 6-MeU.

UV resonance Raman spectra of both solutions were obtained at excitation wavelengths of 250, 257, 266, and 275 nm with laser powers of 4-12 mW, as previously described.[6,8,10,11] Spectral slit widths were 5-7 cm^{-1}. The resonance Raman spectra were obtained using three fresh 6-*d*-U and 6-MeU samples at each excitation wavelengths. Absorption spectra (Hewlett-Packard, model 8452A, Sunnyvale, CA) taken before and after each Raman spectrum confirm that the bulk photoalteration parameter is less than 5%.[12]

Theory

The resonance Raman intensities of 6-*d*-U and 6-MeU were obtained by integrating the spectral peaks and converting them into absolute cross sections, as described previously.[6,7,8,11,13] We have also determined the differential resonance Raman cross sections, $d\sigma/d\Omega$, from the relative integrated intensities as described previously.[13-15] The experimental differential cross sections of sulfate were found to be 3.30×10^{-12}, 2.87×10^{-12}, 2.42×10^{-12}, and 2.05×10^{-12} $Å^2$ $molecule^{-1}$ sr^{-1} at 250, 257, 266, and 275 nm, respectively.[11,12,15]

The absorption spectra and resonance Raman excitation profiles were simulated with the time-dependent wave packet propagation formalism[4]

$$\sigma_A = \frac{4\pi\ E_L e^2 M^2}{6\hbar^2 cn} \int_0^\infty dE_0 H(E_0) \left| \int_{-\infty}^{\infty} dt < i \mid i(t) > exp\left\{ i\left(E_L + \varepsilon_i\right)\ t/\hbar \right\} G(t) \right| \qquad (3.1)$$

$$\sigma_R = \frac{8\pi\ E_S^3 E_L e^4 M^4}{9\hbar^6 c^4} \int_0^\infty dE_0 H(E_0) \left| \int_0^\infty dt < f \mid i(t) > exp\left\{ i\left(E_L + \varepsilon_i\right)\ t/\hbar \right\} G(t) \right|^2 \qquad (3.2)$$

where M is the transition length, n is the refractive index, E_L is the excitation wavelength and E_S is the scattered wavelength in the Raman process, ε_i is the energy of the initial vibrational state, $|i\rangle$ and $|f\rangle$ are the initial and final vibrational wave functions in the Raman process, respectively, $|i(t)\rangle$ is the initial ground-state vibrational wave function propagated on the excited-state potential energy surface. Within the separable harmonic oscillator approximation, the $\langle i|i(t)\rangle$ and $\langle f|i(t)\rangle$ overlaps are significantly sensitive only to the excited-state potential energy surface slope ($\beta/\hbar$) at the Franck-Condon geometry along each normal mode, where $\beta/\hbar = \Delta\nu$ and Δ is the difference in

ground- and excited-state equilibrium geometries along each normal mode (ν). Therefore, the resonance Raman intensities directly reflect the initial structural dynamics of the excited state. G(t) is the homogeneous line width function and it represents the dynamics of the chromophore-solvent coupling for molecules interacting with a bath. The solute-solvent interactions that contribute to the solvent-induced homogeneous broadening are modeled using the Brownian oscillator model developed by Mukamel and co-workers.[16] $H(E_0)$ is a normalized Gaussian distribution of zero-zero energies around an average energy ($\bar{E}_0$) expressed as,

$$H(E_0) = (2\pi)^{-1/2}\theta^{-1}\int_0^{\infty} dE_0 exp\left\{\frac{-(E_0 - \bar{E}_0)^2}{2\theta^2}\right\}^{a} \qquad (3.3)$$

where θ is the standard deviation of the distribution. The parameters are optimized iteratively to obtain the best fit between the resonance Raman excitation profiles and experiment. The general implementation of these equations for absorption and resonance Raman spectroscopy have been described in detail previously.[4-13, 15, 16]

The vibrational mode assignments described in Tables 3.1 and 3.2 were obtained by DFT computation at the B3LYP/6-311G(d,p) level of theory, with the default gradients implemented in the Gaussian09 package performed on the initial planar C_s structures of uracil and 6-MeU in the diketo tautomer form.[17] The isotope effect was calculated for 6-*d*-U from the uracil frequencies, which are not scaled. A single-point calculation was used on the optimized uracil structure by replacing natural abundance mass H with the isotopic mass of 2 for deuterium at the C6 substituent. The set of non-redundant symmetry coordinates of 6-*d*-U were constructed by GAR2PED.[19]

Table 3.1 Harmonic mode parameters of 6-deuterouracil[a]

Mode (cm^{-1})	Assignment[b] (PED%)	β/ħ (cm^{-1})
580	γ(N3H9) [88]	144
786	γ(C5H11) [66], γ(C6D12) [16], Ring def 4 [7], γ(C4O10) [-5]	204
1235	be(C5H11) [45], be(N1H7) [-17], be(C6D12) [-8], ν(C2N3) [-7], ν(N1C2) [6]	469
1337	ν(C2N3) [20], ν(N1C2) [-15], ν(C4C5) [-10], be(C4O10) [-9], be(C2O8) [9], Ring def. 3 [8], be(N1H7) [-8], ν(N3C4) [5]	214
1410	be(N1H7) [44], ν(N1C6) [26], ν(C2O8) [-9]	212
1606	ν(C5C6) [64], ν(N1C6) [-10], be(C6D12) [6]	434
1667	ν(C4O10) [69], ν(C4C5) [-9], Ring def. 2 [5]	533

[a] Wavenumbers listed are the experimental wavenumbers of 6-*d*-U. Fitting the absorption spectra and excitation profiles in Figures 3.2 and 3.3 with Eqs. 3.1 and 3.2, respectively, provided displacements (Δ) in dimensionless normal coordinates and the following parameters: temperature T = 298 K, Brownian oscillator line shape $\kappa = \Lambda/D = 0.1$, Gaussian homogeneous line width Γ_G =1020 cm^{-1}, inhomogeneous line width θ = 1220 cm^{-1}, zero-zero energy E_0 = 37350 cm^{-1}, and transition length M = 0.58 Å. The estimated errors in the parameters used in the calculation are as follows: zero-zero energy (E_0) ±1%, transition length (M) ±1%, homogeneous line width (Γ) ±5%, inhomogeneous line width (θ) ±5%, and displacements ±5%. [b]Mode assignments are obtained by Gaussian09 computations and GAR2PED decomposition into internal coordinates. Potential energy distributions (PEDs) of the listed internal coordinate(s) in % are shown in square brackets. Only the internal coordinates with PEDs > 5% are reported. The sign indicates the phase of the internal coordinate. Abbreviations: ν, stretch; be, bend; def., deformation; γ**,** out-of-plane torsion. The definition of the Ring def. coordinates is shown in Table A of Appendix.

Table 3.2 Harmonic mode parameters of 6-methyluracil[a]

Mode (cm^{-1})	Assignment[b] (PED%)	$\beta/\hbar$ (cm^{-1})
520	Ring def. 2 [54] , Ring def. 3 [-30]	140
550	γ(C6C12) [28] , γ(N1H7) [21] , γ(C2N3) [11] , Ring def. 6 [10] , γ(C4O10) [9] , γ(C5H11) [8]	140
605	be(C2O8) [35] , be(C4H10) [35] , be(C6H12) [-14]	160
657	γ(C2N3) [75] , γ(C6H12) [-8] , Ring def. 4 [-7]	110
1235	be(C5H11) [22] , ν(C2N3) [17] , ν(N3C4) [-17] , ν(N1C2) [-9] , ν(C4C5) [8]	590
1361	be(C5H11) [34] , be(N1H7) [-26] , ν(C2N3) [-7] , ν(N1C2) [6]	180
1397	ν(C2N3) [21] , ν(N1C2) [-11] , be(C2N3) [10] , be(C4O10) [-8] , Ring def. 3 [8] , ν(C4O10) [-8] , ν(C4C5) [-8] , ν(C2O8) [6]	410
1660	ν(C5C6) [60] , ν(C6C12) [-6]	850

[a]Wavenumbers listed are the experimental wavenumbers of 6-MeU. Fitting the absorption spectra and excitation profiles in Figures. 3.2 and 3.3 with Eqs. 3.1 and 3.2, respectively, provided displacements (Δ) in dimensionless normal coordinates and the following parameters: temperature T = 298 K, Brownian oscillator line shape $\kappa = \Lambda/D = 0.1$, Gaussian homogeneous line width Γ_G =1470 cm^{-1}, inhomogeneous line width θ = 1040 cm^{-1}, zero-zero energy E_0 = 36700 cm^{-1}, and transition length M = 0.72 Å. The estimated errors in the parameters used in the calculation are as follows: zero-zero energy (E_0) ±1%, transition length (M) ±1%, homogeneous line width (Γ) ±5%, inhomogeneous line width (θ) ±5%, and displacements ±5%. [b]Mode assignments are from Gaussian09 computations and GAR2PED decomposition into internal coordinates. Potential energy distributions (PEDs) of the listed internal coordinate(s) in % are shown in square brackets. Only the internal coordinates with PEDs > 5% are reported. The sign indicates the phase of the internal coordinate. Abbreviations: ν, stretch; be, bend; def., deformation; γ**,** out-of-plane torsion. The definition of the Ring def coordinates is shown in Table A of Appendix.

3.3 Results

Figure 3.2 shows the UV resonance Raman spectra of 6-*d*-U and 6-MeU excited at 266 nm. The 6-MeU resonance Raman spectrum exhibits intense modes assigned to the C5C6 stretch at 1660 cm^{-1}, ring breathing at 1397 cm^{-1} and the C5H bend at 1235 cm^{-1}. The resonance Raman spectrum of 6-*d*-U is also shown in Figure 3.2, in which the most intense modes are the C4O10 stretch at 1667 cm^{-1}, the C5C6 stretch at 1606 cm^{-1}, the ring breathing at 1337 cm^{-1} and the C5H bend at 1235 cm^{-1}. Figures 3.3 and 3.4 show the resonance Raman spectra of 6-*d*-U and 6-MeU, respectively, as a function of excitation wavelength. They show no frequency shift or relative intensity change, which indicates that the resonance Raman spectra are enhanced by a single electronic transition.

Figure 3.5 shows the experimental and calculated absorption spectra of 6-*d*-U (A) and 6-MeU (B). Deviations observed at energies greater than 38,000 cm^{-1} between the experimental and calculated absorption spectra (Figure 3.5) are due to transitions to higher electronic excited states that were not modeled here (vide infra). The resonance Raman profiles of both 6-*d*-U and 6-MeU are shown in Figure 3.6, that indicate a good fit between experimental and simulated profiles of each peak in all the four excitation wavelengths. As all of the simulated absorption and resonance Raman profiles are obtained by one set of harmonic parameters, the best resulting fit was obtained through these specific parameters (Tables 3.1 and 3.2). A poorer fit is observed in 1235 cm^{-1} of 6-*d*-U and 6-MeU. Generally, a Guassian shape is expected for the experimental resonance Raman excitation profile. However, an unexpectedly upward trend is observed in the 1235 cm^{-1} mode, which causes a poorer fit on the calculated and experimental resonance Raman excitation profiles of this normal mode. The shape of this resonance Raman cross section excitation profile may be due to resonance with the higher electronic transition.

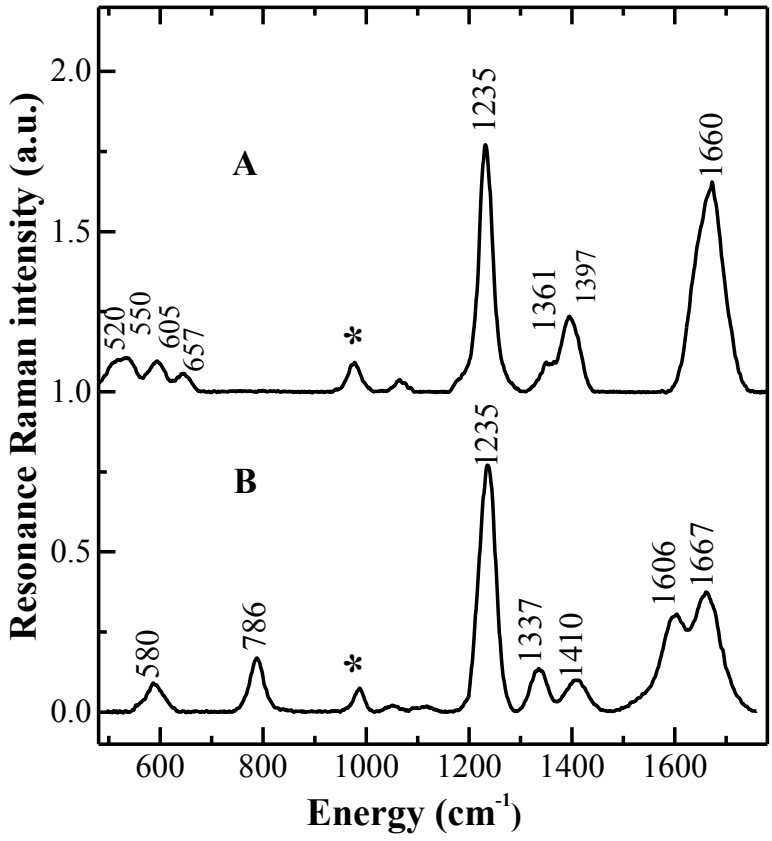

Figure 3.2 Resonance Raman spectra of ca. 3 mM 6-MeU (A) and 6-*d*-U (B) in water excited at 266 nm. The asterisk (*) indicates the 0.3 M sulfate internal standard peak. Each spectrum is the sum of 3-9 scans. The spectrum in A has been offset along the y-axis for clarity.

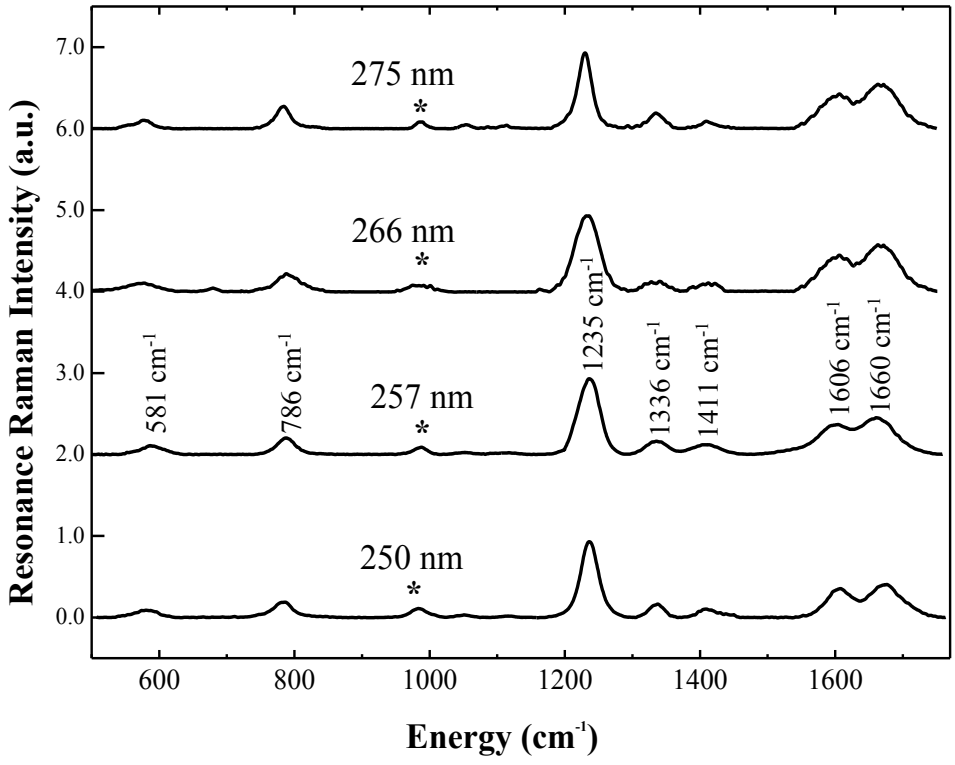

Figure 3.3 Resonance Raman spectra of 3 mM solutions of 6-*d*-U containing 0.3 M lithium sulfate as internal standard at excitation wavelengths throughout its ~260 nm absorption band. The bands due to the internal standard are indicated by asterisks (*). The spectra all have been scaled by the most intense peak and are offset along the y axis for clarity.

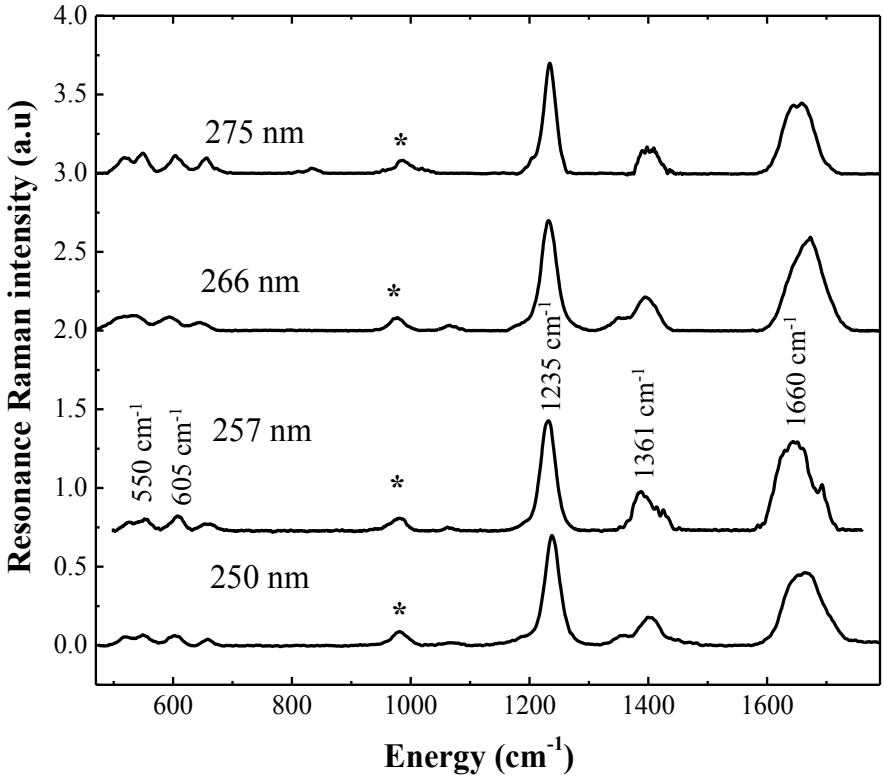

Figure 3.4 Resonance Raman spectra of 3 mM solutions of 6-MeU containing 0.3 M lithium sulfate as internal standard at excitation wavelengths throughout its ~260 nm absorption band. The bands due to the internal standard are indicated by asterisks (*). The spectra all have been scaled by the most intense peak and are offset along the y axis for clarity.

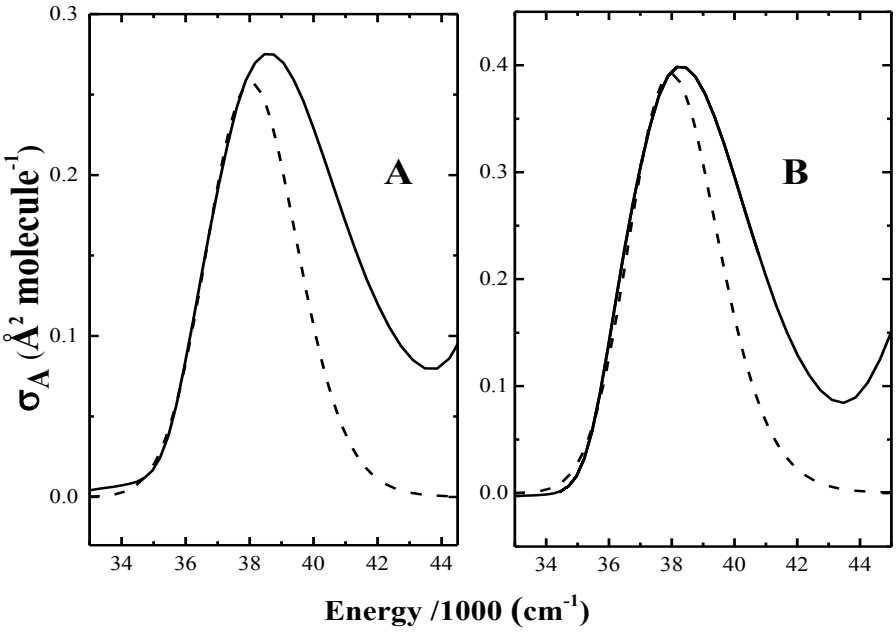

Figure 3.5 Experimental (solid line) and simulated (dashed line) absorption spectra of 6-*d*-U (A) and 6-MeU (B). The simulated absorption spectra were obtained by using Eq. 3.1 and the parameters in Tables 3.1 and 3.2, respectively.

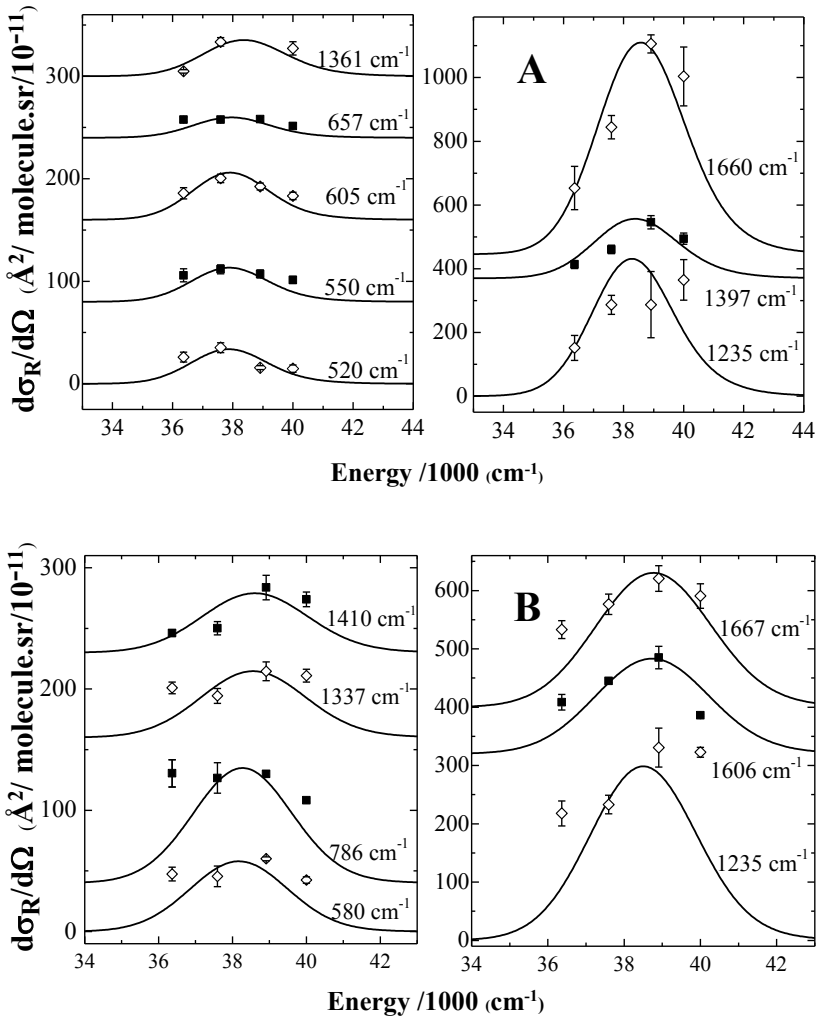

Figure 3.6 Experimental (points) and calculated (solid line) resonance Raman excitation profiles of 6-MeU (A) and 6-*d*-U (B). The excitation profiles were calculated with Eq. 3.2 using the parameters in Tables 3.1 and 3.2, respectively. The excitation profiles were offset along the ordinate for greater clarity of presentation.

Figure 3.7 shows the comparison of the resonance Raman spectra of uracil and its C5 and C6 deuterated and methylated derivatives, in which a gradual change in spectral properties (relative intensities, number of peaks and peak frequencies) is observed. In general, the resonance Raman spectrum is changed more when a heavier substituent (deuterium or CH_3 group) is positioned on C5 than when it is on C6. 5-MeU (T) displays more change in the resonance Raman spectrum than 6-MeU, in comparison to uracil. By increasing the mass of the C5 substituent, a gradual rise is observed in the intensity of the 1397 cm^{-1} peak attributed to the ring breathing (stretch) and a gradual drop is observed in the intensity of the 1235 cm^{-1} peak attributed to the C5H bend. However, a general resemblance is observed on the relative peak intensities of uracil and both the C6 substituted derivatives (Figure 3.7 (B)).

In addition, methyl group substituent changes the general feature of the spectra more than deuterium. Uracil, 5-*d*-U and 6-*d*-U show two peaks in the 1600-1660 cm^{-1} region that are attributed to the C5C6 and C4O10 stretches, respectively (Figure 3.7). The similarity of these three spectra in this region shows that the presence of deuterium on C5 and C6 has no significant effect on the C5C6 or C4O10 stretches. The spectrum of 5-*d*-U is intermediate in overall appearance (the frequencies and relative intensities of the peaks) between those of uracil and 5-MeU (T)[8]. This claim is confirmed through the peaks at 1200, 1400, and 1600 cm^{-1}. However, the 6-*d*-U spectrum in Figure 3.7 (B) exhibits more uracil-like spectral behavior, particularly in the 1230 and 1600 cm^{-1} spectral regions (as showed in Chapter 2).[7] However, two peaks are observed for uracil, 5-*d*-U and 6-*d*-U in the 1600-1666 cm^{-1} region, but only a single peak in this region attributed to C5C6 stretch, is seen for 5-MeU and 6-MeU. The very similar integrated peak intensities of the 1600 cm^{-1} bands in 5-MeU and 6-MeU predict that the C5C6 stretch or the bond lengthening coordinate is similarly affected by the presence of a CH_3 group on C5 or C6. A quantitative comparison on the reorganization energies of the normal modes and the involving internal coordinates of uracil and its C5 and C6 deuterated and methylated derivatives is discussed in more detail below.

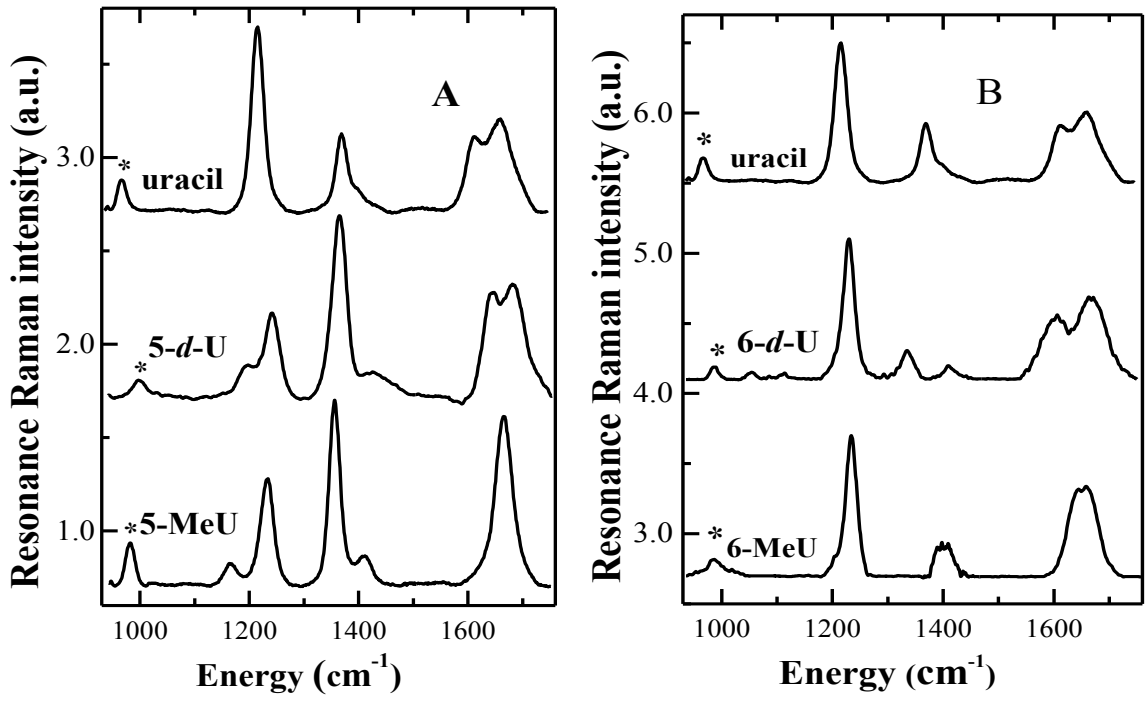

Figure 3.7 Resonance Raman spectra of 3 mM uracil, its C5 (A) derivatives and C6 (B) derivatives excited at 275 nm. The asterisks (*) indicate the 0.3 M sulfate internal standard peak. Intensities have been normalized to the most intense peak in each spectrum. The spectra have been offset along the y axis for clarity

Table 3.3 Experimental and calculated absolute resonance Raman overtone and combination band cross sections of 6-*d*-U[a]

Mode (cm^{-1})	Mode Assignment	$d\sigma_{experimental}/d\Omega$ ($Å^2$/molecule × 10^{10})	$d\sigma_{calculated}/d\Omega$ ($Å^2$/molecule × 10^{10})
1813	1235 + 586	0.98 ± 0.23	1.27
2019	1235 + 786	1.02 ± 0.08	2.20
2318	1606 + 786	0.68 ± 0.12	0.77
2474	2 × 1235	1.42 ± 0.03	3.14
2575	1336 + 1235	0.23 ± 0.23	1.08
2659	1411 + 1235	0.14 ± 0.28	0.93

[a]Excitation wavelength, 257 nm. Cross sections were calculated using Eq. 3.2 with the parameters in Table 3.1.

Table 3.4 Experimental and calculated absolute resonance Raman overtone and combination band cross sections of 6-MeU[a]

Mode (cm^{-1})	Mode assignment	$d\sigma_{experimental}/d\Omega$ ($Å^2$/molecule × 10^{10})	$d\sigma_{calculated}/d\Omega$ ($Å^2$/molecule × 10^{10})
2201	1660 + 520, 1660 + 550	2.5 ± 0.15	1.44
2301	1660 + 650, 1660 + 605	2.19 ± 0.12	1.38
2478	2 × 1235	2.77 ± 0.05	3.13
2644	1397 + 1235	2.21 ± 0.03	2.47
2903	1660 + 1235	6.12 ± 0.05	7.44

[a]Excitation wavelength, 257 nm. Cross sections were calculated using Eq. 3.2 with the parameters in Table 3.2.

The experimental and simulated overtones and combination bands for both 6-*d*-U and 6-MeU are shown in Tables 3.3 and 3.4. A good agreement was observed between the experimental and calculated resonance Raman cross sections of these bands using the parameters in Tables 3.1 and 3.2. The greater sensitivity of the overtone and combination band intensities to the excited-state parameters and the good agreement observed in Tables 3.3 and 3.4 confirm the accuracy of the resonance Raman-derived excited-state parameters in Tables 3.1 and 3.2. However, the overtone and combination intensities have a high dependence on focusing in the Raman microscope, which contributed significantly to the errors. The general low intensity of these peaks caused also a higher degree of error in the experimental overtone and combination band cross sections compared to the fundamental cross sections.

3.4 Discussion

Although, a previous study on the electronic excited-state dynamics has shown that uracil and 6-MeU have similar fluorescence decays (100 fs), it is necessary to look more deeply in the initial excited-state structural dynamics of the photochemical active internal coordinates of these compounds in the first few femtoseconds of excitation.[21] The resonance Raman spectra and the derived initial excited-state structural dynamics of the two 6-substituted uracil derivatives were studied to provide a comparison between uracil and its C5 and C6 substituted derivatives. The excited-state PES slopes ($\beta/\hbar$) are considered as the initial excited-state structural dynamics projection along the normal modes, which are constructed of the photochemical active internal coordinates, such as the C5C6 stretch and C5X and C6X bends, as well as non-photochemical internal coordinates, such as the C4O10 stretch and ring breathing. However, as these internal coordinates are observed in more than one particular normal mode, the direct comparison of the slopes for a normal mode between uracil and its C5 and C6 substituted derivatives cannot provide an accurate description of the initial excited-state structural dynamics. Because each internal coordinate appears in different modes (Tables 3.1 and 3.2) with different potential energy distributions (PEDs), the comparison of the calculated reorganization energy along each *internal coordinate* provide a proper and better description of the initial excited-state structural dynamics

and a better basis for comparison.[4,9]

A convenient parameter for quantitatively comparing initial excited-state structural dynamics is the reorganization energy, borrowed from Marcus theory of electron transfer[5,190].The excited-state reorganization energy of each normal mode (E) is calculated by using $E = (\beta/\hbar)^2/2\tilde{\upsilon}$, where $\tilde{\upsilon}$ is the ground-state wavenumber and $\beta/\hbar$ refers to the excited-state PES slope in cm^{-1}. By using the potential energy distribution (PED), the excited-state reorganization energies along the internal coordinates can be calculated by Eq. 3.4 and are shown in Table 3.5

$$\%\, reorganization\ energy = \frac{\sum_{j=1}^{n}\left\{\left(\frac{\left(\frac{\beta}{\hbar}\right)^2}{2\tilde{\upsilon}}\right)_j c_{ij}\right\}}{\sum_{j=1}^{n}\left(\frac{\left(\frac{\beta}{\hbar}\right)^2}{2\tilde{\upsilon}}\right)_j} \times 100\% \qquad (3.4)$$

where the contribution of each internal coordinate to a normal mode is c_{ij}.

Table 3.5 shows a number of interesting trends that are reflective of the spectral patterns of these uracil derivatives. For example, the C5C6 stretch proportion of the excited-state reorganization energy is low for uracil and its deuterated derivatives, consistent with previous work and as discussed in Chapter 2, but much higher for the methylated derivatives.[6, 7, 20] The reorganization energy of the C5C6 stretch coordinate in uracil (6%) doubles upon deuteration of either the C5 or C6 positions (16% and 12%, respectively). It also quadruples upon methylation of these positions (24% in 5-MeU and 26% in 6-MeU), which clearly reiterates the similarity of C5 and C6 in the C5C6 stretch coordinate. The heavier the substitution on C5 or C6 is, the more the reorganization energy is localized along the C5C6 stretch coordinate, consistent with previous resonance Raman-derived initial excited-state structural dynamics.[7, 8] Recently, Sasidharanpillai and Loppnow demonstrated that the reorganization energy of the C5C6 stretch in 5,6-Me_2-U (25%) is similar to those of 5-MeU and 6-MeU.[20] This result suggests that the presence of a methyl group on the C5C6 bond limits the initial excited-state structural dynamics.

Comparison of the C5X and C6X bends, which are attributed to the in-plane angle changes in all the nucleobase analogues indicates that a larger mass (either deuterium or methyl group) on

Table 3.5 Reorganization energy contributions of different internal coordinates for uracil derivatives[a]

Compound	C5C6 str.	C5 be.	C6 be.	C5 + C6 be.	active	ring def.	C4O10 str.
Uracil	6	13	9	22	28	5	23
5-*d*-U	16	2	16	18	34	4	21
6-*d*-U	12	13	3	16	28	4	20
5-MeU (T)	24	8	15	23	47	5	2
6-MeU	26	7	3	10	36	5	4
5,6-Me_2U[b]	25	7	6	13	38	4	2

[a]In this Table, all reorganization energies are in percent (%). "C5C6 str." is the C5C6 stretch, "C5 be." is all the C5H, C5C and C5D bending coordinates, "C6 be." is all the C6H, C6C and C6D bending coordinates, "C5 + C6 bends" is the sum of the C5X + C6X bends, "active" is the sum of the C5C6 stretch and bending coordinates, "ring def." is the ring deformation and "C4O10 str." is the C4O10 stretch.[b]Data from Ref. 20.

C5 or C6 decreases the reorganization energy along the C5X or C6X bend.[6] This result is expected due to the higher reduced mass. The reorganization energy of C5X bends in uracil (13%) drops to 2% in 5-*d*-U, 8% in 5-MeU, 3% in 6-*d*-U, and 3% in 5-MeU.[6, 7]

Considering the bends in total, as indicated by the "C5 + C6 be." column in Table 3.5, it is interesting that this reorganization energy remains the same in 5-MeU 23% and in uracil (22%), whereas it drops to 10% in 6-MeU. [6, 7] The high reorganization energy value of "C5 + C6 be." clearly shows that the initial excited-state dynamics of C5X and C6X bends remain as high as uracil. However, the initial excited-state dynamics along the C5X and C6X bend coordinates are reduced by the methyl substituent on the C6 position. The previous experimental and calculation studies on the electronic structure and the transition energy around C5 position of uracil and thymine supports the significance of the C5 position on the excited-state potential energy surface and the subsequent reorganization energies of the involved internal coordinates.[21, 22] The recent initial excited-state structural dynamics study on 5,6-Me_2U shows a lower reorganization energies of C5X bends (7%), C6X bends (6%), and consequently in C5X + C6X coordinates (13%). Comparison of this result with those of 6-MeU (10%), 5-MeU (23%), and uracil (22%) indicates that it is the presence of methyl group on C6 that reduces the initial excited-state dynamics on the C5X + C6X bend coordinates and the presence of a H atom on C6 increases the initial excited-state dynamics along this internal coordinates.[20]

By looking at the reorganization energies of all the photochemical active internal coordinates (C5C6 stretch and the sum of C5X + C6X bends), shown as "active" in Table 3.5, it is clearly emphasized that 5-*d*-U with 34% reorganization energy is intermediate between uracil (28%) and 5-MeU (47%), consistent with the resonance Raman spectral patterns.[8] The same comparison shows that the reorganization energies of the "active" internal coordinates are the same in uracil and 6-*d*-U (28%) and increases to 36% in 6-MeU, which is still less than 5-MeU (47%). All these show the significance of the C5 position in increasing the initial excited-state structural dynamics along photochemically active internal coordinates.

All these results clearly show that the initial excited-state structural dynamics of C5X + C6X bends in uracil are increased by the methyl substitution on C5 and are increased along the C5C6

stretch by one or more heavy substituents on C5 and/or C6. The high reorganization energies of both the photochemical active internal coordinates (C5C6 stretch and in-plane C5 and C6 bends) in 5-MeU explains why these coordinates are highly involved in the photochemical reaction. In 6-MeU, the low reorganization energy of C5X + C6X leads 6-MeU to exhibit a more uracil-like behavior in its initial excited-state structural dynamics, even though the reorganization energy of the C5C6 stretch is as high as 5-MeU. All these results confirm the importance of the C5 position in the initial excited-state structural dynamics of C5- and C6-substituted uracil derivatives.

The reorganization energy of the C4O10 stretch coordinate of deuterated uracil derivatives (5-*d*-U and 6-*d*-U) are the same as uracil and much greater than all the methylated derivatives. On the other hand, a relative high reorganization energy along the C5C6 stretch is observed in all the methylated derivatives. Considering these results, one can perceive that the methyl group on C5 or C6 channels the reorganization energy from the C4O10 stretch to the more photochemically relevant coordinate, i.e. the C5C6 stretch. In addition, the small reorganization energies along the ring deformation of all the compounds indicate the low significance of these internal coordinates as the photochemically active coordinates.

3.5 Conclusion

In this Chapter, a clearer insight is provided to understand the initial excited-state structural dynamics of these uracil derivatives. It is clear that substituents rearrange the internal coordinates among the normal modes differentially. This rearrangement also changes the partitioning of the modes between photochemically active and inactive modes, as well as the excited-state PES slopes and resulting initial excited-state structural dynamics. In particular, the initial excited-state structural dynamics along the photochemically active normal modes appear to be more sensitive to C5 than C6 substituents. More experimental studies on other derivatives of uracil and other molecular systems are necessary to understand this effect more generally.

3.6 References

(1) Lemaire, D. G. E.; Ruzsicska, B. P. In *Organic Photochemistry and Photobiology*; Horspool, W. M.; Song, P.-S. Eds.; DNA Damage and Repair; CRC Press: 1995; pp 1295-1329.

(2) He, Y. G.; Wu, C. Y.; Kong, W. Decay Pathways of Thymine and Methyl-Substituted Uracil and Thymine in the Gas Phase. *J. Phys. Chem. A* **2003**, *107*, 5145-5148.

(3) Kang, H.; Lee, K. T.; Jung, B.; Ko, Y. J.; Kim, S. K. Intrinsic Lifetimes of the Excited State of DNA and RNA Bases. *J. Am. Chem. Soc.* **2002**, *124*, 12958-12959.

(4) Myers, A. B.; Mathies, R. A., Eds.; In *Biological applications of Raman spectroscopy*; Spiro, T. G., Ed.; Resonance Raman spectra of polyenes and aromatics; Wiley-Interscience: New York, 1987; Vol. 2, pp 1-58.

(5) Kelley, A. M. Resonance Raman Intensity Analysis of Vibrational and Solvent Reorganization in Photoinduced Charge Transfer. *J. Phys. Chem. A* **1999**, *103*, 6891-6903.

(6) Yarasi, S.; Brost, P.; Loppnow, G. R. Initial Excited-State Structural Dynamics of Thymine are Coincident with the Expected Photochemical Dynamics. *J. Phys. Chem. A* **2007**, *111*, 5130-5135.

(7) Yarasi, S.; Ng, S.; Loppnow, G. R. Initial Excited-State Structural Dynamics of Uracil from Resonance Raman Spectroscopy are Different from those of Thymine (5-Methyluracil). *J. Phys. Chem. B* **2009**, *113*, 14336-14342.

(8) Billinghurst, B. E.; Yeung, R.; Loppnow, G. R. Excited-State Structural Dynamics of 5-Fluorouracil. *J. Phys. Chem. A* **2006**, *110*, 6185-6191.

(9) Marcus, R. A.; Sutin, N. Electron Transfers in Chemistry and Biology. *Biochim. Biophys. Acta* **1985**, *811*, 265-322.

(10) Billinghurst, B. E.; Loppnow, G. R. Excited-State Structural Dynamics of Cytosine from Resonance Raman Spectroscopy. *J. Phys. Chem. A* **2006**, *110*, 2235-2359.

(11) Oladepo, S. A.; Loppnow, G. R. Initial Excited-State Structural Dynamics of 9-Methyladenine from UV Resonance Raman Spectroscopy. *J. Phys. Chem. B* **2011**, *115*, 6149-6156.

(12) Fraga, E.; Webb, M. A.; Loppnow, G. R. Charge-Transfer Dynamics in Plastocyanin, a Blue Copper Protein, from Resonance Raman Intensities. *J. Phys. Chem.* **1996**, *100*, 3278-3287.

(13) Mathies, R.; Oseroff, A. R.; Stryer, L. Rapid-Flow Resonance Raman-Spectroscopy of Photolabile Molecules - Rhodopsin and Isorhodopsin. *Proc. Natl. Acad. Sci. U. S. A.* **1976**, *73*, 1-5.

(14) Mukamel, S. In Principles of nonlinear optical spectroscopy; Oxford University Press: New York, 1995.

(15) Loppnow, G. R.; Fraga, E. Proteins as Solvents: The Role of Amino Acid Composition in the Excited-State Charge Transfer Dynamics of Plastocyanins. *J. Am. Chem. Soc.* **1997**, *119*, 896-905.

(16) Li, B.; Johnson, A. E.; Mukamel, S.; Myers, A. B. The Brownian Oscillator Model for Solvation Effects in Spontaneous Light-Emission and their Relationship to Electron-Transfer. *J. Am. Chem. Soc.* **1994**, *116*, 11039-11047.

(17) Frisch, M. J.; Trucks, G. W.; Schlegel, H. B.; Scuseria, G. E.; Robb, M. A.; Cheeseman, J. R.; Scalmani, G.; Barone, V.; Mennucci, B.; Petersson, G. A.; et al. In Gaussian 09; revision B.01.2009; Gaussian, Inc.:Wallingford,: CT, 2010.

(18) Martin, J. M. L.; Van Alsenoy, C. In GAR2PED; University of Antwerp: Antwerp: The Netherlands, 1995.

(19) Marcus, R. A. Electron-Transfer Reactions in Chemistry - Theory and Experiment. *Rev. Mod. Phys.* **1993**, *65*, 599-610.

(20) Sasidharanpillai, S.; Loppnow, G. R. Initial Excited-State Structural Dynamics of 5,6-Dimethyluracil from Resonance Raman Spectroscopy. *J. Phys. Chem. A* **2014**, *118*, 4680-4687.

(21) Gustavsson, T.; Sarkar, N.; Lazzarotto, E.; Markovitsi, D.; Improta, R. Singlet Excited State Dynamics of Uracil and Thymine Derivatives: A Femtosecond Fluorescence Upconversion Study in Acetonitrile. *J. Chem. Phys. Lett.* **2006**, *429*, 551-557.

(22) Hudock, H. R.; Levine, B. G.; Thompson, A. L.; Satzger, H.; Townsend, D.; Gador, N.; Ullrich, S.; Stolow, A.; Martınez, T. J. Ab Initio Molecular Dynamics and Time-resolved Photoelectron Spectroscopy of Electronically Excited Uracil and Thymine. *J. Phys. Chem. A* **2007**, *111*, 8500-8508.

Chapter 4

C5 Substituent Affect the Initial Excited-state Structural Dynamics of Uracil more than C6 Substituents from Resonance Raman Intensities.

4.1 Introduction

Studying the photochemistry of pyrimidine nucleobases in nucleic acids is interesting because it is the initial step in the complex chain of events that results in UV-induced damage, and ultimately carcinogenesis.[1] Much of the photochemistry of the nucleic acids is localized in the pyrimidine nucleobases, thymine and uracil, which have a very similar structure. They differ only in their C5 substituent, which is H in uracil and CH_3 in thymine. However, the photoproduct quantum yields of uracil and thymine are different (Figure 4.1). UVC irradiation, the major photoproducts of thymine and uracil are cyclobutyl photodimer (CPD) and the photohydrate, respectively. It seems that C5 and C6 play a significant role in the excited-state dynamics.[2]

Many studies of the *electronic* excited-state dynamics have been performed, both theoretically and experimentally.[3-6] Fluorescence lifetime studies and femtosecond transient absorption spectroscopy report very short excited-state lifetimes of <100 and 540 fs for uracil and thymine, respectively, which result from ultrafast internal conversion.[4-7] Thymine and all the C5-substituted uracil derivatives exhibit longer excited-state lifetimes and biexponential fluorescence decays.[4] Also, the S_0/S_1 conical intersection is characterized by pyramidalization and bend motions of the C5 substituents.[4] Therefore, more *structural* dynamics studies are needed to understand the role of the C5 substituent and its difference with C6 in excited state. The short excited-state lifetimes of uracil and thymine restrict the probes for studying the initial excited-state *structural* dynamics to time-resolved resonance Raman and IR spectroscopy. [8-9]

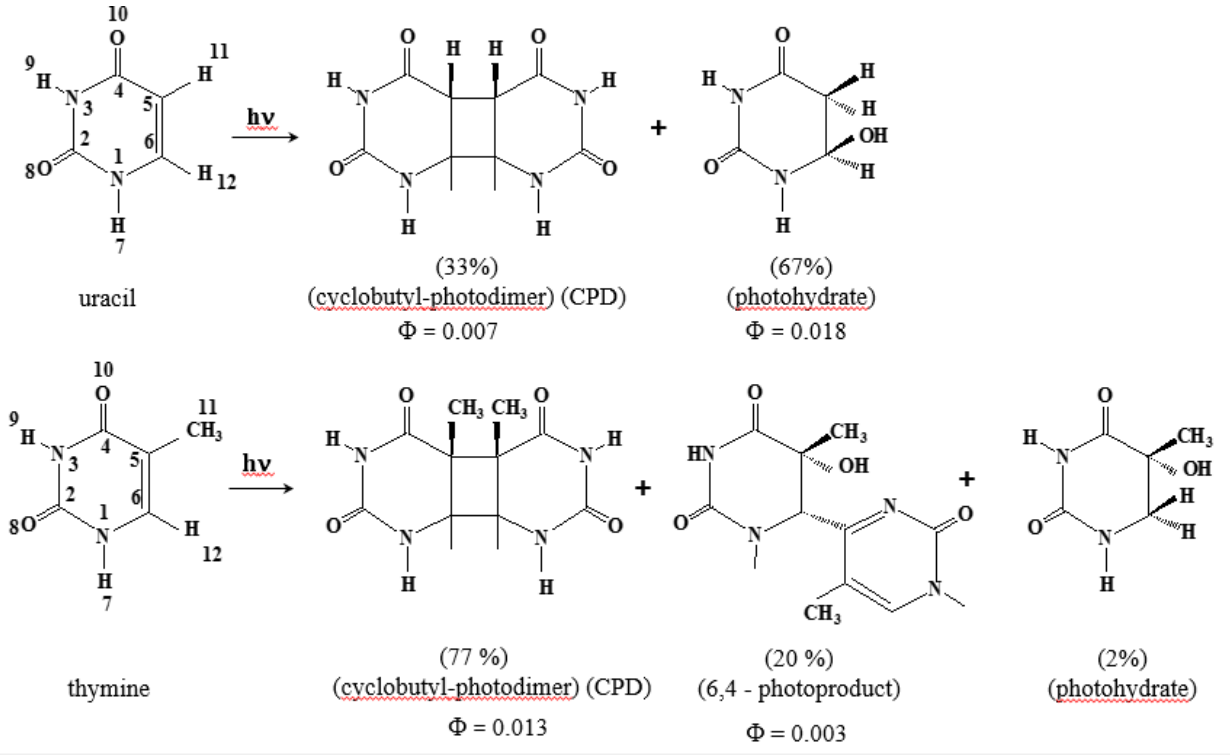

Figure 4.1 Photochemistry of uracil and thymine.[2]

The initial excited-state structural dynamics of nucleobases with short-lived excited-states can be obtained by using resonance Raman peak intensities, absorption spectra and a self-consistent time-dependent formalism. Such an analysis has been performed on numerous uracil derivatives in an attempt to elucidate photochemical mechanisms in DNA components.[10-14] Previous elucidation of the initial excited-state structural dynamics of C5 and C6 methylated uracil derivatives have shown that methyl substitution increases the initial excited-state structural dynamics along the C5C6 bond lengthening coordinate.[10-11, 13-14] Similarly, methyl substitution at C6 shows lower initial excited-state structural dynamics along the C5X and C6X in-plane bends.[13] To complete these studies we here examine the initial excited-state structural dynamics of 5,6-d_2-U (Figure 4.1) using resonance Raman and absorption spectroscopy.

4.2 Experimental

A solution of 5,6-dideuterouracil (5,6-d_2-U, 99%, C/D/N isotopes, Pointe-Claire, Quebec) and 0.3 M lithium sulfate (99%, EMD Chemicals Inc., Gibbstown, NJ) was prepared by dissolving the solid samples in nanopure water obtained from a Barnstead (Boston, MA) water filtration system. The addition of lithium sulfate did not noticeably change the absorption or resonance Raman spectra of 5,6-d_2-U. The UV resonance Raman spectra of solutions containing 1 mM 5,6-d_2-U and 0.3 M lithium sulfate internal standard were obtained at excitation wavelengths of 250, 257, 266, and 275 nm with laser powers of 5-12 mW as previously described.[10, 15-16] Spectral slit widths were 5-7 cm^{-1} and the total accumulation time was 20-30 min in each spectrum. The same sample was used to obtain the 257 nm resonance Raman spectrum with the laser power of 5-8 mW in the overtone and combination band region by using a UV resonance Raman microscope (Renishaw, Chicago, IL).[11]

Absorption spectra (Hewlett-Packard, model 8452A, Sunnyvale, CA) of the samples were taken before and after each Raman spectrum.[11] A few solvents (cyclohexane, ethanol, N,N-dimethylformamide, acetic acid) with known peak positions were used for frequency calibration with an accuracy of ± 5 cm^{-1}. All the other data analyses have been described previously.[10, 17]

The methods used for converting the resonance Raman intensities to differential cross section have been described previously.[18-20] The experimental resonance Raman differential cross sections of sulfate used for the calculations were 3.30×10^{-12}, 2.87×10^{-12}, 2.42×10^{-12}, and 2.05×10^{-12} $Å^2$ molecule^{-1} sr^{-1} at 250, 257, 266 and 275 nm, respectively.[15-16, 20-22]

Theory

Simulation of the absorption spectrum and resonance Raman excitation profiles was performed with the time-dependent wave-packet propagation formalism[17]

$$\sigma_A = \frac{4\pi\ E_L e^2 M^2}{6\hbar^2 cn} \int_0^\infty dE_0 H(E_0) \int_{-\infty}^{\infty} dt < i \mid i(t) > exp\left\{\ i\left(E_L + \varepsilon_i\right)\ t/\hbar\right\}\ G(t) \qquad (4.1)$$

$$\sigma_R = \frac{8\pi\ E_s^3 E_L e^4 M^4}{9\hbar^6 c^4} \int_0^\infty dE_0 H(E_0) \left| \int_0^\infty dt < f \mid i(t) > exp\left\{\ i\left(E_L + \varepsilon_i\right)\ t/\hbar\right\}\ G(t) \right|^2 \qquad (4.2)$$

where E_L and E_S are the energies of incident and scattered photons, respectively, M is the transition length, n is the refractive index, $H(E_0)$ is the normalized inhomogeneous distribution of the zero-zero energies around an average electronic energy ($\bar{E}_0$) expressed as

$$H(E_0) = (2\pi)^{-1/2} \theta^{-1} \int_0^\infty dE_0 exp\left\{\frac{-(E_0 - \bar{E}_0)^2}{2\theta^2}\right\} \qquad (4.3)$$

where θ is the standard deviation of the distribution, $\left|\mathrm{i}\right\rangle$ and $\left|\mathrm{f}\right\rangle$ are the initial and final vibrational wave functions in the Raman process, $\left|\mathrm{i(t)}\right\rangle$ is the initial ground state vibrational wave function propagated on the excited-state potential energy surface, ε_i is the energy of initial vibrational state and *G(t)* is the homogenous line width function as represented by solvent-chromophore coupling within the Brownian oscillator model.[23]

Within the separable harmonic oscillator approximation, the $\langle \mathrm{i} \mid \mathrm{i(t)} \rangle$ and $\langle \mathrm{f} \mid \mathrm{i(t)} \rangle$ overlaps depend only on the excited-state potential energy surface slopes ($\beta/\hbar$) at the Franck-Condon geometry along each normal mode. The parameters are optimized iteratively to obtain the best simulated results in agreement with the experimental absorption spectroscopy and the resonance

Table 4.1 Harmonic mode parameters of 5,6-d_2-U[a]

Mode ν(cm^{-1})	Assignment[b] (PED%)	β/ħ (cm^{-1})
571	Ring def. 3 [53], be(C2O8) [-10], ν(N3C4) [-7], ν(C4C5) [6], be(C4O10) [-6]	108
777	be(C5D11) [52], be(C6D12) [31], ν(C5C6) [-6]	178
1191	ν(C2N3) [17], ν(C4C5) [14], be(N1H7) [12], ν(N1C2) [-11], be(C5D11) [-9], ν(C5C6) [-8], be(C6D12) [8], be(C2O8) [6], ν(N1C6) [5]	202
1274	ν(C2N3) [20], ν(N1C2) [-16], ν(C4C5) [-10], be(C4O10) [-9]	369
1403	be(N1H7) [47], ν(N1C6) [24], ν(C2O8) [-10]	168
1593	ν(C5C6) [63], ν(N1C6) [-11], be(C6D12) [6]	382
1661	ν(C4O10) [71], ν(C4C5) [-8], Ring def. 2 [5]	448

[a] Normal modes listed here are the experimental wavenumbers of 5,6-d_2-U. The excited-state PES slopes (β/ħ) were obtained by fitting the excitation profiles and absorption spectra in Figs. 2 and 3 with Eq.s 1 and 2 and the following parameters: temperature T = 298 K, Brownian oscillator line shape $\kappa = \Lambda/D = 0.1$, Gaussian homogeneous line width Γ_G =1310 cm^{-1}, inhomogeneous line width θ = 1150 cm^{-1}, zero-zero energy E_0 = 37280 cm^{-1}, and transition length M= 0.67 Å. The errors in the parameters are estimated in the calculation as follows: zero-zero energy (E_0), ±1%; transition length (M), ±1%; homogeneous line width (Γ), ±5%; inhomogeneous line width (θ), ±5%; and displacements, ±5%.[b] Gaussian09 and GAR2PED computation was used to obtain mode assignments and internal coordinates. Abbreviations: ν, stretch; be, bend; def., deformation. The definition of the Ring def. coordinates is shown in Table A of Appendix. The numbers in square brackets represent the potential energy distributions (PEDs) of the internal coordinate(s) in %. The internal coordinates with PEDs < 5% are not reported. The sign refers to the phase of the internal coordinate.

Raman excitation profiles. The general implementation of these equations for absorption and resonance Raman spectroscopy has been previously described in detail.[11-12, 14-15, 17, 20-27]All experimental fundamental modes of 5,6-d_2-U were considered in the time-dependent calculation.

The mode assignments were obtained by a density functional theory (DFT) computation at the B3LYP/6-311G(d,p) level of theory using the default gradients in the Gaussian09 package and performed on the initial planar Cs structure of uracil to give the minimum energy structure.[28] The isotope effect was calculated on the uracil frequencies, which are not scaled. A single point calculation was used on the optimized structure, replacing the natural abundance mass of H with the isotopic mass of 2 for deuterium at both C5 and C6. The set of nonredundant symmetry coordinates of 5,6-d_2-U was constructed by GAR2PED.[29]

4.3 Results

The wavelength-dependent UV resonance Raman spectra of 5,6-dideuterouracil (5,6-d_2-U) are shown in Figure 4.2 and all the mode assignments and excited-state PES slopes are described in Table 4.1, where the internal coordinates involved in each mode and their contributions to the normal mode are introduced. The most intense modes observed in the resonance Raman spectra of 5,6-d_2-U include the 1661 cm^{-1} peak corresponding to the C4O10 stretch, 1593 cm^{-1} corresponding to the C5C6 stretch, 1274 cm^{-1} and 1191 cm^{-1} corresponding to ring stretches, 777 cm^{-1} corresponding to the C5D11 and C6D12 in-plane bends and 571 cm^{-1} corresponding to a ring deformation. The experimental and simulated absorption spectra of 5,6-d_2-U are shown in Figure 4.3, which also shows the excitation wavelengths used for measuring the resonance Raman spectra. Deviations between the experimental and calculated absorption spectra (Figure 4.3) at wavenumbers greater than 38,000 cm^{-1} are due to transitions to higher electronic excited states that were not considered in this model (vide infra).

Figure 4.4 shows the experimental and simulated resonance Raman excitation profiles that are modeled with Eqs. 4.1 and 4.2 by using the parameters in Table 4.1. The overtones and combination bands between 1700 and 3000 cm^{-1} were obtained by the UV resonance Raman

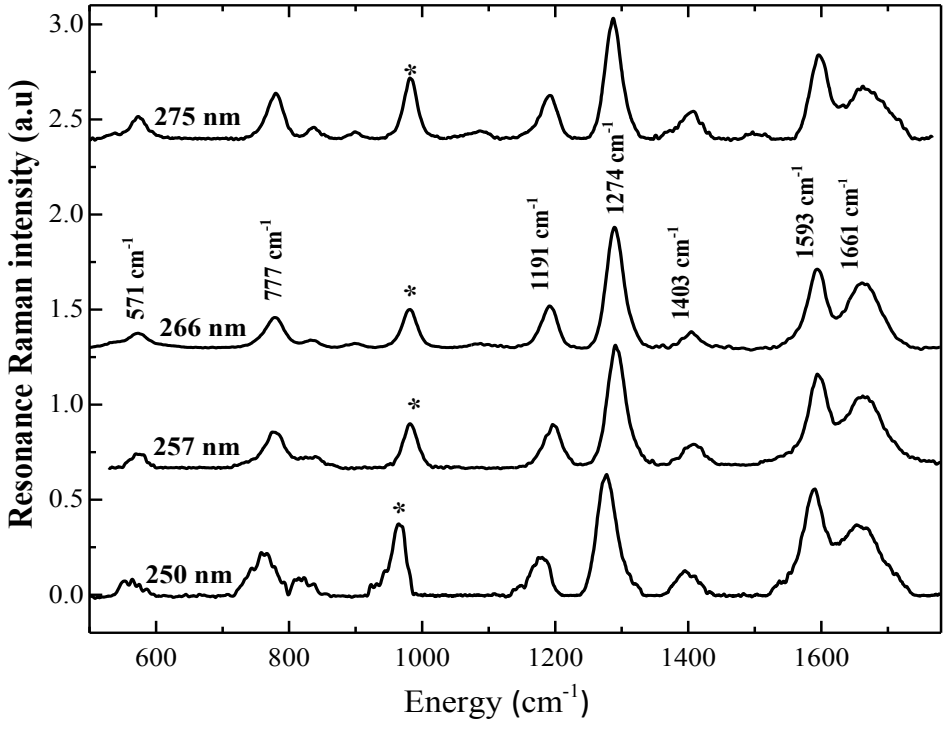

Figure 4.2 Resonance Raman spectra of 1 mM solutions of 5,6-d_2-U containing 0.3 M lithium sulfate as an internal standard at excitation wavelengths throughout its ~ 260 nm absorption band. Asterisks (*) indicate the internal standard bands. The spectra all have been scaled by the most intense peak and offset along the y axis for clarity.

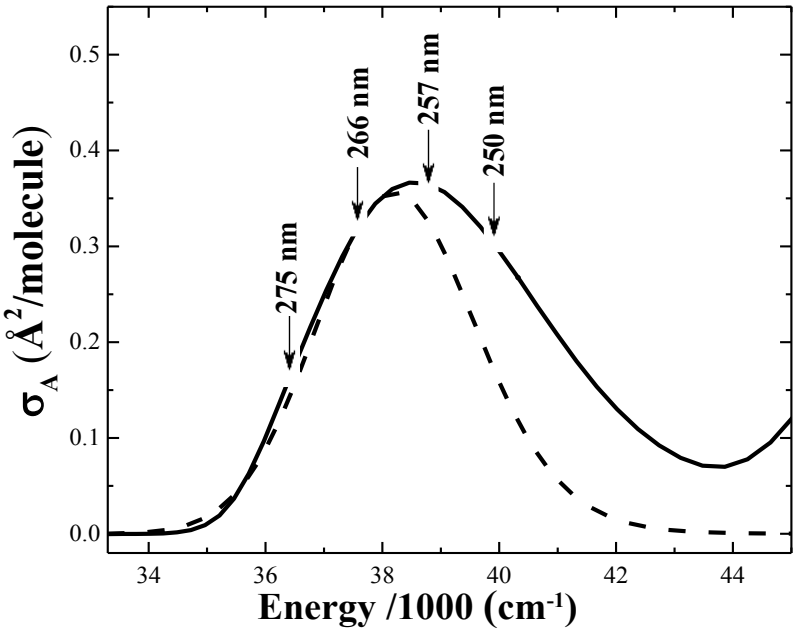

Figure 4.3 Experimental (solid line) and simulated (dashed line) absorption spectra of 5,6-d_2-U. The simulated absorption spectrum was obtained by using Eq. 4.1 and the parameters in Table 4.1. The discrepancies at wavenumbers greater than 38,000 cm^{-1} are due to higher energy electronic transitions that are not modeled here

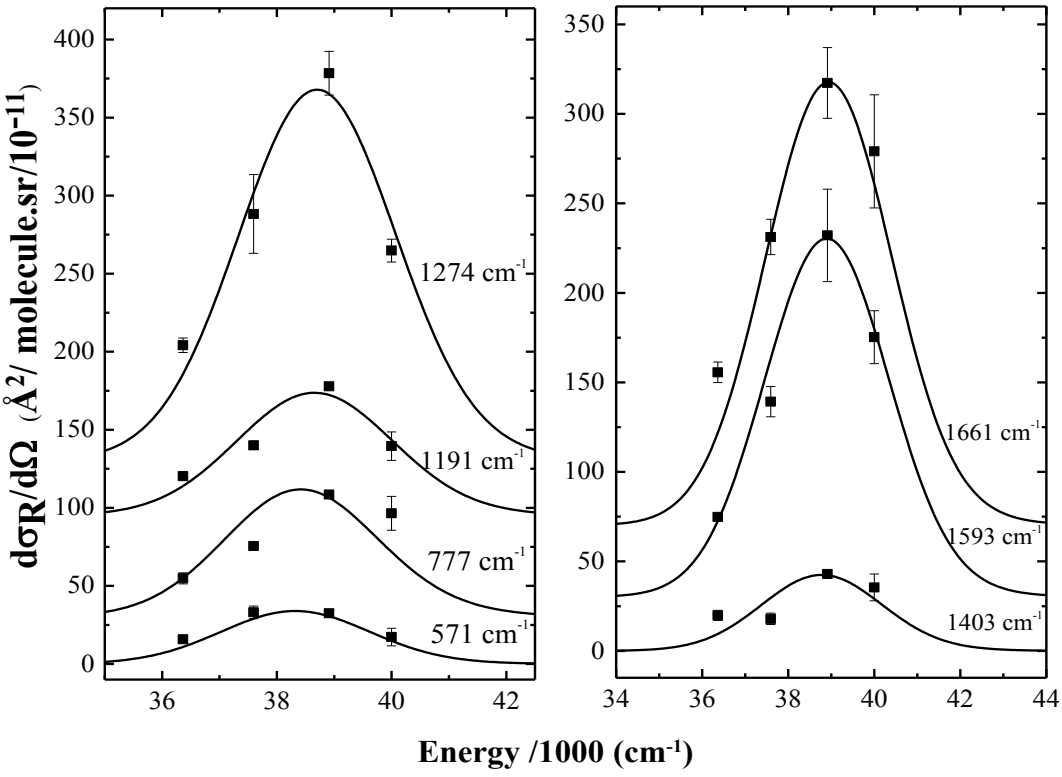

Figure 4.4 Calculated (solid line) and experimental (points) and resonance Raman excitation profiles of 5,6-d_2-U. Using the parameters in Table 4.1, the excitation profiles were calculated with Eq. 4.2. For greater clarity of presentation, the excitation profiles were offset along the coordinate.

microscope at an excitation wavelength of 257 nm and the results are shown in Table 4.2. Because the overtone and combination band intensities are more sensitive to the excited-state parameters and the same derived excited-state parameters (Table 4.1) were used for the overtone and combination bands in the spectrum, proper agreement between experimental and calculated resonance Raman cross sections of this region of spectrum (as shown in Table 4.2) is confirmed.

The observed errors in the overtone and combination band cross sections are attributed to the high dependence of the peak intensities on the focusing point in the Raman microscope. However, the calculated resonance Raman cross sections of this region of spectrum are still within the experimental error range, except for the 2337 cm^{-1} mode. In this way, the harmonic parameter set are constrained and the accuracy of the absorption spectra and fundamental resonance Raman profiles is confirmed. The mass effect on the initial excited-state structural dynamics around the C5 and C6 sites in uracil provide insight into the photochemical mechanism. Comparing all of the resonance Raman spectra of C5- and C6-substituted uracils provides this insight.[12-14] The resonance Raman spectra of uracil and its C5- and C6-methylated and deuterium substituted derivatives are shown in Figure 4.5. Similar main peaks in the fingerprint region (1000-1660 cm^{-1}) are observed in all the methylated and deuterated derivatives of uracil, though they differ in the relative peak intensities and their mode assignments.

A gradual change is observed in the spectral properties, such as the relative intensities, number of peaks and peak frequencies, of all the deuterated uracil derivatives as the number of deuteriums increases. Generally, more change is observed in the resonance Raman spectrum by positioning a heavier substituent (deuterium or CH_3 group) on C5 than on C6. As shown in Figure 4.5, the intensity of the 1397 cm^{-1} peak, attributed to the ring stretch increases, while the intensity of the 1235 cm^{-1} peak, attributed to the C5H bend is reduced. However, the methylated uracil derivatives show more change in the resonance Raman spectra with increasing number of methylated groups, compared to the deuterated derivatives.

Table 4.2 Experimental and calculated absolute resonance Raman overtone and combination band cross sections of and 5, 6-d_2-U[a]

Mode (cm^{-1})	Mode assignment	$d\sigma_{experimental}/d\Omega$ ($Å^2$/molecule × 10^{10})	$d\sigma_{calculated}/d\Omega$ ($Å^2$/molecule × 10^{10})
2081	1273 + 777	0.41 ± 0.37	0.49
2337	(1593 + 777) + (1191 * 2)	0.92 ± 0.13	0.41
2480	(1661 + 777) + (1191 + 1273)	0.72 ± 0.17	0.85
2589	(1191 + 1403) + (1273 * 2)	0.63 ± 0.11	0.74

[a]Excitation wavelength, 257 nm. Cross sections were calculated using Eq. 4.1 with the parameters in Table 4.1.

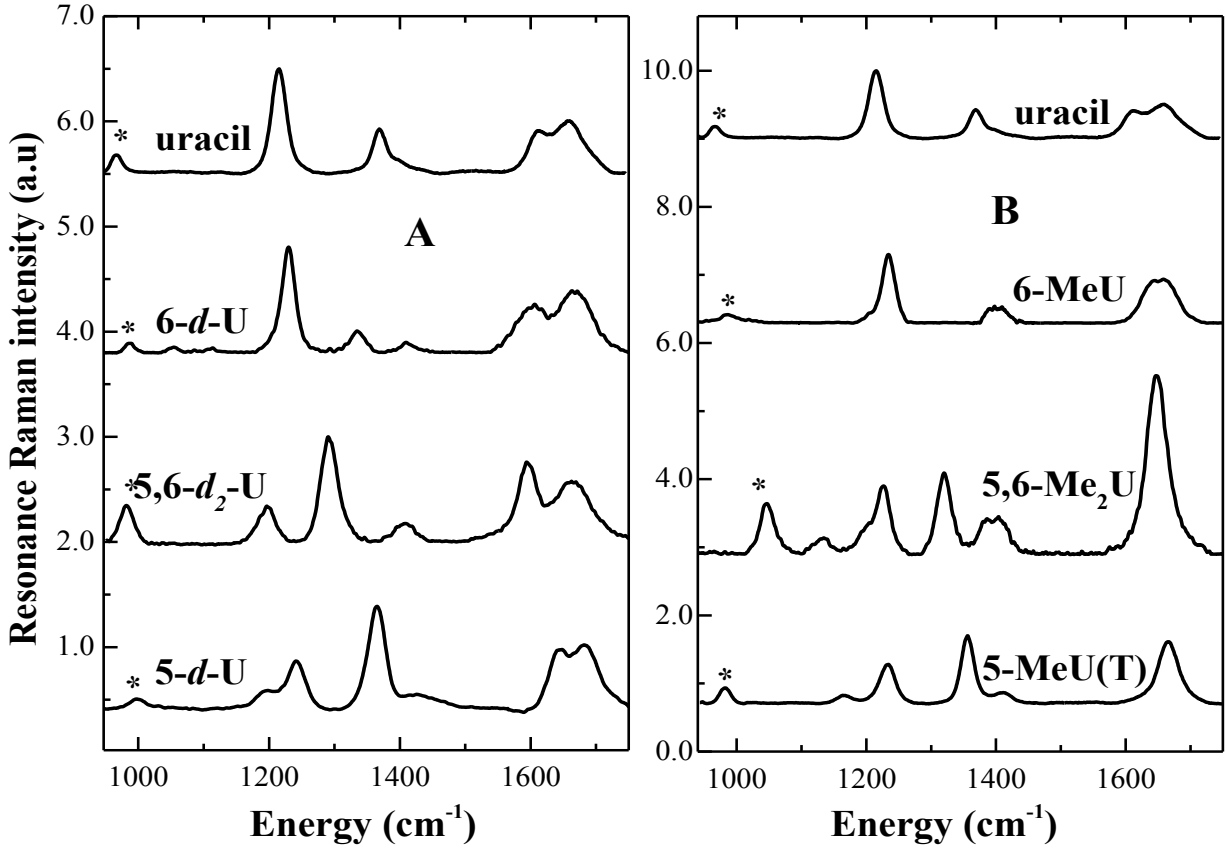

Figure 4.5 Resonance Raman spectra of aqueous solution of (A) uracil, 5-*d*-U, 6-*d*-U and 5,6-d_2-U A and (B) uracil, 5-MeU (T), 6-MeU, 5,6-Me_2U, excited at 275 nm. The asterisks (*) indicate the sulfate internal standard peak in all the compounds except 5,6-Me_2U, in the nitrate peak was used as the internal standard. The spectra have been offset along the y axis for clarity. Intensities have been normalized to the most intense peak in each spectrum.

As observed in Figure 4.5, the comparison of resonance Raman spectra of the deuterated uracil derivatives shows that the spectrum of 5,6-d_2-U is a combination of 5-*d*-U and 6-*d*-U in the range 1200-1400 cm^{-1}. This range corresponds to the C5X and C6X bending coordinates. However, more similarity is observed between the spectra of 6-*d*-U and 5,6-d_2-U, than for either with 5-*d*-U. The similar behavior is also observed in the methylated derivatives in the same region. This result shows that the C5 substituent is more significant in affecting the initial excited-state structural dynamics of uracil derivatives.

The two peaks in 1600 and 1660 cm^{-1} which are observed in uracil and all the deuterated uracil derivatives, correspond to the C5C6 and C4O10 stretches, respectively (Table 4.1). Among all the deuterated compounds, the general feature (the frequencies and relative intensities of the peaks) of these two peaks in 5-*d*-U (as shown in Chapter 2) is more similar to the methylated derivatives peaks. This result is another piece evidence as to the importance of substituents on C5 affecting the initial excited-state dynamics more than those on C6.

4.4 Discussion

Each normal mode is constructed of a few internal coordinates (Table 4.1), including the photochemically active coordinates, such as the C5C6 stretch and C5X and C6X bends, and the non-photochemical internal coordinates, such as the C4O10 stretch and the ring breathing modes. However, the internal coordinates mix differently in the normal modes dependent on the uracil analogue being examined. Therefore, it is more appropriate to discuss the structural dynamics from the internal coordinate perspective, rather than the normal mode perspective, to provide an easier comparison between different uracil analogues and identify trends in their respective initial excited-state structural dynamics. Here, the excited-state PES slope ($\beta/\hbar$) for each normal mode is used as the initial excited-state structural dynamics reporter.

The reorganization energy (E) along each internal coordinate from electron transfer theory can be used as a quantitative measure to compare initial excited-state structural dynamics among different uracil analogues.[25, 28] As shown in Table 4.1, each internal coordinate is observed in

more than one normal mode. Therefore, the contribution of a particular internal coordinate to all the normal modes must be taken into account. The reorganization energy of each internal coordinate is obtained by Eq. 4.5

$$\%\ \text{reorganization energy} = \frac{\sum_{j=1}^{n}\left\{\left(\frac{\left(\frac{\beta}{\hbar}\right)^2}{2\bar{\upsilon}}\right)_j c_{ij}\right\}}{\sum_{j=1}^{n}\left(\frac{\left(\frac{\beta}{\hbar}\right)^2}{2\bar{\upsilon}}\right)_j} \times 100\% \qquad (4.5)$$

where ῡ is the ground-state wavenumber, β/ħ is the excited-state PES slope of each mode, and the contribution of each internal coordinate to the normal mode is c_{ij}.

The reorganization energies of the photochemically active internal coordinates of uracil and its methylated and deuterated derivatives are shown in Table 4.3. Along the C5C6 stretch, Table 4.3 shows that the reorganization energy along this internal coordinate increases from 6% in uracil to 16% and 12% in 5-*d*-U and 6-*d*-U (as discussed in Chapters 2 and 3), respectively. [11] Interestingly, the presence of the second deuterium has no additional effect on the initial excited-state structural dynamics of C5C6 stretch coordinate (14% in 5,6-d_2-U).

A similar effect is observed in singly and doubly methylated uracil; the presence of a single methyl group increases the reorganization energy along the C5C6 stretch from 6% in uracil to 24% and 26% in 5-MeU (T) and 6-MeU (as discussed in Chapter 3), respectively, but the presence of a second methyl group does not lead to any significant increase in the reorganization energy along this internal coordinate (25% in 5,6-Me_2U).[10, 12] In other words, the reorganization energy of doubly deuterated and methylated uracil is the same as the reorganization energy of the singly substituted uracil.

The C5X and C6X bends are another photochemically active internal coordinate. A significant decrease is expected in the reorganization energy of the initial excited-state structural dynamics of the C5X or C6X bends due to the heavier mass of the substituent compared to H. It is observed

that the reorganization energy along the C5X bend in uracil reduces from 13% to 2% in 5-*d*-U. Similarly, the reorganization energy along the C6X bend in uracil reduces from 9% to 3% in 6-*d*-U. With deuteriums on both C5 and C6 , the reorganization energies along both the C5X and C6X bends reduces more considerably from 13% and 9% in uracil to 6% and 2% in 5,6-d_2-U, respectively. These decreases appear along the C5 + C6 bends sum, in which the reorganization energy is reduced from 22% in uracil to 18% and 16% in 5-*d*-U (as discussed in Chapter 2) and 6-*d*-U (as discussed in Chapter 3) and to 8% in 5,6-d_2-U. These results were predicted by the presence of the heavier mass on any of the C5 or C6 sites.[10-12]

A similar behavior is expected along the C6X bends coordinate in singly and doubly methylated uracil derivatives. The reorganization energy along C5X bend in uracil (13%) decreases to 8% in 5-MeU and the reorganization energy along C6X bend in uracil (9%) decreases to 3% in 6-MeU. Similar to 5,6-d_2-U, the reorganization energy along the C5 + C6 bends coordinate is reduced from 22% in uracil to 13% in 5,6-Me_2U. However, less of a decrease along the C5 + C6 bends coordinate is observed in the C5-substituted derivatives - 5-*d*-U and 5-MeU with 18% and 23%, respectively, - compared to C6-substituted uracil derivatives (6-*d*-U and 6-MeU with 16% and 10%, respectively).[10] All these results confirm the greater significance of the C5 position in increasing the initial excited-state structural dynamics along the C5 + C6 bends sum.

Comparing the reorganization energies along the C5X + C6X bends sum in 5,6-d_2-U and 5,6-Me_2U, we can observe that the reorganization energy along the sum in 5,6-Me_2U with 13% is more than those of 5,6-d_2-U with 8%. Due to the greater mass of CH_3 group compared to deuterium, it is an unexpected result. It must be explained by any other properties of CH_3 group (electronic structure, etc.) rather than mass. This result confirms the significance of CH_3 substituent in increasing the initial excited-state structural dynamics of these internal coordinates.

Comparison of the sum of the reorganization energies of C5C6 stretch and C5 + C6 bends sum (represented as “active” in Table 4.3) in all the deuterated and methylated uracil derivatives indicates that the highest reorganization energies along these photochemical active internal coordinates belong to the C5 substituted uracil derivatives (34% and 47% in 5-*d*-U and 5-MeU(T),

Table 4.3 Internal coordinate reorganization energies of singly and doubly C5- and C6-deuterated and methylated uracil derivatives[a]

Compound	C5C6 str.	C5 be.	C6 be.	C5 + C6 be.	active	ring def.	C4O10 str.
uracil	6	13	9	22	28	5	23
5-*d*-U	16	2	16	18	34	4	21
6-*d*-U	12	13	3	16	28	4	20
5,6-d_2-U	14	6	2	8	22	4	22
5-MeU (T)	24	8	15	23	47	5	2
6-MeU	26	7	3	10	36	5	
5,6-Me_2U[b]	25	7	6	13	38	4	2

[a] In this Table, all reorganization energies are in percent (%). "C5C6 str." is the C5C6 stretch, "C5 be." is all the C5H, C5C and C5D bending coordinates, "C6 be." is all the C6H, C6C and C6D bending coordinates, "C5 +C6 be." is the sum of the C5X + C6X bends, "active" is the sum of the C5C6 stretch and bending coordinates, "ring def." is the ring deformation and "C4O10 str." is the C4O10 stretch. [b] Data from Ref. 12.

respectively). This result confirms the significance of C5 in the initial excited-state structural dynamics of these internal coordinates. Thus, it is obviously confirmed that the high initial excited-state structural dynamics of 5-MeU(T) along the photochemical active internal coordinates depend on a CH_3 group only on C5, which increases the initial excited-state dynamics of C5C, involved in angle change versus bond lengthening.

The higher reorganization energies of C4O10 stretch coordinates in uracil and all the deuterated derivatives (~ 20%) clearly indicate their resemblance to uracil in the initial excited-state dynamics, which is also obvious on the spectra (1660 cm^{-1}). Considering the relative high reorganization energy along the C5C6 stretch in all the methylated derivatives (< 20%), it is perceived that the methyl group on C5 or C6 channels the reorganization energy from the C4O10 stretch to the C5C6 stretch, which is a more photochemical active internal coordinate. It therefore leads to the lower reorganization energy along the C4O10 stretch coordinates in all the methylated derivatives (~ 2-4%). The ring deformation coordinate includes all the bends in the ring. This internal coordinate exhibits little initial excited-state structural dynamics in all compounds (~ 5%). This low reorganization energy along this ring deformation coordinate shows that it is not a photochemically active internal coordinate.

4.5 Conclusion

We have compared the initial excited-state structural dynamics of C5 and C6 uracil derivatives provided by using absorption and UV resonance Raman spectroscopy. The substituent rearrangement alters the internal coordinates of each normal mode, the position of a number of the normal modes, their excited-state PES slopes and resulting initial excited-state structural dynamics. The higher sensitivity of the initial excited-state structural dynamics on the C5 position of uracil is confirmed by comparing the resonance Raman-derived initial excited-state structural dynamics of all the C5 and C6 deuterated and methylated uracil derivatives. Therefore, the first step has been taken in understanding the complex mechanism of the excited-state dynamics of uracil and thymine and their photoproduct formation. Further time dependent studies can complete the excited-state mechanism to provide the full dynamics of these vital molecules in the excited-

state.

4.6 References

(1) Kraemer, K. H. Sunlight and Skin Cancer: Another Link Revealed. *Proc. Natl. Acad. Sci. USA* **1997,** *94*, 11-14.

(2) Lemaire, D. G. E.; Ruzsicska, B. P. In *Organic Photochemistry and Photobiology*. In *DNA Damage and Repair*, Horspool, W. M.; Song, P.-S. Eds. CRC Press: 1995; pp 1295-1329.

(3) Gustavsson, T.; Sarkar, N.; Lazzarotto, E.; Markovitsi, D.; Improta, R. Singlet Excited State Dynamics of Uracil and Thymine Derivatives: A Femtosecond Fluorescence Upconversion Study in Acetonitrile. *Chem. Phys. Lett.* **2006,** *429*, 551-557.

(4) Gustavsson, T.; Banyasz, A.; Lazzarotto, E.; Markovitsi, D.; Scalmani, G.; Frisch, M. J.; Barone, V.; Improta, R. Singlet Excited-state Behavior of Uracil and Thymine in Aqueous Solution: A Combined Experimental and Computational Study of 11 Uracil Derivatives. *J. Am. Chem. Soc.* **2006,** *128*, 607-619.

(5) Merchan, M.; Gonzalez-Luque, R.; Climent, T.; Serrano-Andres, L.; Rodriuguez, E.; Reguero, M.; Pelaez, D. Unified Model for the Ultrafast Decay of Pyrimidine Nucleobases. *J. Phys. Chem. B* **2006,** *110*, 26471-26476.

(6) Hare, P. M.; Crespo-Hernandez, C. E.; Kohler, B. Internal Conversion to the Electronic Ground State Occurs via Two Distinct Pathways for Pyrimidine Bases in Aqueous Solution. *Proc. Natl. Acad. Sci. USA* **2007,** *104*, 435-440.

(7) Cohen, B.; Hare, P. M.; Kohler, B. Ultrafast Excited-state Dynamics of Adenine and Monomethylated Adenines in Solution: Implications for the Nonradiative Decay Mechanism. *J. Am. Chem. Soc.* **2003,** *125*, 13594-13601.

(8) Cohen, B.; Crespo-Hernandez, C. E.; Kohler, B. Strickler-Berg Analysis of Excited Singlet State Dynamics in DNA and RNA Nucleosides. *Faraday Discuss.* **2004,** *127*, 137-147.

(9) Crespo-Hernandez, C. E.; Cohen, B.; Hare, P. M.; Kohler, B. Ultrafast Excited-state Dynamics in Nucleic Acids. *Chem. Rev.* **2004,** *104*, 1977-2019.

(10) Yarasi, S.; Brost, P.; Loppnow, G. R. Initial Excited-state Structural Dynamics of Thymine are Coincident with the Expected Photochemical Dynamics. *J. Phys. Chem. A* **2007,** *111,* 5130-5135.

(11) Yarasi, S.; Ng, S.; Loppnow, G. R. Initial Excited-State Structural Dynamics of Uracil from Spectroscopy are Different from Those of Thymine (5-Methyluracil). *J. Phys. Chem. B* **2009,** *113*, 14336-14342.

(12) Sasidharanpillai, S.; Loppnow, G. R. Initial Excited-state Structural Dynamics of 5,6-Dimethyluracil from Spectroscopy. *J. Phys. Chem. A* **2014,** *118*, 4680-4687.

(13) Fraga, E.; Webb, M. A.; Loppnow, G. R. Charge-transfer Dynamics in Plastocyanin, a Blue Copper Protein, from Intensities. *J. Phys. Chem.* **1996,** *100*, 3278-3287.

(14) Webb, M. A.; Kwong, C. M.; Loppnow, G. R. Excited-state Charge-transfer Dynamics of Azurin, a Blue Copper Protein, from Intensities. *J. Phys. Chem. B* **1997,** *101*, 5062-5069.

(15) Myers, A. B.; Mathies, R. A., Eds.; In *Biological applications of Raman spectroscopy;* Spiro, T. G., Ed.; Resonance Raman Spectra of Polyenes and Aromatics; Wiley-Interscience: New York, 1987; Vol. 2, pp 1-58.

(16) Lee, S. Y.; Heller, E. J. Time-Dependent Theory of Raman-Scattering. *J. Chem. Phys.* **1979,** *71*, 4777-4788.

(17) Myers, A. B. *Laser Techniques in Chemistry*. Wiley: New York, 1995; pp 325-384.

(18) Kelley, A. M. Intensity Analysis of Vibrational and Solvent Reorganization in Photoinduced Charge Transfer. *J. Phys. Chem. A* **1999,** *103*, 6891-6903.

(19) Loppnow, G. R.; Fraga, E. Proteins as solvents: The Role of Amino Acid Composition in the Excited-state Charge Transfer Dynamics of Plastocyanins. *J. Am. Chem. Soc.* **1997,** *119*, 896-905.

(20) Mathies, R.; Oseroff, A. R.; Stryer, L. Rapid-Flow -Spectroscopy of Photolabile Molecules - Rhodopsin and Isorhodopsin. *Proc. Natl. Acad. Sci. USA* **1976,** *73*, 1-5.

(21) Billinghurst, B. E.; Loppnow, G. R. Excited-state Structural Dynamics of Cytosine from Spectroscopy. *J. Phys. Chem. A* **2006,** *110*, 2235-2359.

(22) Fraga, E.; Loppnow, G. R. Proteins as solvents: Blue Copper Proteins as a Molecular Rules for Solvent Effects on Intensities. *J. Phys. Chem. B* **1998,** *102*, 7659-7665.

(23) Li, B.; Johnson, A. E.; Mukamel, S.; Myers, A. B. The Brownian Oscillator Model for Solvation Effects in Spontaneous Light-Emission and their Relationship to Electron-Transfer. *J. Am. Chem. Soc.* **1994,** *116*, 11039-11047.

(24) Billinghurst, B. E.; Yeung, R.; Loppnow, G. R. Excited-state Structural Dynamics of 5-Fluorouracil. *J. Phys. Chem. A* **2006,** *110*, 6185-6191.

(25) Marcus, R. A.; Sutin, N. Electron Transfers in Chemistry and Biology. *Biochim. Biophys. Acta* **1985,** *811*, 265-322.

(26) Frisch, M. J.; Trucks, G. W.; Schlegel, H. B.; Scuseria, G. E.; Robb, M. A.; Cheeseman, J. R.; Scalmani, G.; Barone, V.; Mennucci, B.; Petersson, G. A.; et al. In Gaussian 09; revision B.01.2009; Gaussian, Inc.:Wallingford,: CT, 2010.

(27) Martin, J. M. L.; Van Alsenoy, C. GAR2PED. University of Antwerp: Antwerp: The Netherlands, 1995.

(28) Marcus, R. A. Electron-Transfer Reactions in Chemistry - Theory and Experiment. *Rev. Mod. Phys.* **1993,** *65*, 599-610.

Chapter 5

Conclusion and Future Work

5.1 Conclusion

Uracil and thymine have similar structures (Figure 1.2) with the only difference at the C5 substituent, in which a CH_3 group in thymine replaces the H atom in uracil. Previous photochemical studies on the pyrimidines have shown that the photohydrate and cyclobutyl photodimer (CPD) are the main photoproducts of uracil and thymine, respectively.[1] The C5 and C6 substituents of uracil-like pyrimidines are important in the photoproduct formation, because the most of the initial excited-state dynamics of these molecules are directed along C5H and C6H bending modes and C5C6 stretching modes. Gustavsson et al., using a computational study, have shown that the pyramidalization at C5 is one of the key motions to reach the *S*1/*S*0 conical intersection.[2] In addition, they found that an out of plane motion of the hydrogen atom on C5 leads the hydrogen toward a "pseudo perpendicular" arrangement with respect to the molecular plane.[2] These studies have clearly shown that the C5 substituent plays a major role in determining the excited-state *electronic* dynamics.

Previously, the studies of initial excited-state structural dynamics of thymine and 5-fluorouracil, in Loppnow's group, confirmed the significance of the C5 substituent mass in changing the resonance Raman spectra and the excited-state PES slope along each vibrational mode. The structures of the CPD and photohydrate and their different quantum yields as the main photoproducts of uracil and thymine indicate the role of the C6 substituents in determining the excited-state structural dynamics. By the excited-state *electronic* dynamics study, Gustavsson et al. have shown that the excited state lifetime of 6-MeU is very similar to that of uracil and much longer than that of thymine with the help of quantum mechanics calculations. The steady-state fluorescence spectrum, also, showed more similarity of 6-MeU and uracil, compared to thymine.[2] However, it is necessary to study the mass effect on the excited-state *structural* dynamics along

the C6 substituent of uracil and thymine. Therefore, in this thesis, I have mainly focused on studying the mass effect on the initial excited-state *structural* dynamics of the deuterated and methylated uracil derivatives by resonance Raman spectroscopy. In addition, the mass effect was studied on the initial excited-state structural dynamics of the C5 and C6 deuterated uracil derivatives; 5-*d*-U in Chapter 2, 6-*d*-U, and 5,6-d_2-U in Chapters 3 and 4, respectively, by UV absorption and resonance Raman spectroscopy. In Chapter 3 of this thesis, I studied the initial excited-state structural dynamics of 6-MeU that enabled me to make a comparison with those of 5,6-Me_2U, which were previously studied in our group.[3] In addition, we used the reorganization energies along the photochemically active internal coordinates (C5C6 stretch and C5X and C6X bends) as a more precise picture of the initial excited-state structural dynamics of the C5 and C6 mass-tuned uracil derivatives. The results of this comparison clearly showed the lesser effect of the C6 substituents of the uracil derivatives in the initial excited-state structural dynamics. Therefore, it turns out that the highest initial excited-state structural dynamics along C5C6 stretch were only observed by the presence of the CH_3 group on C5, which increases the probability of addition of two thymines on the C5 and C6. All these more detailed results, which are in agreement with the more general excited-state *electronic* dynamics, are consistent with the higher quantum yield of the CPD formation in thymine.[2]

The importance of the C5 and C6 substituents in the photoproducts formation comes from the initial difference of the C5 substituents in uracil and thymine, the structures of uracil and thymine photoproducts, and as well, the different quantum yields of these photoproducts. The previous research within our group has shown different initial excited-state structural dynamics for uracil and thymine.[4, 5] By a different project, Billinghurst and Yeung in our group studied the initial excited-state structural dynamics of 5-fluorouracil by resonance Raman spectroscopy. This project was interesting, because CH_3 group was replaced with fluorine, with similar mass and different electronic structure, steric and vibrational coupling properties of CH_3 group. Interestingly, no significant change was observed between the initial excited-state structural dynamics of 5-MeU and 5-fluorouracil.[6] This result was consistent with our model where the initial excited-state structural dynamics depend on the mass of the C5 substituent. As both the C5 and C6 positions

are involved in the structure of the CPD and photohydrate, we found it necessary to study the dependence of the initial excited-state structural dynamics of uracil and thymine on the C6 substituent, too. Therefore, we decided to compare the mass effect by replacing the C5, C6 or both substituents with deuterium. The initial excited-state structural dynamics of 5-*d*-U were studied by resonance Raman spectroscopy in Chapter 2. The result of this study showed that the minimal increasing of the C5 substituent mass could increase the reorganization energy along the C5C6 stretch. Therefore, we observed the initial excited-state structural dynamics of 5-*d*-U is intermediate between uracil and thymine and consistent with a model where excited-state structural dynamics depend on the mass of the C5 substituent.[4, 5] In Chapter 3, the effect of C6 substituents on the initial excited-state structural dynamics was studied in 6-*d*-U and 6-MeU. The comparison of the reorganization energies along the C5C6 stretch internal coordinate showed that a heavy substituent on either C5 or C6 causes a similar increase in the initial excited-state dynamics of this internal coordinate. However, CH_3 substitution on the C5 or C6 results in a four-fold increase of the initial excited-state dynamics along C5C6 stretch. Whereas, deuterium increases twice as much reorganization energy as hydrogen does. In addition, it was found that the C5X and C6X bends demonstrated much higher reorganization energies when the deuterium or CH_3 group is located on C5 not on C6, which clearly confirmed the importance of the C5 position in increasing the initial excited-state structural dynamics along C5X and C6X bends.

In Chapter 4, we studied 5,6-d_2-U and made a comparison with 5,6-Me_2U and all the other C5 and C6 deuterated and methylated uracil derivatives.[3] These results showed that the presence of the first substitution of deuterium or CH_3 on C5 or C6 saturates the reorganization energies along the C5C6 stretch internal coordinate. In other words, the presence of the second substituent cannot increase the reorganization energies along the C5C6 stretch internal coordinate any further. Also, the lower reorganization energies along the C5X and C6X bending coordinates in 5,6-d_2-U was recognized as the main reason for reducing the overall initial excited-state structural dynamics of 5,6-d_2-U .

The electronic excited-state dynamics is a key to understanding the photophysical and photochemical behavior of nucleobases and have been studied in previous computational and

experimental techniques, such as time-resolved absorption and fluorescence spectroscopy. Ab initio calculations suggest that the lowest energy transition is a forbidden nπ* transition for both uracil and thymine.[7-9] By using femtosecond transient absorption spectroscopy, Kohler et al. measured the excited-state lifetimes of adenine, guanine, cytosine, and thymine to be 290, 460, 720, and 540 fs, respectively.[10] Also, Phillips et al. reported an ultrafast, single base-localized, stepwise mechanism in studying thymidine and thymine by femtosecond time-resolved fluorescence and transient absorption spectroscopy.[11] The studies of the electronic excited-state dynamics via computational and experimental techniques show a femtosecond timescale for decaying the allowed ππ* transition of DNA nucleobases to the ground electronic state. Ultrafast time-resolved techniques and ab initio calculations have measured the excited-state lifetimes to provide the ultrafast radiationless decay mechanisms. They also show the non-radiatively decay of the nucleobases in the excited state on a sub-picosecond time scale. This very short-lived excited state with very low fluorescence quantum yields may explain the photostability of the nucleobases and the photoproducts quantum yield. Conical intersections between the excited states and ground state PESs are often attributed to the ultrafast excited-state dynamics of the nucleobases.[2, 12-40] These studies and much other experimental and computational research on the *electronic* excited-state dynamics of the pyrimidine nucleobases provided a valuable, but general, introduction to understand the excited-state structural dynamics of these molecules.[2, 7, 11, 23, 40-48] This very short-lived excited state of the nucleobases with very low fluorescence quantum yields has been known for many years, however, understanding the underlying quenching mechanism and excited state dynamics is necessary.[49] The excited state lifetimes may explain the photostability of the nucleobases and the photoproducts quantum yields. Conical intersections between the excited states and ground state potential energy surfaces (PESs), are usually required for ultrafast internal conversion dynamics.[7, 50] Photochemistry is often attributed to the ultrafast excited-state dynamics of the nucleobases.[2, 7, 10, 12-40, 50] But they differ quantitatively on the nature of conical intersection structures and the simulation of excited-state dynamics.[51-57] For example, we see much larger excited-state slopes and little evidence of any excited-state barriers in the photochemical pathways. However, more structural dynamics studies are required to enrich our understanding of the excited-state dynamics, the repairing mechanism or photoproducts

formation. However, studying the excited-state *structural* dynamics of uracil and thymine is a more specific approach to the photoproduct formation mechanism. Therefore, Loppnow's research on the initial excited-state *structural* dynamics of uracil, thymine and their derivatives use different approach to reach the goal of understanding the mechanism of the photoproduct formation.

Myers et al. have discussed how the resonance Raman intensities provide detailed information about excited-state structure and dynamics on such a short time. Resonant enhancement of the normal modes coupled to the electronic excitation occurs by tuning the exciting laser into an absorption band. Upon excitation to an electronic excited state, the resonance Raman intensities directly reflect the conformational distortion of the molecule along each normal mode. A set of resonance Raman excitation profiles are obtained by measurement of the resonance Raman intensity of each vibration as a function of excitation wavelength within an absorption band. Self-consistent analysis of the resonance Raman excitation profiles and the absorption spectrum yield a set of harmonic molecular parameters, which include the excited-state lifetime, the distortion along each normal mode upon photoexcitation, transition moment.[58] The excited-state PES slope is obtained by using those parameters, by which the contributions of the reorganization energies along the internal coordinates are calculated. The reorganization energies reflect the initial excited-state *structural* dynamics. Myers and Kelley used the efficient theory for studying different systems such as, bacteriorhodopsin, but Loppnow's group used it to study the initial excited-state *structural* dynamics of nucleobases.[3-6, 59-62] In our model, we studied the mass effect of the C5 and C6 substituents on the initial excited-state *structural* dynamics of uracil and thymine, by measuring the reorganization energies along the C5C6 stretch and C5X/C6X bends. The higher reorganization energies along these photochemical active internal coordinates, when CH_3 group is on C5, reflect the higher initial excited-state structural dynamics along these photochemical active internal coordinates.

Although the elucidation of the Franck-Condon region of the excited-state is still early in the excited-state evolution to predict the photoproduct formation mechanism, the higher initial excited-state structural dynamics of the C5C6 stretch coordinate may equally increase the

probability of addition of two thymines at both C5 and C6. This must compensate for the unequal initial excited-state structural dynamics in the C5X and C6H bends, which could suggest a higher probability of forming the photohydrate. This is because we see equal magnitudes of distortions at the two carbon sites (Table 4.3). Therefore, formation of the CPD is expected to occur with simultaneous addition at both C5 and C6. This great result is consistent with the higher quantum yield of CPD. The extremely short electronic lifetime of thymine (540 fs) suggests low probability of additional structural dynamics other than those probed in the Franck-Condon region. In fact, a time-resolved IR study has shown that the CPD is formed within a few hundred femtoseconds, essentially along a barrierless trajectory.[63] Therefore, according to the short excited-state electronic lifetime and all the initial excited-state structural dynamics of the photochemical active internal coordinates, the probability of CPD formation over photohydrate or the other possible photoproducts is strongly indicated. However, much more excited-state structural dynamics study is required after this initial point to make an accurate judgment for the possible excited-state mechanism toward photoproducts formation of uracil and thymine.

However, the low reorganization energy along C5C6 stretch in uracil - in the absence of the CH_3 group on C5 - and the greater reorganization energies along C5X/C6X bends are more consistent with the photohydrate formation. Although, the photohydrate, also, has a C5-C6 single bond and sp^3 carbons at C5 and C6, just as the CPD does, the different mechanisms are expected for CPD and photohydrate formation. Photohydrate forms sequentially via a zwitterionic intermediate.[64] Therefore, the initial excited-state structural dynamics that we observe in the short excited-state electronic lifetime of thymine from the resonance Raman experiment are consistent with the more probability of CPD formation over photohydrate or the other possible photoproducts.

Martinez et al. found a low-lying S2/S1 conical intersection, which is separated from an S2 minimum by an intervening barrier. They suggested that the picosecond component of the lifetime may correspond to electronic relaxation from S2 to S1 through this conical intersection. They found that although it is possible to reach directly the S2/S1 minimal energy conical intersection from the Franck-Condon point without any intervening barrier, the steepest slope belongs to the

S2 PES in the direction of the S2 minimum. Our experimental initial excited-state structural dynamics of the individual nucleobases are *qualitatively* consistent with the various computational predictions of relaxation pathways, but differ quantitatively on the conical intersection structures and the simulation of excited-state dynamics.[51-56] However, more structural dynamics studies are required to explain the excited-state dynamics and the mechanism of repairing or photoproducts formation.

The resonance Raman spectroscopy is a unique technique for probing the initial excited-state *structural* dynamics of the pyrimidine nucleobases. However, we also confronted the inherent deficiency of Raman spectroscopy, which is the low intensity of the Raman signals.[65, 66] The intensity enhancement of the resonance Raman peaks has dwindled this issue significantly. The more intense peaks could also be obtained by using a laser with higher power, better laser focusing on the sample and more concentrated sample. However, it requires more caution, since the pyrimidine nucleobases are good chromophores and absorb UV light.

In our time-dependent two state model, we use some assumptions to simplify the calculation of absorption and resonance Raman excitation profiles. These assumptions include the Born-Oppenheimer approximation, the Condon approximation, and the multidimentional separable harmonic approximation. In the latter, the same harmonic frequencies are considered for the ground and excited states, which only differ in the equilibrium positions. The contribution of the nonresonant vibrational states are also neglected. Duschinsky effects, which state that the internal coordinates, are mixed or rotated from the ground to excited state, are also neglected.[4] The displacement of the excited-state PES of each normal mode is only considered in this two state model. It is worth mentioning that, despite all these assumptions, the resulted absorption and resonance Raman excitation profiles are still in a good agreement with experiment, which confirms the accuracy of the excited-state harmonic parameters and the PES slopes for the individual normal modes.

All these assumptions were used in the two state calculation in absorption and resonance Raman cross section simulation. A more accurate calculation with less of these assumptions can make the

absorption and resonance Raman cross sections closer to those obtained by the experiment. Designing a better calculation model can also help to obtain the best match between the experimental and calculated absorption and excited-state resonance Raman profiles and provide a more accurate harmonic parameters and excited-state PES slopes. Now, the first steps have been taken in developing the molecular mechanism of UV-induced nucleic acid damage. It can be improved by further studies on the photochemistry of these uracil derivatives in a longer time-scale to establish a relationship with the initial excited-state structural dynamics. In the grander scheme of things, it will help to complete our understanding in the excited-state structural dynamics of dinucleotides, oligonucleotides and finally the nucleic acids that is essential for the implications of the origins of life.

5.2 Future Work

In this thesis, the initial excited-state structural dynamics were studied on deuterated and methylated photochemical active site (C5 and C6) of uracil by using resonance Raman spectroscopy in the few first femtoseconds after excitation (10-30 fs). To measure longer time structural dynamics, time-resolved IR and time-resolved resonance Raman spectroscopy can be used.[67-70] For example, Mathies et al. have used picosecond time-resolved resonance Raman spectroscopy to probe the structural changes in rhodopsin's retinal chromophore.[71] Also, this technique has been used to study proteins.[72-74] Similarly, time-resolved resonance Raman spectroscopy can be used for studying excited-state structural dynamics of pyrimidine nucleobases in a longer time. Understanding the longer time excited-state structural dynamics of uracil and thymine takes us closer to a more complete understanding of the mechanism of photoproduct formation. In the bigger picture, this initial excited-state structural dynamics predict and measure the factors which control the formation of the photoproducts.

In addition, what was generally focused on in this thesis was the mass effect on the initial excited-state structural dynamics of a number of deuterated and methylated uracil derivative. These experiments were performed by studying the change of partitioning of the reorganization energies of each photochemically active normal mode upon changing the mass of the substituents

on C5 or/and C6. Replacing the H substituents of C5 or/and C6 of uracil with fluorine can show us the effect of the electronic structure change on partitioning the reorganization energies of the related normal modes, as the CH_3 group and F atom have the same mass with different size and electronic structure. Therefore, as the initial excited-state structural dynamics of 5-fluorouracil was previously studied by Loppnow's research group, it would be interesting to study the initial excited-state structural dynamics of 6-fluorouracil and 5,6-difluorouracil.[6] The comparison of these fluorouracil derivatives with 5-fluorouracil, 5-MeU, 6-MeU, and 5,6-Me_2U can provide interesting initial excited-state structural dynamics information. Eventually, the results of these experiments can explain the role of the electronic structure of the C5 and C6 substituents of uracil on the initial excited-state structural dynamics of uracil and thymine.

Alternatively, the study of the initial excited-state structural dynamics by resonance Raman spectroscopy of 5-hydroxyuracil, which is the main photoproduct of uracil, and 6-hydroxythymine, which is a minor photoproduct of thymine, can assist in the understanding of the excited-state dynamics and mechanisms of these pyrimidine photoproducts. This study can also be done under different environmental conditions to study the effect of different environmental conditions, such as solvents, pH, temperature, etc. on the initial excited-state structural dynamics of these photoproducts.

5.3 References

(1) Lemaire, D. G. E.; Ruzsicska, B. P. In *Organic Photochemistry and Photobiology;* Horspool, W. M., Song, P. S., Eds.; DNA Damage and Repair; CRC Press: 1995; pp 1295-1329.

(2) Gustavsson, T.; Banyasz, A.; Lazzarotto, E.; Markovitsi, D.; Scalmani, G.; Frisch, M. J.; Barone, V.; Improta, R. Singlet Excited-State Behavior of Uracil and Thymine in Aqueous Solution: A Combined Experimental and Computational Study of 11 Uracil Derivatives. *J. Am. Chem. Soc.* **2006**, *128*, 607-619.

(3) Sasidharanpillai, S.; Loppnow, G. R. Initial Excited-State Structural Dynamics of 5,6-

Dimethyluracil from Resonance Raman Spectroscopy. *J. Phys. Chem. A* **2014**, *118*, 4680-4687.

(4) Yarasi, S.; Brost, P.; Loppnow, G. R. Initial Excited-State Structural Dynamics of Thymine are Coincident with the Expected Photochemical Dynamics. *J. Phys. Chem. A* **2007**, *111*, 5130-5135.

(5) Yarasi, S.; Ng, S.; Loppnow, G. R. Initial Excited-State Structural Dynamics of Uracil from Resonance Raman Spectroscopy are Different from those of Thymine (5-Methyluracil). *J. Phys. Chem. B* **2009**, *113*, 14336-14342.

(6) Billinghurst, B. E.; Yeung, R.; Loppnow, G. R. Excited-State Structural Dynamics of 5-Fluorouracil. *J. Phys. Chem. A* **2006**, *110*, 6185-6191.

(7) Crespo-Hernandez, C. E.; Cohen, B.; Hare, P. M.; Kohler, B. Ultrafast Excited-State Dynamics in Nucleic Acids. *Chem. Rev.* **2004**, *104*, 1977-2019.

(8) Broo, A.; Pearl, G.; Zerner, M. C. Development of a Hybrid Quantum Chemical and Molecular Mechanics Method with Application of Solvent Effects on the Electronic Spectra of Uracil and Uracil Derivatives. *J. Phys. Chem. A* **1997**, *101*, 2478-2488.

(9) Shukla, M. K.; Leszczynski, J. Phototautomerism in Uracil: A Quantum Chemical Investigation. *J. Phys. Chem. A* **2002**, *106*, 8642-8650.

(10) Pecourt, J. M. L.; Peon, J.; Kohler, B. DNA Excited-State Dynamics: Ultrafast Internal Conversion and Vibrational Cooling in a Series of Nucleosides. *J. Am. Chem. Soc.* **2001**, *123*, 10370-10378.

(11) Kwok, W.; Ma, C.; Phillips, D. L. A Doorway State Leads to Photostability or Triplet Photodamage in Thymine DNA. *J. Am. Chem. Soc.* **2008**, *130*, 5131-5139.

(12) Matsika, S. Radiationless Decay of Excited States of Uracil through Conical Intersections. *J. Phys. Chem. A* **2004**, *108*, 7584-7590.

(13) Sobolewski, A. L.; Domcke, W. On the Mechanism of Nonradiative Decay of DNA Bases: Ab initio and TDDFT Results for the Excited States of 9H-Adenine. *Eur. Phys. J. D* **2002**, *20*, 369-374.

(14) Ismail, N.; Blancafort, L.; Olivucci, M.; Kohler, B.; Robb, M. A. Ultrafast Decay of Electronically Excited Singlet Cytosine via ππ* to n_0π* State Switch. *J. Am. Chem. Soc.* **2002**, *124*, 6818-6819.

(15) Merchan, M.; Serrano-Andres, L. Ultrafast Internal Conversion of Excited Cytosine via the Lowest ππ* Electronic Singlet State. *J. Am. Chem. Soc.* **2003**, *125*, 8108-8109.

(16) Broo, A. A Theoretical Investigation of the Physical Reason for the very Different Luminescence Properties of the Two Isomers Adenine and 2-Aminopurine. *J. Phys. Chem. A* **1998**, *102*, 526-531.

(17) Mennucci, B.; Toniolo, A.; Tomasi, J. Theoretical Study of the Photophysics of Adenine in Solution: Tautomerism, Deactivation Mechanisms, and Comparison with the 2-Aminopurine Fluorescent Isomer. *J. Phys. Chem. A* **2001**, *105*, 4749-4757.

(18) Matsika, S. Three-State Conical Intersections in Nucleic Acid Bases. *J. Phys. Chem. A* **2005**, *109*, 7538-7545.

(19) Kistler, K. A.; Matsika, S. Radiationless Decay Mechanism of Cytosine: An Ab initio Study with Comparisons to the Fluorescent Analogue 5-Methyl-2-Pyrimidinone. *J. Phys. Chem. A* **2007**, *111*, 2650-2661.

(20) Perun, S.; Sobolewski, A. L.; Domcke, W. Ab Initio Studies on the Radiationless Decay Mechanisms of the Lowest Excited Singlet States of 9H-Adenine. *J. Am. Chem. Soc.* **2005**, *127*, 6257-6265.

(21) Chen, H.; Li, S. H. Theoretical Study Toward Understanding Ultrafast Internal Conversion

of Excited 9H-Adenine. *J. Phys. Chem. A* **2005**, *109*, 8443-8446.

(22) Blancafort, L.; Robb, M. A. Key Role of a Threefold State Crossing in the Ultrafast Decay of Electronically Excited Cytosine. *J. Phys. Chem. A* **2004**, *108*, 10609-10614.

(23) Merchan, M.; Serrano-Andres, L.; Robb, M. A.; Blancafort, L. Triplet-State Formation along the Ultrafast Decay of Excited Singlet Cytosine. *J. Am. Chem. Soc.* **2005**, *127*, 1820-1825.

(24) Chen, H.; Li, S. H. Ab initio Study on Deactivation Pathways of Excited 9H-Guanine. *J. Chem. Phys.* **2006**, *124*, 154315 (1-10).

(25) Sobolewski, A. L.; Domcke, W. Ab Initio Studies on the Photophysics of the Guanine-Cytosine Base Pair. *Phys. Chem. Chem. Phys.* **2004**, *6*, 2763-2771.

(26) Tomic, K.; Tatchen, J.; Marian, C. M. Quantum Chemical Investigation of the Electronic Spectra of the Keto, Enol, and Keto-Imine Tautomers of Cytosine. *J. Phys. Chem. A* **2005**, *109*, 8410-8418.

(27) Nielsen, S. B.; Solling, T. I. Are Conical Intersections Responsible for the Ultrafast Processes of Adenine, Protonated Adenine, and the Corresponding Nucleosides? *Chemphyschem* **2005**, *6*, 1276-1281.

(28) Zgierski, M. Z.; Patchkovskii, S.; Fujiwara, T.; Lim, E. C. On the Origin of the Ultrafast Internal Conversion of Electronically Excited Pyrimidine Bases. *J. Phys. Chem. A* **2005**, *109*, 9384-9387.

(29) Zgierski, M. Z.; Patchkovskii, S.; Lim, E. C. Ab Initio Study of a Biradical Radiationless Decay Channel of the Lowest Excited Electronic State of Cytosine and its Derivatives. *J. Chem. Phys.* **2005**, *123*, 081101.

(30) Merchan, M.; Gonzalez-Luque, R.; Climent, T.; Serrano-Andres, L.; Rodriuguez, E.; Reguero, M.; Pelaez, D. Unified Model for the Ultrafast Decay of Pyrimidine Nucleobases. *J.*

Phys. Chem. B **2006**, *110*, 26471-26476.

(31) Hare, P. M.; Crespo-Hernandez, C. E.; Kohler, B. Internal Conversion to the Electronic Ground State Occurs via Two Distinct Pathways for Pyrimidine Bases in Aqueous Solution. *Proc. Natl. Acad. Sci. U. S. A.* **2007**, *104*, 435-440.

(32) Gustavsson, T.; Sarkar, N.; Lazzarotto, E.; Markovitsi, D.; Improta, R. Singlet Excited State Dynamics of Uracil and Thymine Derivatives: A Femtosecond Fluorescence Upconversion Study in Acetonitrile. *Chem. Phys. Lett.* **2006**, *429*, 551-557.

(33) Yoshikawa, A.; Matsika, S. Excited Electronic States and Photophysics of Uracil-Water Complexes. *Chem. Phys.* **2008**, *347*, 393-404.

(34) Cohen, B.; Crespo-Hernandez, C. E.; Kohler, B. Strickler-Berg Analysis of Excited Singlet State Dynamics in DNA and RNA Nucleosides. *Faraday Discuss.* **2004**, *127*, 137-147.

(35) Hare, P. M.; Crespo-Hernandez, C. E.; Kohler, B. Solvent-Dependent Photophysics of 1-Cyclohexyluracil: Ultrafast Branching in the Initial Bright State Leads Nonradiatively to the Electronic Ground State and a Long-Lived $\pi\pi^*$ State. *J. Phys. Chem. B* **2006**, *110*, 18641-18650.

(36) Peon, J.; Zewail, A. H. DNA/RNA Nucleotides and Nucleosides: Direct Measurement of Excited-State Lifetimes by Femtosecond Fluorescence Upconversion. *Chem. Phys. Lett.* **2001**, *348*, 255-262.

(37) Gustavsson, T.; Sharonov, A.; Onidas, D.; Markovitsi, D. Adenine, Deoxyadenosine and Deoxyadenosine 5'-Monophosphate Studied by Femtosecond Fluorescence Upconversion Spectroscopy. *Chem. Phys. Lett.* **2002**, *356*, 49-54.

(38) Gustavsson, T.; Sharonov, A.; Markovitsi, D. Thymine, Thymidine and Thymidine 5'-Monophosphate Studied by Femtosecond Fluorescence Upconversion Spectroscopy. *Chem. Phys. Lett.* **2002**, *351*, 195-200.

(39) Onidas, D.; Markovitsi, D.; Marguet, S.; Sharonov, A.; Gustavsson, T. Fluorescence Properties of DNA Nucleosides and Nucleotides: A Refined Steady-State and Femtosecond Investigation. *J. Phys. Chem. B* **2002**, *106*, 11367-11374.

(40) Haupl, T.; Windolph, C.; Jochum, T.; Brede, O.; Hermann, R. Picosecond Fluorescence of Nucleic Acid Bases. *Chem. Phys. Lett.* **1997**, *280*, 520-524.

(41) Nir, E.; Kleinermanns, K.; Grace, L.; de Vries, M. S. On the Photochemistry of Purine Nucleobases. *J. Phys.Chem. A* **2001**, *105*, 5106-5110.

(42) Middleton, C. T.; de La Harpe, K.; Su, C.; Law, Y. K.; Crespo-Hernandez, C. E.; Kohler, B. DNA Excited-State Dynamics: From Single Bases to the Double Helix. *Annu. Rev. Phys. Chem.* **2009**, *60*, 217-239.

(43) Barbatti, M.; Aquino, A. J. A.; Szymczak, J. J.; Nachtigallova, D.; Hobza, P.; Lischka, H. Relaxation Mechanisms of UV-Photoexcited DNA and RNA Nucleobases. *Proc. Natl. Acad. Sci. U. S. A.* **2010**, *107*, 21453-21458.

(44) Pancur, T.; Schwalb, N. K.; Renth, F.; Temps, F. Femtosecond Fluorescence Up-Conversion Spectroscopy of Adenine and Adenosine: Experimental Evidence for the πσ* State? *Chem. Phys.* **2005**, *313*, 199-212.

(45) Kwok, W.; Ma, C.; Phillips, D. L. Femtosecond Time- and Wavelength-Resolved Fluorescence and Absorption Spectroscopic Study of the Excited States of Adenosine and an Adenine Oligomer. *J. Am. Chem. Soc.* **2006**, *128*, 11894-11905.

(46) Buchvarov, I.; Wang, Q.; Raytchev, M.; Trifonov, A.; Fiebig, T. Electronic Energy Delocalization and Dissipation in Single- and Double-Stranded DNA. *Proc. Natl. Acad. Sci. U. S. A.* **2007**, *104*, 4794-4797.

(47) Li, M.; Liu, M.; Zhao, Y.; Pei, K.; Wang, H.; Zheng, X.; Fang, W. H. Excited State Structures and Decay Dynamics of 1,3-Dimethyluracils in Solutions: Resonance Raman and Quantum Mechanical Calculation Study. *J. Phys. Chem. B* **2013**, *117*, 11660-11669.

(48) Crespo-Hernandez, C. E.; Cohen, B.; Kohler, B. Base Stacking Controls Excited-State Dynamics in A-T DNA. *Nature* **2005**, *436*, 1141-1144.

(49) Pecourt, J. M. L.; Peon, J.; Kohler, B. Ultrafast Internal Conversion of Electronically Excited RNA and DNA Nucleosides in Water. *J. Am. Chem. Soc.* **2000**, *122*, 9348-9349.

(50) Cohen, B.; Hare, P. M.; Kohler, B. Ultrafast Excited-State Dynamics of Adenine and Monomethylated Adenines in Solution: Implications for the Nonradiative Decay Mechanism. *J. Am. Chem. Soc.* **2003**, *125*, 13594-13601.

(51) Epifanovsky, E.; Kowalski, K.; Fan, P.; Valiev, M.; Matsika, S.; Krylov, A. I. On the Electronically Excited States of Uracil. *J. Phys. Chem. A* **2008**, *112*, 9983-9992.

(52) Mercier, Y.; Santoro, F.; Reguero, M.; Improta, R. The Decay from the Dark nπ* Excited State in Uracil: An Integrated CASPT2/CASSCF and PCM/TD-DFT Study in the Gas Phase and in Water. *J. Phys. Chem. B* **2008**, *112*, 10769-10772.

(53) Merchan, M.; Serrano-Andres, L.; Robb, M. A.; Blancafort, L. Triplet-State Formation along the Ultrafast Decay of Excited Singlet Cytosine. *J. Am. Chem. Soc.* **2005**, *127*, 1820-1825.

(54) Hudock, H. R.; Levine, B. G.; Thompson, A. L.; Satzger, H.; Townsend, D.; Gador, N.; Ullrich, S.; Stolow, A.; Martinez, T. J. Ab Initio Molecular Dynamics and Time-Resolved Photoelectron Spectroscopy of Electronically Excited Uracil and Thymine. *J. Phys. Chem. A* **2007**, *111*, 8500-8508.

(55) Nachtigallova, D.; Aquino, A. J. A.; Szymczak, J. J.; Barbatti, M.; Hobza, P.; Lischka, H. Nonadiabatic Dynamics of Uracil: Population Split among Different Decay Mechanisms. *J. Phys.*

Chem. A **2011**, *115*, 5247-5255.

(56) Zeleny, T.; Ruckenbauer, M.; Aquino, A. J. A.; Mueller, T.; Lankas, F.; Drsata, T.; Hase, W. L.; Nachtigallova, D.; Lischka, H. Strikingly Different Effects of Hydrogen Bonding on the Photodynamics of Individual Nucleobases in DNA: Comparison of Guanine and Cytosine. *J. Am. Chem. Soc.* **2012**, *134*, 13662-13669.

(57) Improta, R.; Barone, V.; Lami, A.; Santoro, F. Quantum Dynamics of the Ultrafast ππ*/ nπ * Population Transfer in Uracil and 5-Fluorouracil in Water and Acetonitrile. *J. Phys. Chem. B* **2009**, *113*, 14491-14503.

(58) Myers, A. B.; Mathies, R. A., Eds.; In *Biological applications of Raman spectroscopy;* Spiro, T. G., Ed.; Resonance Raman Spectra of Polyenes and Aromatics; Wiley-Interscience: New York, 1987; Vol. 2, pp 1-58.

(59) Billinghurst, B. E.; Loppnow, G. R. Excited-State Structural Dynamics of Cytosine from Resonance Raman Spectroscopy. *J. Phys. Chem. A* **2006**, *110*, 2235-2359.

(60) El-Yazbi, A. F.; Palech, A.; Loppnow, G. R. Initial Excited-State Structural Dynamics of 2'-Deoxyguanosine Determined Via UV Resonance Raman Spectroscopy. *J. Phys. Chem. A* **2011**, *115*.

(61) Oladepo, S. A.; Loppnow, G. R. Initial Excited-State Structural Dynamics of 9-Methyladenine from UV Resonance Raman Spectroscopy. *J. Phys. Chem. B* **2011**, *115*, 6149-6156.

(62) Myers, A. B.; Harris, R. A.; Mathies, R. A. Resonance Raman Excitation Profiles of Bacteriorhodopsin. *J. Chem. Phys.* **1983**, *79*, 603-613.

(63) Schreier, W. J.; Schrader, T. E.; Koller, F. O.; Gilch, P.; Crespo-Hernandez, C. E.; Swaminathan, V. N.; Carell, T.; Zinth, W.; Kohler, B. Thymine Dimerization in DNA is an

Ultrafast Photoreaction. *Science* **2007**, *315*, 625-629.

(64) Hovorun, D. M.; Kondratyuk, I. V. The Quantum Mechanical Calculations Evidence Molecular-Zwitterionic Features of Prototropic Tautomerism of Canonical Nucleotide Bases. 1. Pyrimidines. *Biopolimery i Kletka* **1996**, *12*, 42-48.

(65) Skoog, D. A.; Holler, F. J.; Crouch, S. R., Eds.; In *Principles of Instrumental Analysis;* Thomson Brooks/Cole: CA, 2007; pp 1039.

(66) Griffiths, P. R., Ed.; In *Handbook of Vibrational Spectroscopy;* Chalmers, J. M., Griffiths, P. R., Eds.; John-Wiley & Sons Ltd.: Chichester, UK, 2002; Vol. 1, pp 33-43.

(67) Locke, B.; Diller, R.; Hochstrasser, R. M. In *Ultrafast Infrared Spectroscopy and Protein Dynamics;* Clark, R. J. H., Hester, R. E., Eds.; Biomolecular Spectroscopy, part B; John Wiley and Sons Ltd: New York, 1993; Vol. 21, pp 1-47.

(68) Hamm, P.; Zurek, M.; Mantele, W.; Meyer, M.; Scheer, H.; Zinth, W. Femtosecond Infrared-Spectroscopy of Reaction Centers from Rhodobacter-Sphaeroides between 1000 and 1800 Cm^{-1}. *Proc. Natl. Acad. Sci. U. S. A.* **1995**, *92*, 1826-1830.

(69) Petrich, J. W.; Martin, J. L.; Houde, D.; Poyart, C.; Orszag, A. Time-Resolved Raman-Spectroscopy with Subpicosecond Resolution - Vibrational Cooling and Delocalization of Strain-Energy in Photodissociated (Carbonmonoxy)Hemoglobin. *Biochem.* **1987**, *26*, 7914-7923.

(70) Franzen, S.; Bohn, B.; Poyart, C.; Martin, J. L. Evidence for Subpicosecond Heme Doming in Hemoglobin and Myoglobin - A Time-Resolved Resonance Raman Comparison of Carbonmonoxy and Deoxy Species. *Biochem.* **1995**, *34*, 1224-1237.

(71) Kim, J. E.; McCamant, D. W.; Zhu, L. Y.; Mathies, R. A. Resonance Raman Structural Evidence that the Cis-to-Trans Isomerization in Rhodopsin Occurs in Femtoseconds. *J. Phys. Chem. B* **2001**, *105*, 1240-1249.

(72) Doig, S. J.; Reid, P. J.; Mathies, R. A. Picosecond Time-Resolved Resonance Raman-Spectroscopy of Bacteriorhodopsin-J, Bacterlorhodopsin-K, Bacterlorhodopsin-Kl Intermediates. *J. Phys. Chem.* **1991**, *95*, 6372-6379.

(73) Mizutani, Y.; Kitagawa, T. Direct Observation of Cooling of Heme upon Photodissociation of Carbonmonoxy Myoglobin. *Science* **1997**, *278*, 443-446.

(74) Song, L.; El-Sayed, M. A. Primary Step in Bacteriorhodopsin Photosynthesis: Bond Stretch rather than Angle Twist of its Retinal Excited-State Structure. *J. Am. Chem. Soc.* **1998**, *120*, 8889-8890.

Appendix

Table A. Symmetry coordinate definitions for 5-*d*-U , 6-*d*-U, 5,6-d_2-U, and 6-MeU

Coordinate	Definition
Ring def. 1	be (C6C2 N1) - be (N1N3C2) + be (C2C4N3) - be (N3 C5 C4) + be (C4C6C5) - be (C5N1C6)
Ring def. 2	2be (C6C2 N1) - be (N1N3C2) + be (C2C4N3) +2 be (N3 C5 C4) - be (C4C6C5) - be (C5N1C6)
Ring def. 3	be (N1N3C2) - be (C2C4N3) + be (C4C6C5) - be (C5N1C6)
Ring def. 4	τ (C6N1C2N3) - τ (N1C2N3C4) + τ (C2N3C4C5) - τ (N3C4C5C6) + τ (C4C5C6N1) - τ (C5C6N1C2)
Ring def. 5	τ (C6N1C2N3) + τ (C2N3C4C5) + τ (N3C4C5C6) - τ (C5C6N1C2)
Ring def. 6	-τ (C6N1C2N3) + 2τ (N1C2N3C4) - τ (C2N3C4C5) - τ (N3C4C5C6)+2 τ (C4C5C6N1) - τ (C5C6N1C2)

τ shows the a change in the dihedral angle between atoms. Abbreviation: be, bend; def. deformation.